CR 185612

Final Report for the Program

Three-man Solid Electrolyte Carbon Dioxide Electrolysis Breadboard

June 1989

Prepared for:

National Aeronautics and Space Administration
Lyndon B. Johnson Space Center
Houston, Texas

Under Contract No. NAS9-17590

Prepared by:

Arnold O. Isenberg
Science and Technology Center
Westinghouse Electric Corporation
1310 Beulah Road
Pittsburgh, PA 15235

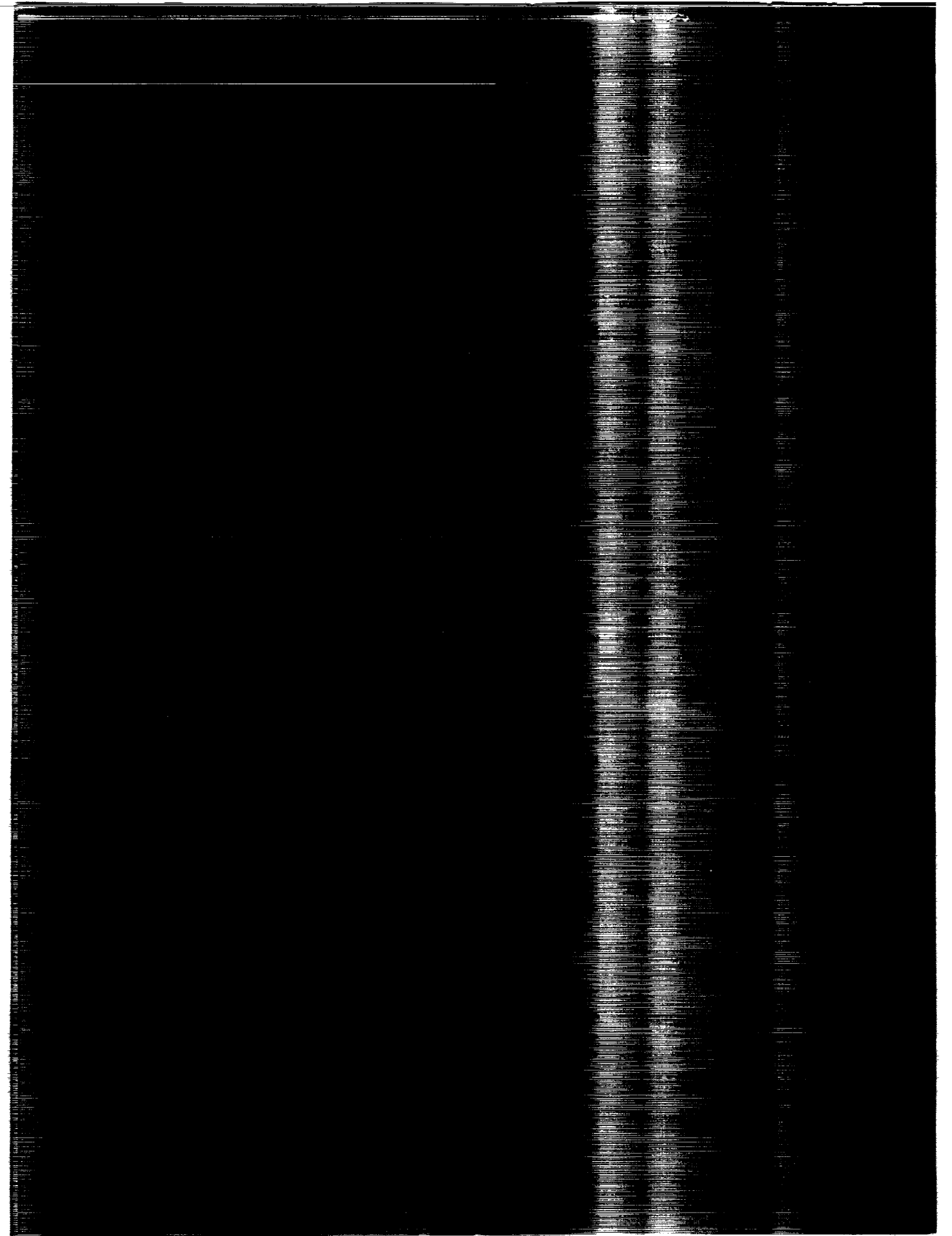

Final Report for the Program

Three-man Solid Electrolyte Carbon Dioxide Electrolysis Breadboard

June 1989

Prepared for:

National Aeronautics and Space Administration
Lyndon B. Johnson Space Center
Houston, Texas

Under Contract No. NAS9-17590

Prepared by:

Arnold O. Isenberg
Science and Technology Center
Westinghouse Electric Corporation
1310 Beulah Road
Pittsburgh, PA 15235

Table of Contents

ABSTRACT

The development of the Three-Man Solid Electrolyte Carbon Dioxide Electrolysis Breadboard consisted of a Phase I and II effort. The Phase I started in May of 1986 and lasted until June 1987 at which time the Phase II started. The Phase I effort constituted fabrication of three electrolysis cell types and performing parametric testing, off-design testing, and cell life testing. The cell type showing the best performance was selected for the breadboard system. Analysis of the test data led to determination of the breadboard conceptual design and operating characteristics of the three-man (2.2 lb CO_2/man-day) CO_2 Electrolysis Cell Breadboard System. The Phase II consisted of the preliminary design, incorporation of palladium (Pd) tubes for hydrogen separation from the electrolyzer cathode feed gases, design support testing, final design, fabrication, and performance testing of the breadboard system. Both Phases I and II were successfully completed. The results of the performance tests have demonstrated that CO_2 electrolysis in an oxygen reclamation system for long duration space-based habitats (Lunar/Mars) is feasible. Closure of the oxygen system loop, therefore, can be achieved by CO_2 electrolysis. In a two step process the metabolic CO_2 and H_2O vapor are electrolyzed into O_2, H_2, and CO. The CO can subsequently be disproportionated into carbon (C) and CO_2 in a carbon deposition reactor and the CO_2 in turn be recycled and electrolyzed for total O_2 recovery. The development effort has demonstrated electrolyzer systems can be designed and built to operate safely and reliably and the incorporation of Pd tubes for hydrogen diffusion can be integrated safely with predictable performance.

SUMMARY

The comparison of three different solid oxide electrolyte cell Types (A, B and C) for carbon dioxide (CO_2) electrolysis resulted in the clear choice of cell Type as a candidate for application in the 3-man breadboard system. The selection was made on the basis of cell fabricability and performance. The cell Type A could not be fabricated within the limits of this program because of materials interaction problems during processing. The other cell Type C was successfully processed and tested; however, some reliability problems in cell fabrication and a lower performance level as compared to cell type B were the reasons for excluding it from further considerations.

Cell test data from individual cells demonstrated a superior current efficiency of nearly 100% (objective 85% min.). This was independently determined by analysis of the anode oxygen and by chemical analysis of the cathode exit gases. The anode oxygen minimum purity measured 99%. This high current efficiency was also achieved in five cells of the breadboard cell stack while others were lower. The average value for the cell stack of 16 cells was 92%.

Parametric cell test were performed on individual cells and on the 16-cell stack including variations of temperature, flow rate, power, cathode feed gas composition, and degrees of CO_2 decomposition. Neither the presence of large quantities (20%) of hydrogen nor the presence of nitrogen (~10%) as contaminant, or the use of pure, dry carbon dioxide as feed gas, precludes the use or limits the performance of individual cells as well as that of the cell stack in the breadboard.

Life performance tests on the individual cells indicated a slow but steady increase in cell voltage with time, which is be attributed to cell resistance increase. The voltage of a breadboard type cell rose nearly 50 mV over a test period of 1100 hours (~1 mV/day).

Five test cells were temperature cycled without mechanical failure prior to constructing the breadboard cell bundle. All test cells operated at 800°C to 1000°C, having an inactive portion of the cell (gas inlet end)

exposed to a temperature gradient of approximately 900°C over a five inch length which begins in the cold (ambient temperature) region of the oxygen manifold. There was not any observed damage to the cell structure.

During performance testing of individual cells a small gas leakage was observed through the detection of CO_2 in the oxygen exhaust (~70 to 360 ppm). A higher CO_2 contamination of the oxygen product (~3-7% CO_2) was measured in breadboard stack cells due to some structural damage. An operational temperature level of 900°C was chosen for the 16-cell breadboard which was tested under similar conditions as individual cells.

There were not any major problems experienced during cell fabrication and breadboard construction. The electrical characteristics of the breadboard electrolysis unit were in close agreement with the expected ones as extrapolated from individual cell tests. The auxiliary systems of the breadboard operated as expected.

Leaks developed in the palladium (Pd) tubes during the breadboard performance test. Subsequently leaks also occurred in the electrolysis cells in the same region of the cell bundle where Pd tubes developed small holes. Thermal stresses on the electrolyzer cells are considered to have caused a sudden and uncontrolled flow of cathode gas at varying temperature levels over the cell tubes. The cell damage occurred in the areas where holes in the Pd tubes had developed. A sudden cathode gas flow disturbance was caused by the cathode gas evacuating through these holes in the Pd tubes. Despite the development of leaks in the electrolysis cells, the breadboard cell bundle did not show significant performance deterioration over a test period of twenty-six (26) days.

The failure mechanism of the Pd tubes was determined after visual inspection of the breadboard cell stack. Separate experiments demonstrated that the interaction of phosphine (PH_3) with Pd tubes resulted in partial melting of palladium and subsequent hole formation.

PH_3 formed by H_2 interaction with a phosphate compound in a structural cement. This was demonstrated by performing interaction tests with Pd tube under cathode gas conditions. The test results were positive.

The cement interaction with the Pd tubes through the gaseous phase had not been anticipated but can be avoided in future stack designs.

The Pd tube failure occurred a short time after breadboard start-up. During this period the hydrogen removal from the cathode gas via diffusion through the evacuated Pd tubes was tested. The hydrogen diffusion rate for the 25 Pd tubes was in agreement with the predicted value which was determined and extrapolated from tests on single Pd tubes.

The disassembly of the electrolysis unit demonstrated easy removal and exchange capability of the cell stack and the soundness of all structural stack components and seals.

CONCLUSIONS

Thin layer solid oxide electrochemical cells, using calcia stabilized porous zirconia tubes as mechanical cell support can be produced reliably and operate well in the electrolysis mode for carbon dioxide (CO_2) and water vapor (H_2O). The cells produce oxygen of high purity (99% plus) and show nearly 100% current efficiency. The internal cell resistance heat losses of state-of-the-art cells are low, so that external heating of cell stacks is required. Further reduction of cell resistance does not lead to reduction of total electrolyzer power consumption (AC plus DC power). Major power reduction for future prototype units will be achieved best through better thermal insulation and reactants gas heat exchange.

Electrolysis cells were tested for over 1600 hours and show slow electrolysis voltage increase. Longer cell and cell stack life-tests using improved electrodes should be performed.

The experimental results obtained from cell fabrication, breadboard construction and testing lead to the following conclusions:

- electrolyzer cells can be fabricated reliably and perform well
- electrolyzer performance can be predicted from individual cell tests
- incorporation of Pd tubes for H_2 extraction from cathode gas can be integrated safely and their performance is predictable
- inactive cell tube extensions withstand temperature gradients between 900°C and 25°C and allow cold-end manifolding of oxygen
- electrolysis cells can produce oxygen efficiently for weeks even when damaged and leaking
- the breadboard operation, including heat-up, shutdown, and data handling is reliable and uncomplicated.

Furthermore, an outcome of this breadboard development program is, that for future prototypical electrolysis units:

- new materials of construction, such as cements, must be tested more rigorously with respect to compatibility with cell stack components
- the incorporation of Pd tubes into the cell bundle must be re-evaluated from a reliability, not a functional point of view
- heat losses by thermal conduction through stack metal containment walls must be reduced by decreasing-wall thickness to a minimum.
- greatly improved thermal insulation for the electrolysis unit must be applied to reduce heat losses
- increased attention must be paid to minimize thermal stresses in active electrolyzer regions which can lead to cell fracture during transient feed gas flows (off-design).

The breadboard electrolyzer unit delivers sufficient oxygen for 3.75 persons at a current density of 250 mA/cm^2 (1.6 lb O_2/person-day), which is a conservative performance level. Therefore, a DC power consumption of 140 watts per person can be expected as a maximum. The AC power consumption for the breadboard electrolysis unit heater is presently too high because the insulation was not engineered for prototype performance. With advanced insulation, the AC power consumption can be greatly reduced, therefore, a total power consumption of less than 200 watt per person can be expected of future more prototype electrolyzers using state-of-the-art solid oxide electrolysis cells.

The excellent electrical performance of the breadboard cell stack regardless of the cell leakage demonstrates to the practicality of oxygen recovery from CO_2 and H_2O for space related activities. However, long-term testing of cells and cell stacks must be performed in order to predict not only the rate of cell deterioration but also the effect of temperature and time on other structural stack components, such as palladium tubes, cell contacts and stack containment.

1. INTRODUCTION

The development of reliable processes for the fabrication of thin and impervious layers of stabilized zirconia in the past decade has substantially increased the potential applications of high temperature electrochemical cells which use such oxide layers as solid electrolyte. The discovery that the same processes can be used to deposit gas impervious layers of electronically conducting complex oxides such as lanthanum chromite was equally important, since it allowed the electrical series connection of such cells were permitted in a simplified way without the use of sealants.

During Phase I of this program these advanced technologies were applied to the fabrication of electrolysis cells for carbon dioxide. Previous studies[1] had investigated cells with machined zirconia electrolytes, having metal to ceramic seals and cell connectors. While these studies demonstrated the possibility of carbon dioxide electrolysis, they fell short of demonstrating reliable sealing techniques. These reported studies also showed that the electrical losses in the electrolyzer cells were not faradayic in nature (e.g., a fraction of the cell current was observed to not contribute towards the decomposition of carbon dioxide into carbon monoxide and oxygen).

During Phase II of this program, the experimental results of Phase I were applied. The cell type, methods of cell fabrication, operational cell conditions, feedgas composition, and cell sealing were evaluated and selected. The breadboard was engineered to produce a minimum of 4.8 lb. of oxygen (O_2) from the electrolysis of carbon dioxide in the presence of other gases, such as hydrogen (H_2) and nitrogen (N_2). The electrolysis of carbon dioxide (CO_2) is not complete and leads to the formation of carbon monoxide (CO) and O_2 according to equations (1), (2). and (3).

$$\text{cathode reaction:} \quad 2CO_2 + 4e^- \xrightarrow{900^\circ C} 2CO + 2O^= \qquad (1)$$

$$\text{anode reaction:} \quad 2O^= \xrightarrow{900^\circ C} O_2 + 4e^- \qquad (2)$$

$$\text{sum reaction:} \quad 2CO_2 \xrightarrow{900^\circ C} 2CO + O_2 \qquad (3)$$

Under the condition that H_2 is present in the CO_2 feed gas, the presence of water (H_2O) in the gaseous form is certain also to be present due to the water gas shift-reaction occurring at elevated temperatures as shown in equation (4).

$$CO_2 + H_2 \xrightarrow{900^\circ C} H_2O + CO \qquad (4)$$

The electrolysis of $CO_2 + H_2$ gas mixtures, therefore, also involves the electrolysis of water vapor, which is represented by equations (5), (6), and (7).

$$\text{cathode reaction:} \quad 2H_2O + 4e^- \xrightarrow{900^\circ C} 2H_2 + 2O^= \qquad (5)$$

$$\text{anode reaction:} \quad 2O^= \xrightarrow{900^\circ C} O_2 + 4e^= \qquad (6)$$

$$\text{sum reaction:} \quad 2H_2O \longrightarrow 2H_2 + O_2 \qquad (7)$$

The direct electrochemical recovery of O_2 from CO_2, which, at this time, is only possible by high temperature electrolysis, cannot be made complete, because it would lead to the deposition of solid carbon (C) at the cathode. Therefore, for complete O_2 recovery the electrochemically produced CO (equation 3) must be chemically disproportionated into solid C and CO_2 in a separate C-deposition reactor according to equation (8).

$$2CO \xrightarrow[\text{Fe-catalyst}]{\sim 600^{\circ}C} CO_2 + C \qquad (8)$$

A complete oxygen recovery system, therefore, includes a CO_2-concentrator, a CO_2/H_2O electrolysis unit, and a carbon deposition reactor.

The total O_2-recovery system operates on a closed loop principle; however, H_2 would accumulate if it were not extracted from the cathode gas. This is accomplished by diffusing H_2 through evacuated palladium (Pd) tubes. These Pd diffusion tubes can be integrated into the electrolyzer cell stack at high temperatures (~900°C), or into the exit gas plenum of the carbon deposition reactor at lower temperatures (~500°C). The location of the Pd diffusion tubes in a closed system loop is critical because carbon deposition can also be triggered by the catalytic action of Pd in a CO-rich cathode gas according to equation 8. In the course of this program it was decided to integrate the Pd diffusion tubes into the breadboard cell stack.

This program deals only with the CO_2/H_2O electrolysis aspect because the other two system components are based on technically proven technologies.

2. OVERALL PROGRAM OBJECTIVES

The guiding principle in the design of the breadboard was to test an arrangement of electrolysis cells which is mechanically sound with respect to high g-forces and which has acceptable power, volume and weight characteristics for outer space applications. Also, the breadboard auxiliary system had to be engineered to provide sufficient operational latitude to test the electrolyzer in off-design conditions as well as allow for an easy exchange of cell stacks if so desired. A NASA requirement was that the data handling system be IBM-PC compatible.

A further design objective for the breadboard was to create a compact stand-alone unit that could easily be transported to and be tested at a NASA test site. The performance objectives for the breadboard

included having the capability to electrolyze a minimum of 2.2 lb of CO_2 per man-day (4.8 lb O_2/man-day) in addition to demonstrating the potential of the breadboard electrolysis unit to be functionally integrated with either steam desorbed solid amine CO_2-removal systems or with electrochemical CO_2 concentrator systems as well as with carbon deposition reactors.

3. PHASE I OBJECTIVES AND TASKS

The solid oxide cell fabrication technologies can be used to produce different cell geometries with varying electrical behavior. Therefore, Phase I activities were directed to fabricate three different types of cells and to determine which cell is best suited for incorporation in the three-man carbon dioxide electrolysis breadboard. Phase I tasks included cell fabrication, construction of a dedicated test station, and testing of cells.

3.1 Cell Fabrication Processes

All cell geometries required the fabrication of porous support tubes. These support tubes are either made of calcia stabilized zirconia, and/or for anode supported cells, of calcia doped lanthanum manganite. For the support tubes and for the processes (like vapor deposition of oxide layers), specific materials had to be prepared.

3.1.1 Porous Support Tubes

The primary ingredient for porous support tubes is calcia stabilized zirconia (0.85 Mol ZrO_2 0.15 Mol CaO) powder containing 0.35% iron oxide (Fe_2O_3) added as a sintering aid.

The purchased powder is wet milled to give an average particle size of 5 to 6 microns. A 1.5 weight percent of polyvinyl alcohol is added to the slurry which is then spray-dried to give small <50 μm ($<2 \times 10^{-3}$ inch) agglomerates. This powder is calcined at 1350°C for three (3) hours.

The calcined and dispersed material, starch (a plasticizer and extrusion aid), cellulose (a pore former) and PWA wetting agent (a napthalated sulfuric acid) are dry mixed (one hour) in a V-cone blender.

The dry blended components are converted into a plastic mass by the addition of a water solution of polyvinyl alcohol to give the proper moisture content for extrusion. The components are mixed for one hour and then sorted in sealed plastic bags, to prevent moisture loss, until the material can be consolidated into dense billets (15 cm diameter by 61 cm length) using a pug mill. The billets are stored for at least two days, in tightly sealed plastic covering, to ensure uniform moisture distribution throughout the billet. The billet is then introduced into an extruder, and the trapped gases are removed by evacuation. The tubes are then extruded through a pin and die assembly as shown in Figure 1.

A plug is formed in one end of the extruded and dried tube by pressing a plastic pellet between two opposed hemispherical rods forcing the material to press against and adhere to the inner wall of the tube. Plugging pellets are prepared by extruding rods from the same tube material composition. Pellets of the desired length are cut from the extruded rods.

A collar is also applied to the outer diameter of the tube at the plugged end to facilitate hanging the tube during sintering. The collar material is prepared from the same tube material composition.

The collared tubes are hung from refractory support plates in the muffle furnace and sintered. The initial heating rate and sintering atmosphere is controlled to remove the organic materials. The rate is increased to 100°C/hr after reaching 600°C (1112°F) to a sintering temperature of 1550°C (2822°F) which is maintained for four hours. Programmed cooling rates are 200°C/hr (390°F/hr) from 1550°C down to 1000°C (1832°F) and 500°C/hr (932°F/hr) down to room temperature.

The sintered tube is cut through the plugged end of the tube with a diamond cut-off wheel and a hemispherical diamond grinder is used to shape the plugged end round. Figure 2 is a schematic cross section

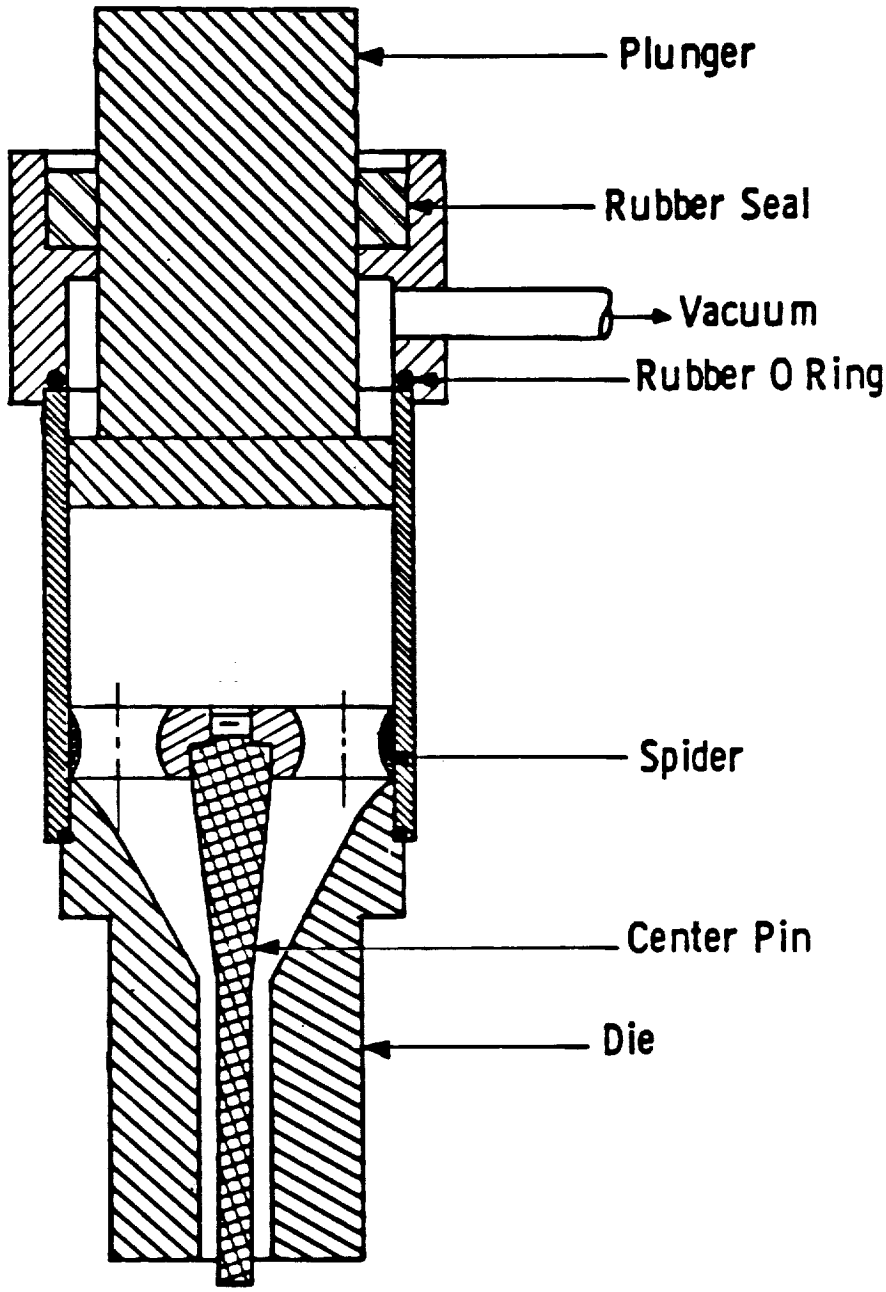

Figure 1. Schematic of Extruder Assembly for Extruding Porous Support Tubes

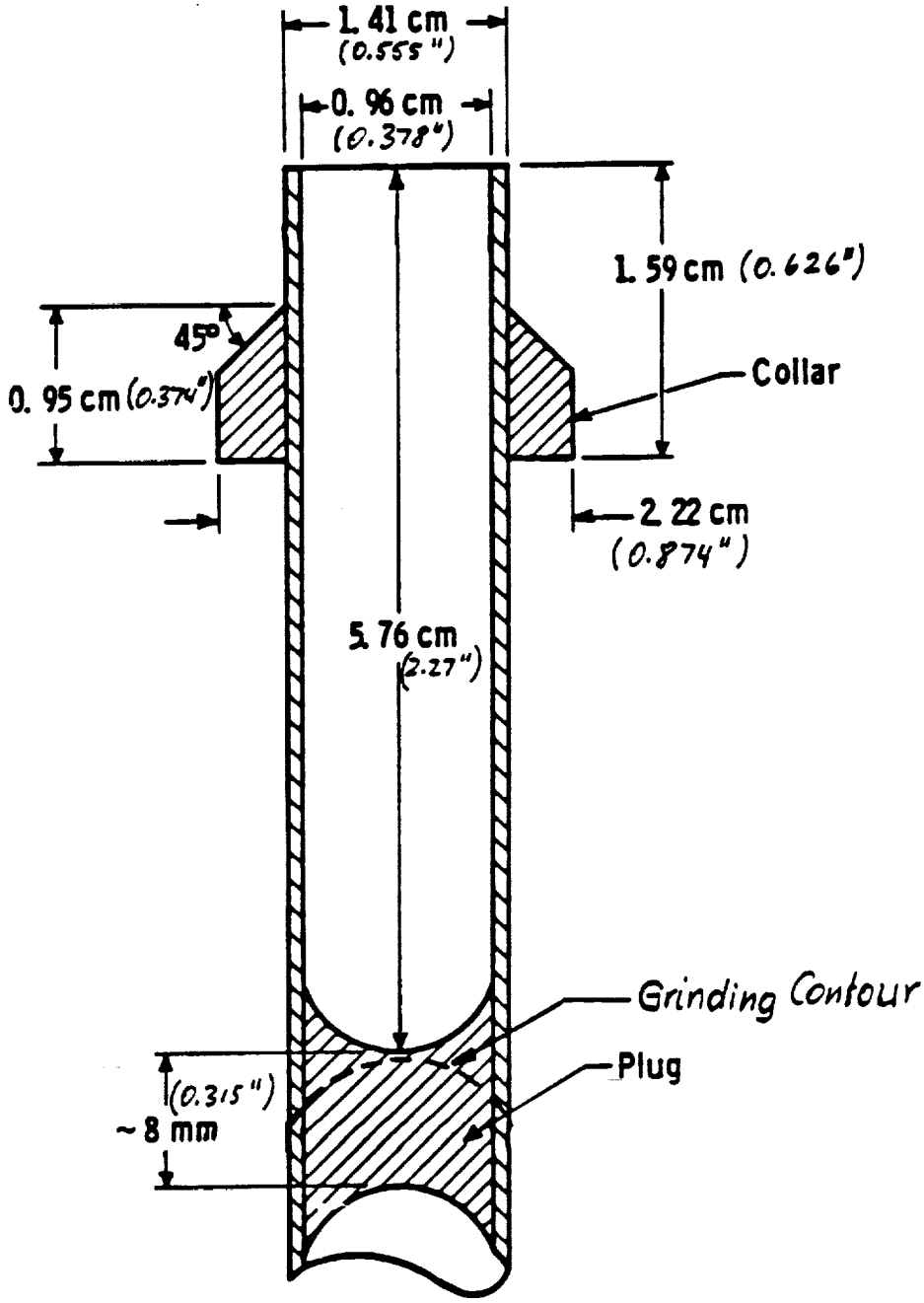

Figure 2. Cross Section of a Plugged and Collared Tube

through a plugged and collared tube. Sixty porous support tubes have been fabricated and finished.

3.1.2 Electrochemical Vapor Deposition (EVD) of Cell Components

Electrochemical vapor deposition (EVD)[2] is the principal method of preparing the solid oxide electrolyte, and for depositing a magnesia-doped lanthanum chromite cell electrical interconnection layers. The electrolyte consists of 8-15 mole % yttria stabilized zirconia 25-50 μm (~10^{-3} inches) thick and is gas tight. The lanthanum chromite layer has similar dimensions and is also gas tight. A schematic representation of these layers are shown in Figure 3. The porous anode serves as the substrate for the dense layers of the electrolyte and interconnection. The layers are formed by passing the respective metal chloride vapors at high temperatures (1200-1350°C, 2190-2460°F) over the porous anode while water vapor passes through the pores from the other side. During this initial growth phase I the pores close up with oxide deposits. This chemical vapor deposition phase (CVD) is followed by the EVD phase II. During this second phase, continued growth of the oxide layer takes place by oxygen ion as well as electron transfer because a large oxygen concentration gradient exists between both sides of the oxide layer. The duration of phase I is one to five minutes and that of phase II varies between 30 and 90 minutes. Both reaction phases take place in the same reactor immediately following each other at the same temperature (1200-1350°C, 2190-2460°F) and pressure (0-1.5 Torr).

The EVD process requires halide source materials for allowing constant and precise delivery of metal chloride vapors. For the magnesium doped lanthanum chromite interconnection materials ($LaCr_{0.9}Mg_{0.1}O_3$), vapor streams of chromium dichloride ($CrCl_2$), lanthanum chromite ($LaCl_3$), and magnesium chloride ($MgCl_2$) are produced. The metal chlorides are produced by either chlorination and instantaneous evaporation, so that the flow rate of chlorine can be used as a measure of the rate of metal

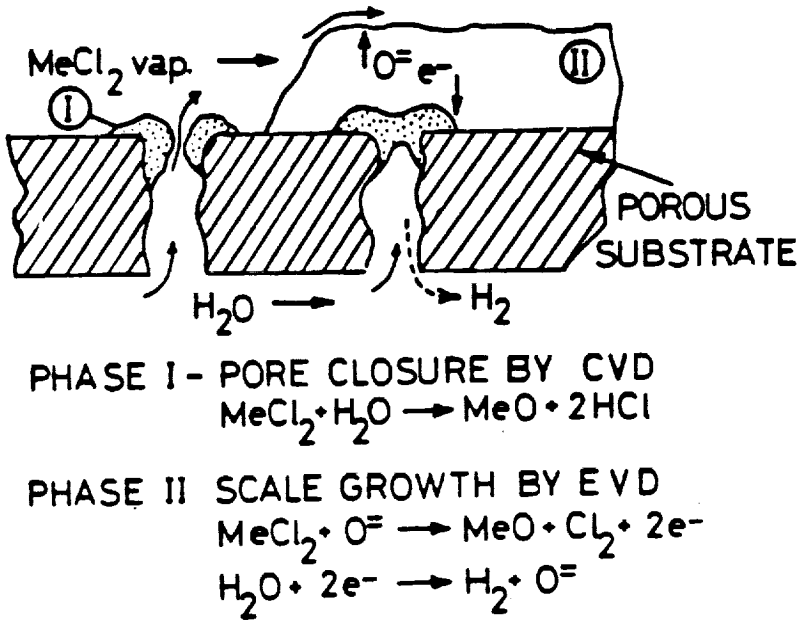

Figure 3. Schematic of Scale Growth by EVD

chlorides delivered into the EVD reactor. The halide source materials had to be prepared because they are not readily available commercially. The materials are: pelletized mixtures of lanthanum oxichloride/carbon, magnesium oxide/carbon, yttria stabilized zirconia/carbon and chromium metal granules. For the interconnection fabrication the respective chlorides are delivered to the EVD reactor by the following chlorination reactions:

$$2LaOCl + 2C + 3Cl_2 \xrightarrow{\sim 1250^\circ C} 2\ LaCl_{3(vap.)} + 2CO \quad (9)$$

$$Cr + Cl_2 \xrightarrow{\sim 1250^\circ C} CrCl_{2(vap.)} \quad (10)$$

$$MgO + C + Cl_2 \xrightarrow{\sim 1250^\circ C} MgCl_{2(vap.)} + CO \quad (11)$$

The chlorination reactions, (9) and (11), are quantitative only when executed in the presence of finely divided carbon (lamp black).

Lanthanum oxichloride was prepared by reacting lanthanum oxide in water with ammonium chloride (equation 12) for several days between 85 and 95°C (185-203°F) while replenishing the evaporating distilled water. Approximately 438 g LaOCl were prepared from 503 g La_2O_3 and 196 g NH_4Cl in 4 ℓ of water. Some product loss (LaOCl) is experienced when washing the LaOCl and decanting the water from the LaOCl. The washing and decanting step is performed after completion of reaction 12 several times in order to remove the excess ammonium chloride present in the LaOCl.

$$La_2O_3 + H_2O + 2NH_4Cl \rightarrow 2LaOCl + 2NH_4OH \quad (12)$$

The dried oxichloride was mixed with 33 g of lamp black and the mixture homogenized in acetone by rolling in a ball mill (2 l polyethylene bottle) with 1/2" steel balls. The homogenized slurry was poured into a dish, dried, and granulized to ~1/8" size granules.

The granules of different source materials are each filled into separate, tubular graphite containers and receive a measured stream of chlorine gas (Cl_2) for chloride delivery control during the vapor deposition process.

For the deposition of yttria-stabilized zirconia electrolyte, the same principle of chloride formation is employed using mixtures of yttria-stabilized zirconium oxide plus carbon, followed by chlorination.

$$ZrO_2 + 2C + 2Cl_2 \xrightarrow{1200^\circ C} ZrCl_4 + 2CO \qquad (13)$$

$$Y_2O_3 + 3C + 3Cl_2 \xrightarrow{1200^\circ C} 2YCl_3 + 3CO \qquad (14)$$

3.1.3 Anode Fabrication

Strontium doped lanthanum manganite $La_{0.9}Sr_{0.1}MnO_3$ (10% ZrO_2) is synthesized from La_2O_3, MnO_2, $SrCO_3$, and ZrO_2. This is accomplished by mixing the powders, compacting, calcining at 1500°C in air, followed by milling. This sequence is repeated two more times to achieve homogenization. The resulting powder (50% ~6μm) is suspended in water. Application to the tube surface is accomplished by the spraying of single tubes or by filtering when several tubes are processed in parallel. We used both processes. In filtering, the porous tubes are submersed into the oxide/water suspension and vacuum is applied to the tube inside, while the tube rotates. A uniform oxide filter cake is formed on the outside. The deposited oxide is dried and sintered at 1400°C for one hour in air.

The platinum-zirconia cermet anodes are applied from the powder slurries by repeated painting and sintering at 1300 to 1400°C. While this process was very reliable in making conductive electrode layers, these electrode layers could not be further processed and applied to cells because of structural and chemical deterioration during EVD processing for the interconnection layers.

3.1.4 Cermet Cathode Fabrication

Cell tubes that have been covered with both the electrolyte and the interconnection layers are tape masked and dipped into metal powder slurries of adjusted composition (binders) to achieve uniform powder coatings. These coatings are fixed to the electrolyte by a further growth of stabilized zirconia into the porous metal layer as described for the electrolyte EVD deposition process. A skeleton of zirconia forms within the porous metal powder layer which is ~100μm thick. This skeleton attaches to the porous metal electrode in a manner as if the electrolyte penetrated into the porous metal matrix. This process is very critical to the performance stability of cells. Nickel and cobalt were the cathode metals of choice. Since the thermal expansion of the metals differs from that of zirconia, interface stresses can be expected which can lead to electrode separation if the zirconia skeleton is too weak.

For one test cell we applied the nickel powder layer by spraying, which results in a more porous electrode structure (larger irregular voids) which allowed enhanced cathode bonding to the electrolyte (see Appendix 1).

3.1.5 Cathode Activation

As-fabricated cermet cathodes exhibit high concentration overvoltage losses, which are reduced by depositing activating oxides into the porous electrode structure. Such oxides are mixed conductors (oxygen-ionic/electronic) and reduce overvoltages and minimize power losses. A lanthanum-doped cerium oxide $(CeO_2)_{0.8}(La_2O_3)_{0.2}$ was selected and tried. It is introduced into the porous cathode by impregnation with a concentrated nitrate solution, followed by drying and thermal decomposition of the nitrates to oxides. This occurs at 1000°C in a N_2 + 10% H_2 + 3% H_2O gas mixture. Activated cathodes contain 2-3 mg/cm^2 of this oxide after one impregnation.

3.2 Fabrication of Different Cell Types

3.2.1 A-Type Cell

The cell geometry of this cell is shown in Figure 4. Fabrication of this cell type was considered to be straightforward when using platinum-zirconia cermet electrodes. Zirconia electrolytes had been produced over such electrodes successfully for other applications. For the deposition of lanthanum chromite interconnection layers, however, the chemical and physical deterioration of the underlying cermet electrode was observed. A structural analysis shows platinum migration out from the cermet electrode structure into the growing lanthanum chromite layer. This fact precluded the use of platinum cermet electrodes as anodes when using present cell fabrication techniques.

Several attempts were made to replace platinum cermet anodes with lanthanum manganite oxide anodes; however, completion of such cells was not possible because of the increased thickness of oxide anodes to achieve the same sheet resistance. The increased thickness of the oxide anodes resulted in a stressed cell structure which led to interconnection layers spalling (chipping) and in some cases causing tube fracture. As a consequence of these difficulties, the fabrication of such cells was abandoned.

3.2.2 B-Type Cell

This cell type is shown in Figures 5 and 6. Four such cells were fabricated and two were tested. The fabrication of these cells did not present problems. Major fabrication steps included:

- tube extrusion, sintering
- anode deposition, sintering
- interconnection deposition by EVD
- electrolyte deposition by EVD
- cathode fixation by EVD
- cathode activation by impregnation

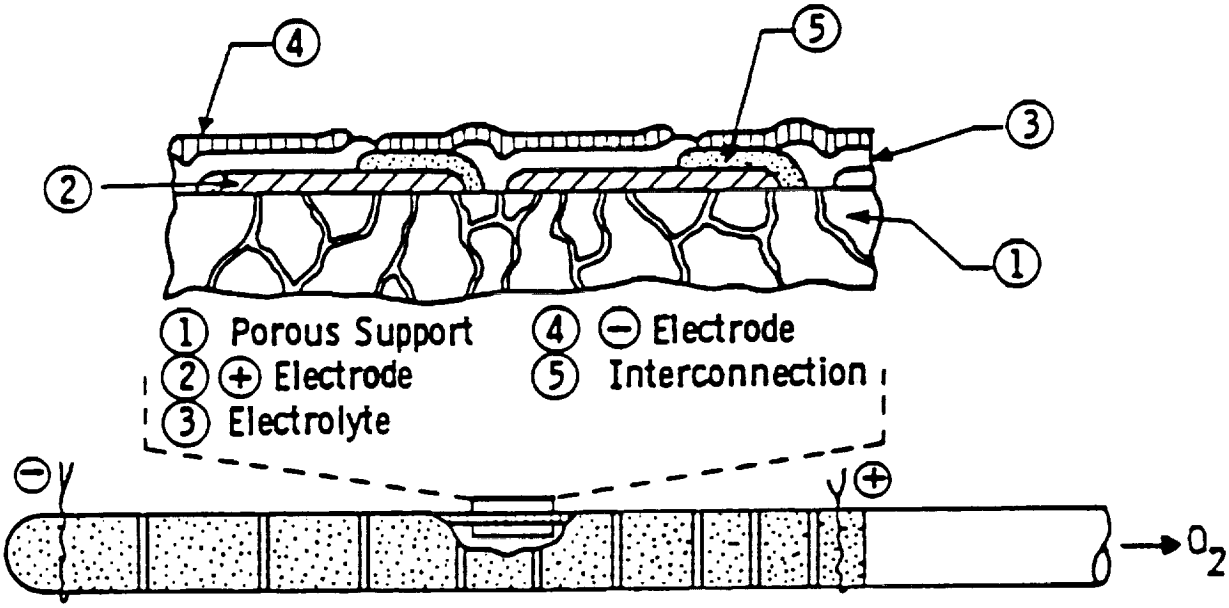

Figure 4. Schematic Structures of Cell Geometry A

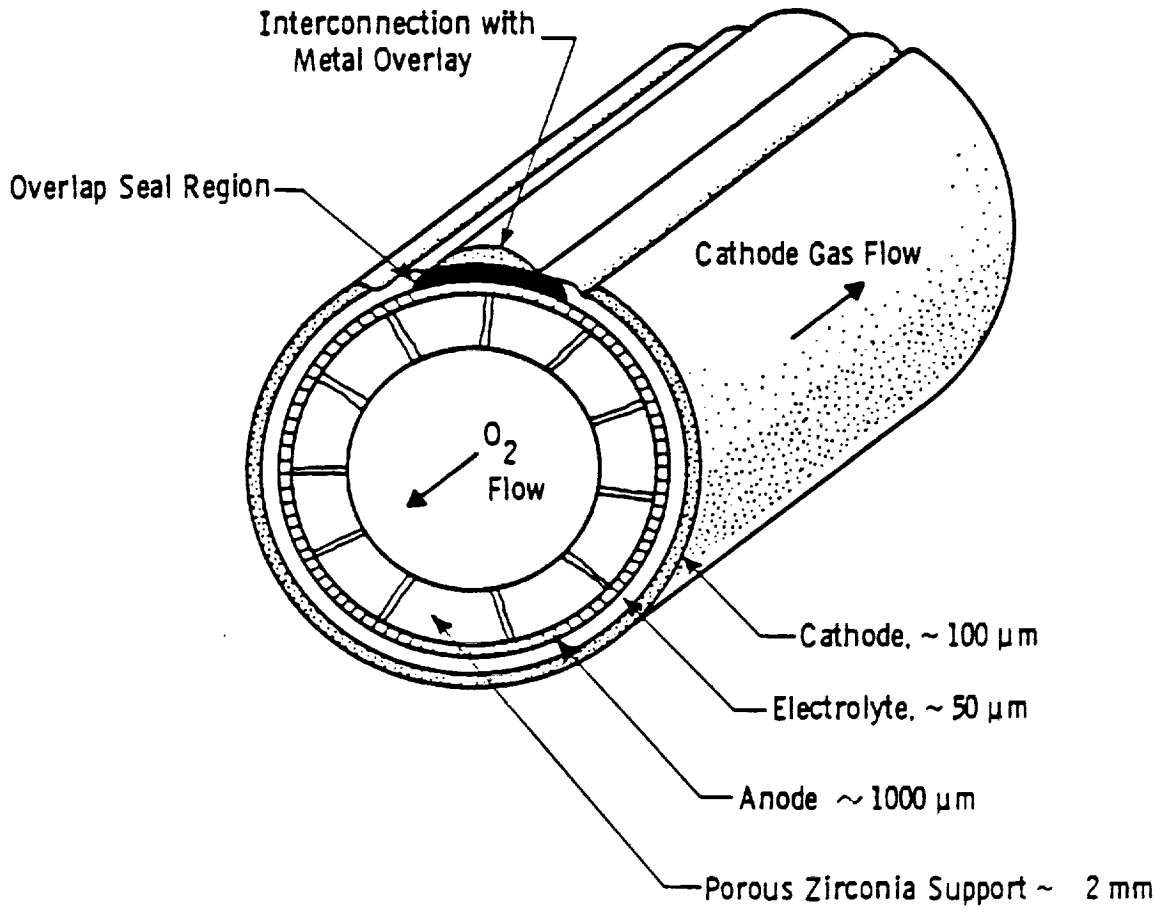

Figure 5. Schematic Section and Arrangement of Components in Cell Geometry B

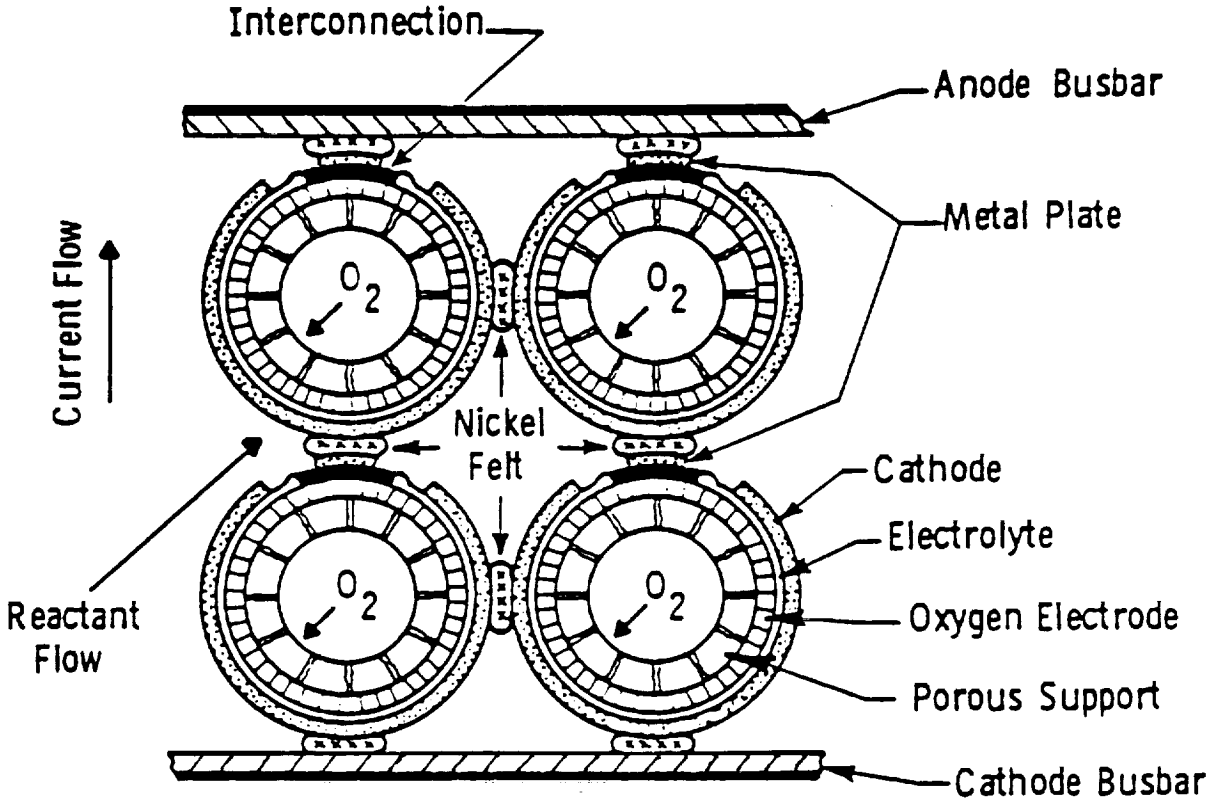

Figure 6. Schematic Arrangement of an Electrolysis Cell Tube Bundle Showing Electrical Series-Parallel Connection of Type B Cells

One of four B-type cells was fabricated as a self-supporting cell; i.e., the oxide anode was made into a support tube by extrusion to achieve a lower cell resistance. The lower resistance is achieved by doubling the oxide layer thickness from 1mm to 2mm. The self-supported cell is shown in Figure 7. It was fabricated and tested as a replacement effort for the abandoned A-type cells. The fabrication processes and sequence is identical to the regular B-type cells except that the anode tube extrusion and sintering replaces the zirconia tube and the anode deposition process.

3.2.3 C-Type Cell

This cells structure is shown in Figure 8. An attempt was made to fabricate six cells. Three were taken to completion. The fabrication sequence is identical to that of zirconia supported B-type cells. The cell geometry, however, exhibits banded interconnection rings. In three attempts, this ring-type structure produced residual stresses which led to cell fracturing after interconnection application. The failure of completing several C-type cells is related to the problems that we faced when attempting to fabricate A-type cells which also have circumferential interconnection bands. It is concluded, that undue stresses in banded cell designs are the cause of mechanical failure. It is our experience that the stress release mechanism in B-type cells is more favorable and does not lead to such failure.

3.3 Cell Test Station

A schematic of a cell test station is shown in Figure 9. Figures 10, 11, and 12 are photographs of the test station, the test assembly of a cell as arranged in the test station furnace, with the gas control and measurement equipment included. The station permits establishing all the anticipated test conditions for the CO_2 electrolysis cells, such as controlling

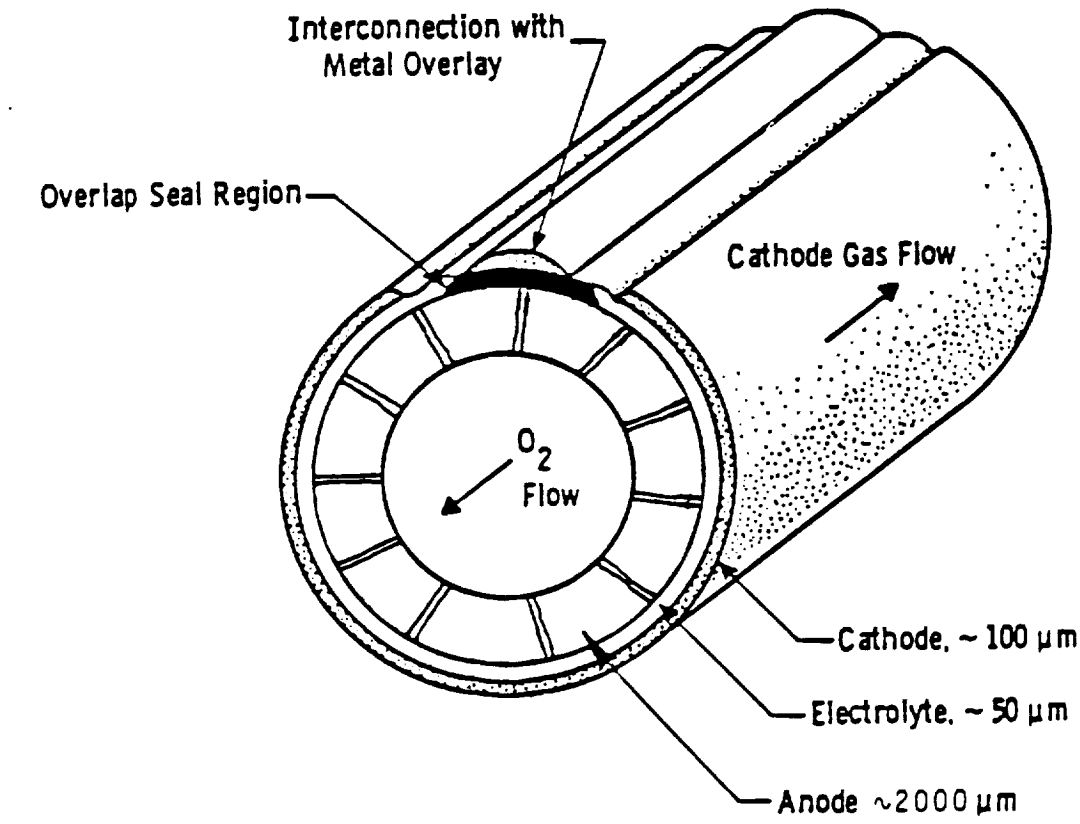

Figure 7. Schematic Section and Arrangement of Components in Cell Geometry B Using Porous Anode Support

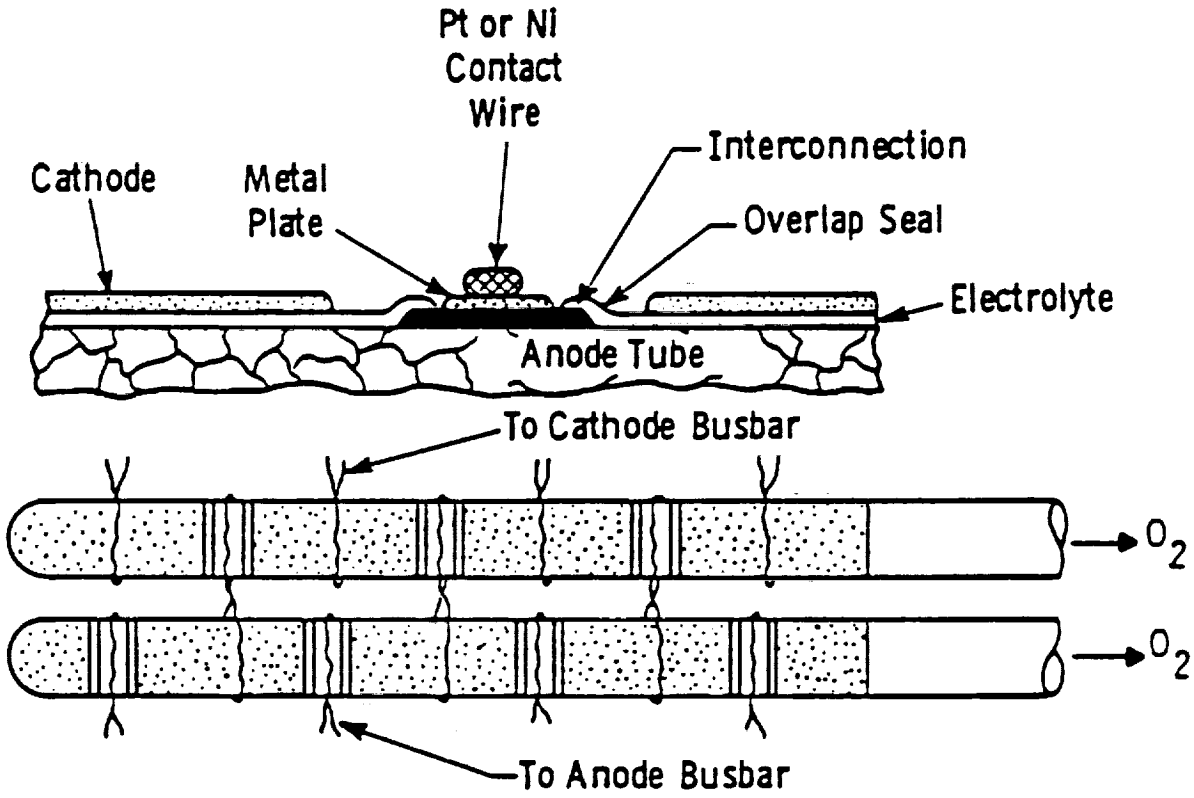

Figure 8. Schematic Section of C-type Cells and Two Cell Electrical Connections

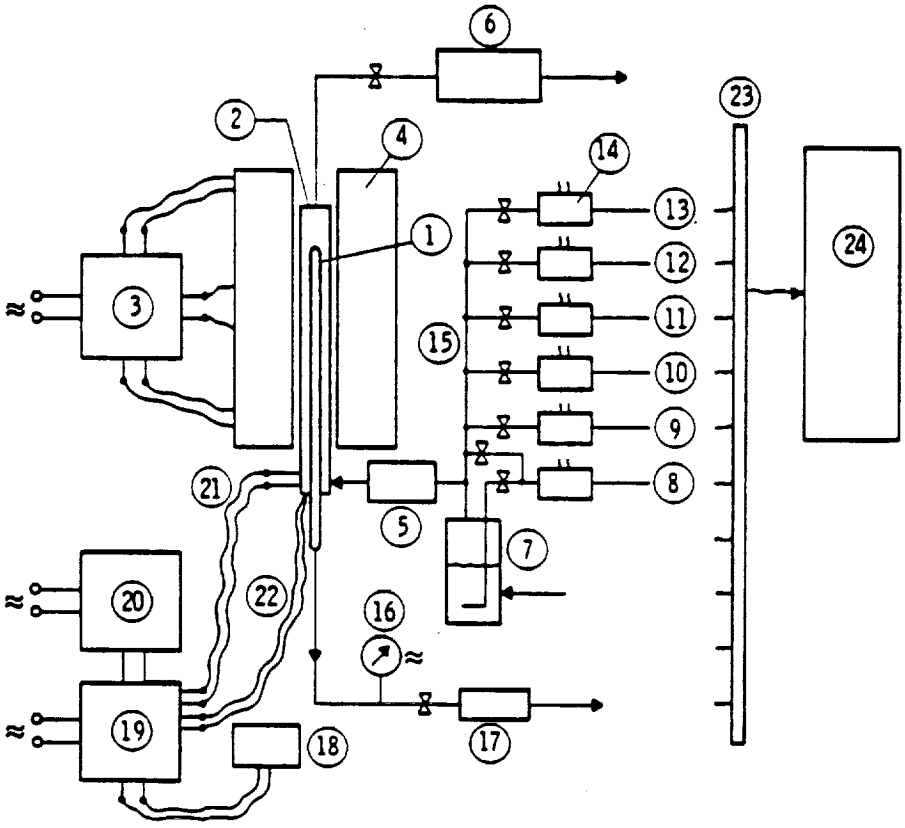

1	Cell
2	Test Envelope
3	A.C. Power Supply
4	3-Zone Test Furnace
5	Oxygen Sensor Inlet
6	Oxygen Sensor Outlet
7	Humidifier
8-13	Gas Inlets for CO_2, CO, H_2, N_2-H_2S, N_2-Freon, N_2
14	Mass Flow Controllers
15	Gas Manifold and Valves
16	Oxygen Pressure Control
17	Mass Flow Meter
18	Oscilloscope
19	Electronic Switch and Test Circuit
20	D.C. Power Supply
21	D.C. Current Line
22	D.C. Potential Line
23	Data Highway
24	Data Acquisition

Figure 9. Essential Components of a Solid Oxide Cell Test Station for CO_2 Electrolysis

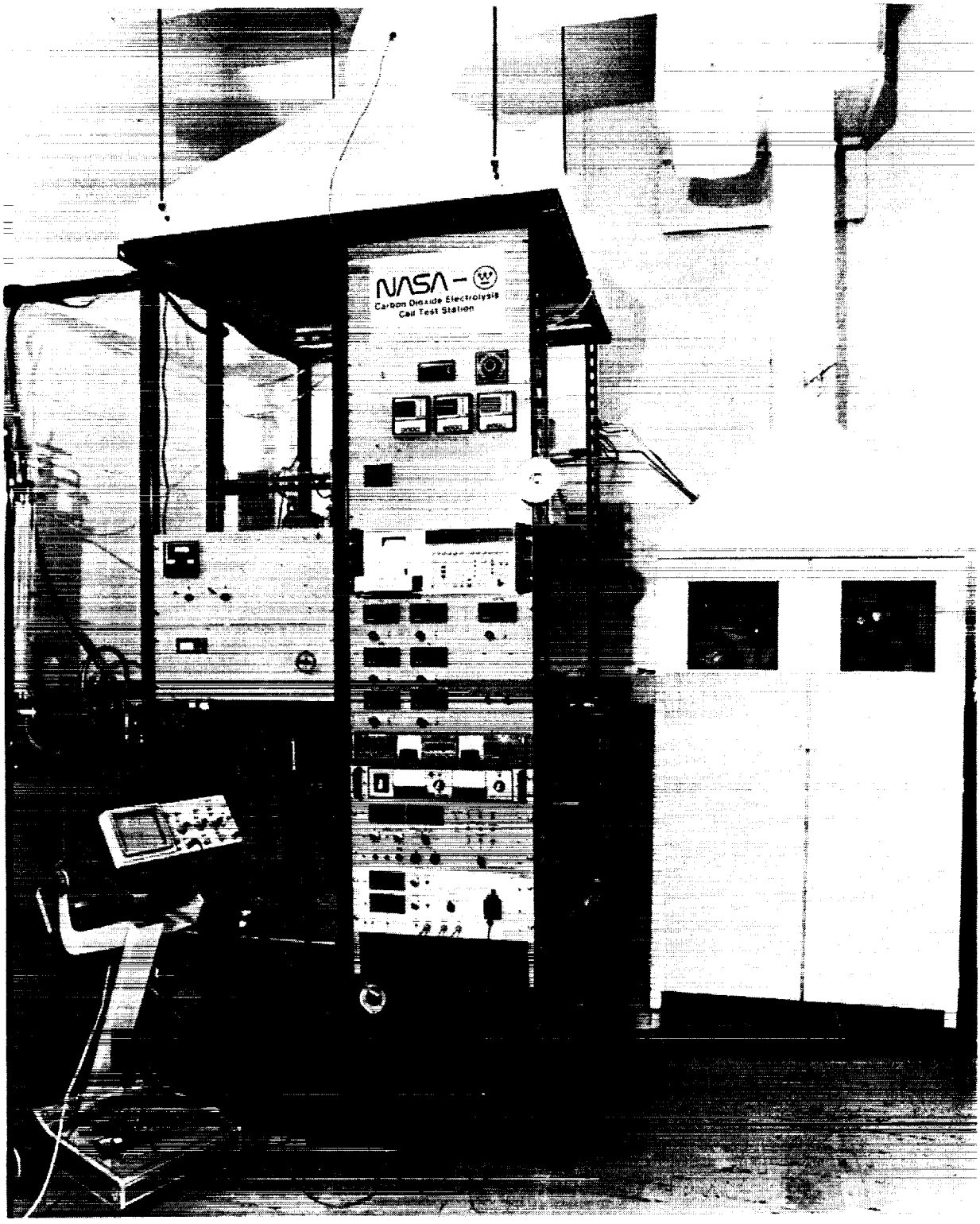

Figure 10. Front View of CO_2 - Electrolysis Cell Test Station

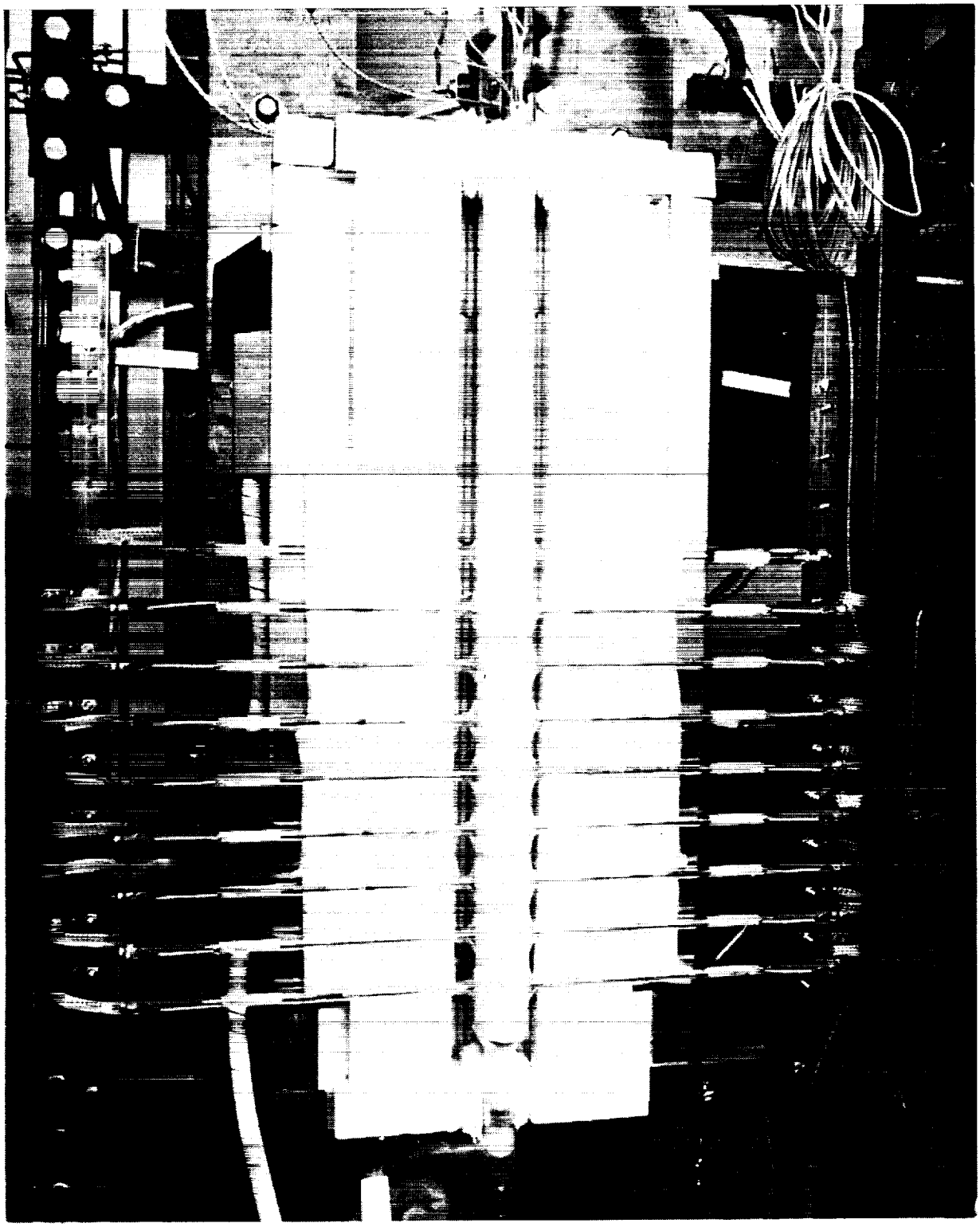

Figure 11. View of Installed Test Cell in Test Envelope as Arranged in Test Furnace and Electrically Contacted

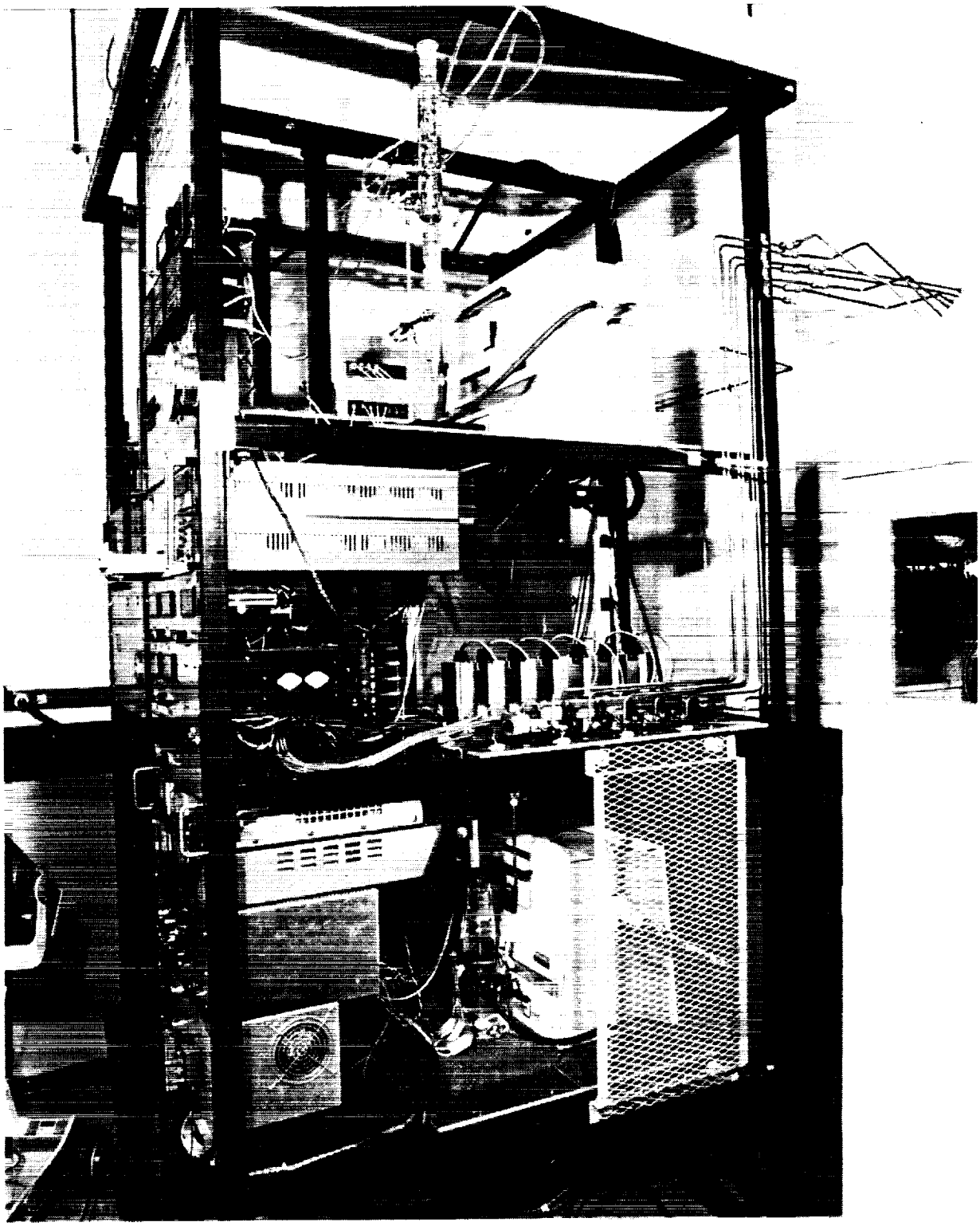

Figure 12. Side View of CO_2-Electrolysis Cell Tests Station Showing Gas Flow Control Units, Water Bubbler, Inlet and Outlet Gas Analyzers (O_2-Gauges), and Gas Manifold

and measuring gas flows of CO_2, CO, H_2, H_2O, N_2, N_2-Freon, N_2-H_2S, O_2, and allowing oxygen generation under pressure.

Cells can be tested at temperatures up to 1000°C. Power supplies, electronic loading and switching devices are installed to achieve foreseeable electrical test conditions for cells. A Fluke data acquisition unit allows periodic recording of gas flows, temperatures, pressure, and voltages. The test station is also used for the testing and qualification of cells for the three-man breadboard system. The construction of the test station did not present any difficulties.

Electrolysis feed gases are synthesized from bottled gases.

During long-term tests, exceeding 1500 hours, the test furnace, power supply, and control units performed as expected.

3.4 Cell Design Support Testing

The objective of this task was to test each cell type parametrically over a range of temperatures, gas flow rates, inlet gas compositions and current densities. The amount of oxygen and carbon monoxide produced was measured under such conditions. Investigation of cell performance at 800, 900, and 1000°C and at current densities from 150 to 300 mA/cm^2 were performed. The feed gas composition was varied within wide margins, using pure CO_2 and CO_2 + 20% H_2 as feed gas. Nitrogen was tested as an inert contaminant. An attempt was made to test each cell configuration for a minimum duration of 1000 hours. The determination of cell leakage and current conversion efficiency was established.

Further objectives were the operation of such test cells at a differential pressure of 200 psi (oxygen side pressurized) and a minimum of two rapid heat-ups from ambient temperature to 900°C.

During the course of Phase I refinements in cell test conditions had been introduced to obtain more meaningful evaluation results for potential spacecraft application. These included additional testing of more realistic cathode gas conditions, which are expected to exist when a CO_2-electrolysis module is integrated with a carbon deposition reactor. In

such an instance, feed gas compositions are not the ones which come from the CO_2-concentrator systems but contain considerable amounts of CO, H_2, H_2O, and CO_2 in a recycle loop. Approximate feed gas compositions were determined on the basis of a previous NASA study.[1] Tests with Freon 23 and with H_2S as contaminants were not performed because of predictable damage to the nickel cermet cathodes and because technology exists which can minimize the presence of these contaminants reliably from cathode feed gases before entering the system loop. Nitrogen, however, is a predictable contaminant in a system loop and was included in the test matrix.

3.4.1 B-Type Cell, Test Cell No. 1

The first B-type cell was equipped with a nickel-zirconia cermet cathode and was mounted in a quartz test envelope and installed in the cell test station. This B-type cell was used to check out (shake-down) the test station and to answer two critical questions for future cell testing, and cell construction.

- Can the inactive ceramic cell tube extension withstand an axial thermal gradient of nearly 900°C over a 13 cm (~5") length?
- What maximum internal cell pressure can the cell maintain at the design operational temperature of 900°C?

Further information was gained on electrical cell contacting with nickel metal. The location of thermocouples for temperature measurements were determined and carbon deposition on contact rods were evaluated for the first time. Some deposition of carbon on colder portions of nickel contacts was observed but was expected according to equation 8. It was estimated that this would not lead to mechanical failure of the quartz test envelope. This concern can be explained through Figure 13, which schematically depicts the test cell in the test envelope. Since the nickel contact rods are exposed to temperatures as high as 900°C (cell side) and as low as room temperature (bus bar side), carbon deposition on nickel in

the 500 to 700°C temperature zone, can be expected from carbon monoxide when it diffuses into the side arms of the quartz test envelope. The carbon deposit will grow in thickness as long as carbon monoxide is available. Over extended test periods this leads to the fracture of the side arms. The use of non-catalytic copper for contact rods was avoided because of its high heat conduction. Figure 13 also shows the axial temperature range of the test envelope. The concentric ceramic housing within the quartz test envelope, is made of alumina. This solid alumina tube accomplished the functions of protecting the quartz envelope from breaking which may be caused by cell rupture when it is pressurized internally. The alumina tube also protects the cell from chemical interaction with gaseous silicon compounds which are formed at high temperature in the presence of hydrogen, carbon monoxide, carbon dioxide, and water vapor.

The cell was tested for 137 hours. The test conditions were the following:

Temperature:	908°C average
Gas Feed:	80% CO_2, 20% H_2 300 ml/min CO_2 75 ml/min H_2
Cell Voltage:	1.38 - 1.39 V
Current Density:	250 mA/cm^2
Oxygen Flow:	87.5 ml/min
Current Efficiency:	100%
CO_2 Impurity in Oxygen:	35 ppm

The initial cell resistance was higher than anticipated (0.75 Ω cm^2 vs. 0.5 - 0.6 Ω cm^2), which appears to be due to an irregularity in the deposition process for electrolyte.

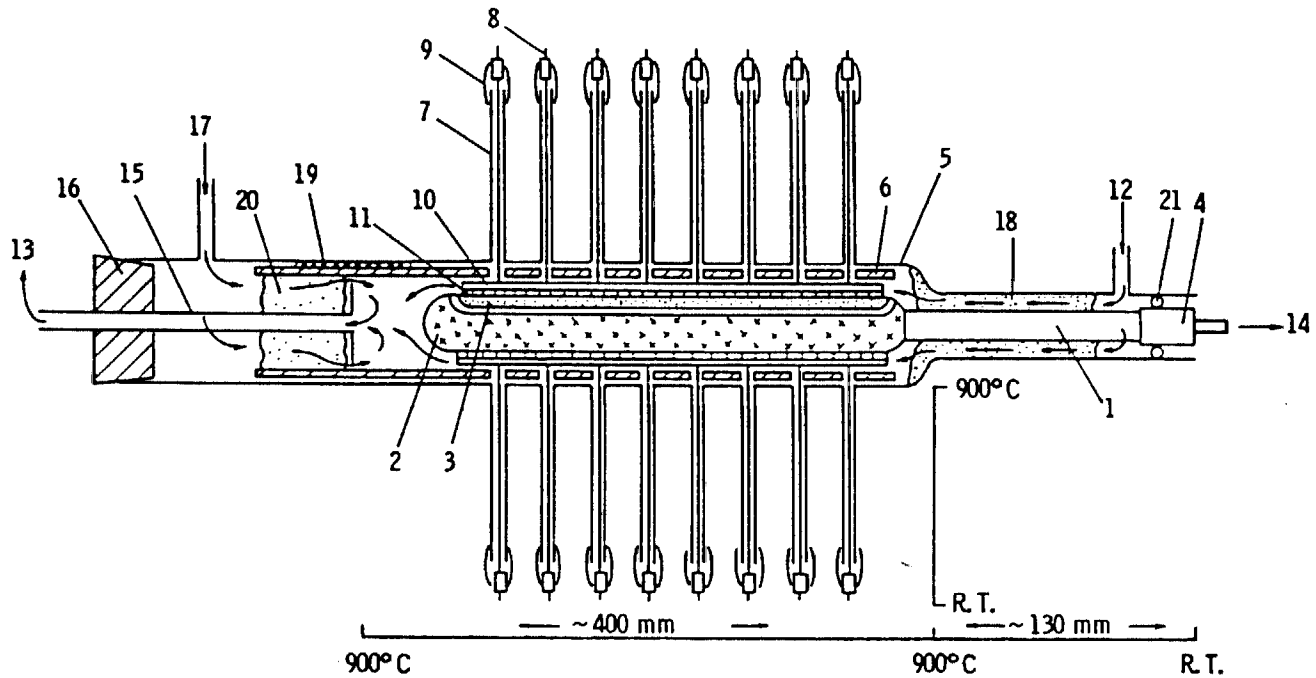

1. Cell Tube, Inactive End Reaching Into Cold Zone
2. Cathode Layer - Negative Electrode
3. Interconnection - Contact to Anode
4. Metal Cell Adapter for O_2 - Manifolding
5. Quartz Outer Test Envelope
6. Aluminia Tube Insert for Cell Protection
7. Side Arm of Quartz Test Envelope
8. Nickel Contact Rod to Cell and to Cold Bus Bar (Not Shown)
9. Silicon Rubber Sleeve for Contact Rod Seal to Test Envelope
10. Nickel Bus Bar Contact to Nickel Felt on Anode and Cathode
11. Nickel Felt Contact to Anode and Cathode
12. Carbon Dioxide Rich Gas Inlet
13. Carbon Monoxide Rich Outlet to Carbon Deposition Reactor
14. Oxygen Outlet
15. Reaction Product Duct (Quartz Tube)
16. Silicon Rubber Seal
17. Nitrogen Inlet
18. Alumina Wool for Thermal Shock Protection of Cell Tube
19. Alumina Wool (Partially Shown) Surrounding Alumina Insert 6
20. Alumina Wool as Diffusion Barrier and Radiation Shield
21. Silicon Rubber O-Ring

Figure 13. Cross Section of Test Envelope for Electrolysis Cells

At the last day of testing, the cell interior was pressurized to determine the high temperature pressure capability of the cell. For this purpose the oxygen pressure was raised in 5 psi intervals until cell rupture occurred, which happened at 30 psi. This burst pressure is much lower than expected. Anticipated differential pressure figures were not based on actual cell tests but rather on extrapolated values obtained from burst tests on porous support tubes at room temperature, which are as high as 7000 psi. A room temperature burst strength of 870 psi is calculated for a 2 mm wall support tube. A factor of four was assumed in calculating the loss of strength at 900°C versus room temperature. The fractured porous support tube did not show separation of actual cell layers, therefore it is believed that the porous cell support tube contained flaws which were responsible for the failure at a relatively low pressure. The alumina tube which surrounded the test cell prevented damage to the quartz test envelope as it was intended.

Upon disassembly of the cell it was observed that a significant deposition of carbon had occurred on nickel contact rods downstream, where the carbon monoxide concentration was the highest. Of the eight pair of contact rods, four pair were affected. The degree of carbon deposition was significant; therefore plating of the nickel rods with non-catalytic copper was used for the following test cells. The problem of carbon deposition on electrical contact rods is only of concern for single test cells. It will not affect the breadboard cell stack, where the colder parts of contacts are located within the inlet gas stream and where carbon deposition will not occur.

The conclusions from this first cell test were that the state-of-the-art CO_2 electrolysis cells cannot withstand high differential pressures when pressurized on the inside and should not be operated at conditions of more than 20 psia. Also, the contact rods for test cells must be plated with copper in temperature zones between 500 to 900°C to avoid carbon deposition.

3.4.2 B-Type Cell, Test No. 2

This cell was considered a candidate for endurance testing. However, before initiation of this test, the cell underwent extensive parametric tests in order to establish test conditions for subsequent test cells. To establish these conditions it was assumed that in a future total oxygen recovery system reasonable constancy of feed gas composition for the carbon deposition reactor is expected because oxygen consumption in a space environment varies little. This means that electrolysis exit gas compositions are expected to be constant. Therefore, cells were operated at "constant degrees of decomposition" (DD) which is given by the mole fraction of combined hydrogen and carbon monoxide in the cathode exit gas. The DD value is a measure of the conversion of CO_2 and H_2O to CO and H_2.

$$DD = \frac{\text{exit CO + exit } H_2}{\text{total exit gas - exit } N_2}$$

Under such test conditions the gas flows are varied widely, corresponding to the cell current. This current is varied with oxygen demand.

Test cell No. 2 was used to establish sensitivity of performance to nitrogen contamination and moist/dry feed gas composition. Figures 14 through 26 summarize all test conditions. Figures 14, 15 and 16 show the cell performance at three different temperatures and its dependence on three different DD values to recycle feed gas. Figures 17, 18 and 19 are obtained with carbon dioxide-hydrogen feed gases at varying DD values for three temperatures. All figures show also the theoretical line for oxygen delivery according to Faraday's Law and the actual measured values. Figures 20, 21 and 22 show cell behavior under dry and humidified CO_2 feed gas conditions. Figure 23 relates to Figure 21 in that it indicates the effect of the addition of 10% nitrogen to the cathode feed gas. Figures 24 and 25 summarize the most important data for test cell No. 2 for recycle gas, dry CO_2, and CO_2 containing 20% H_2.

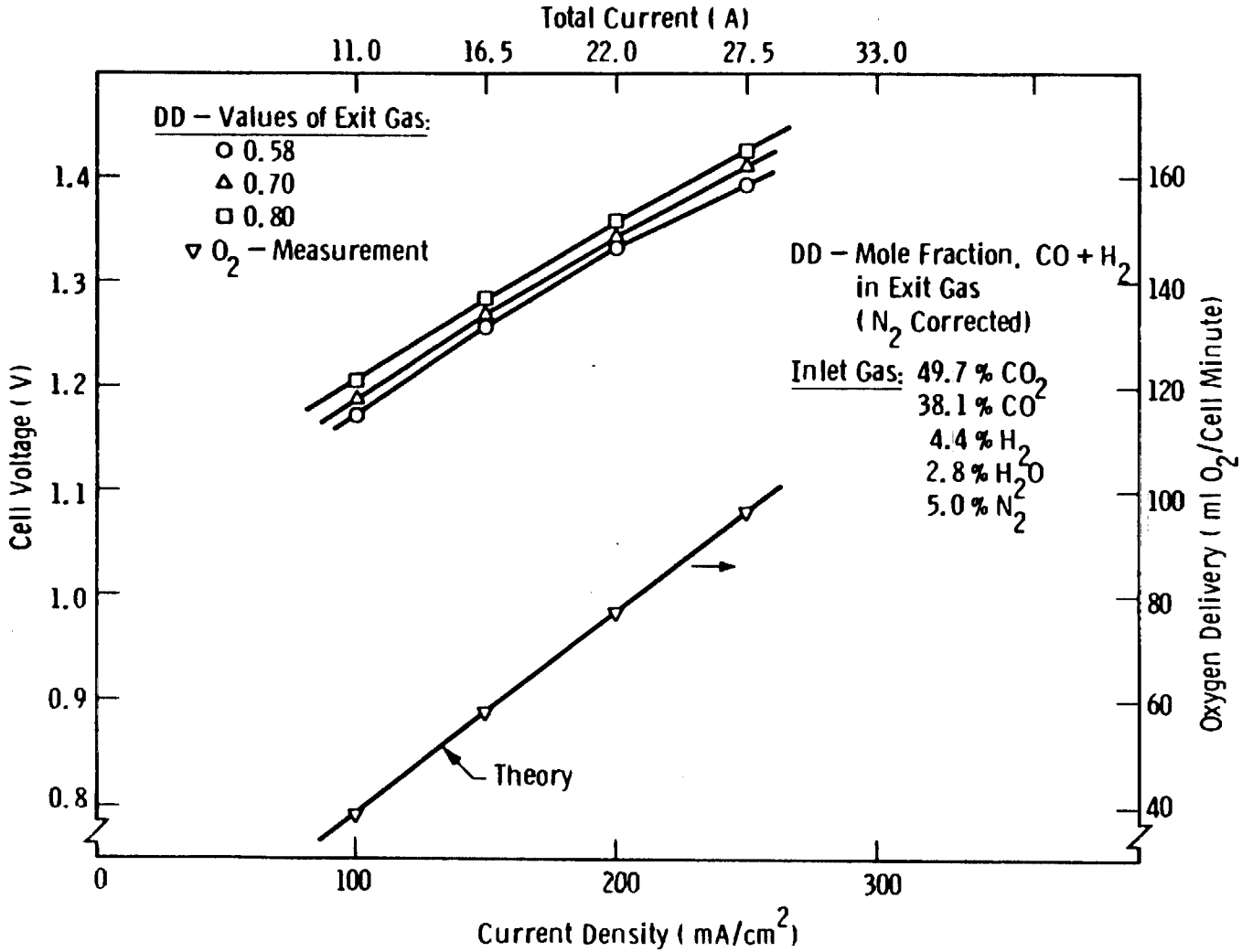

Figure 14. Electrolysis Cell Characteristics at 800°C For Three Constant Degrees of Decomposition (DD) of Carbon Deposition Reactor Recycle Feed Gas Cell Type B Cell No. 2

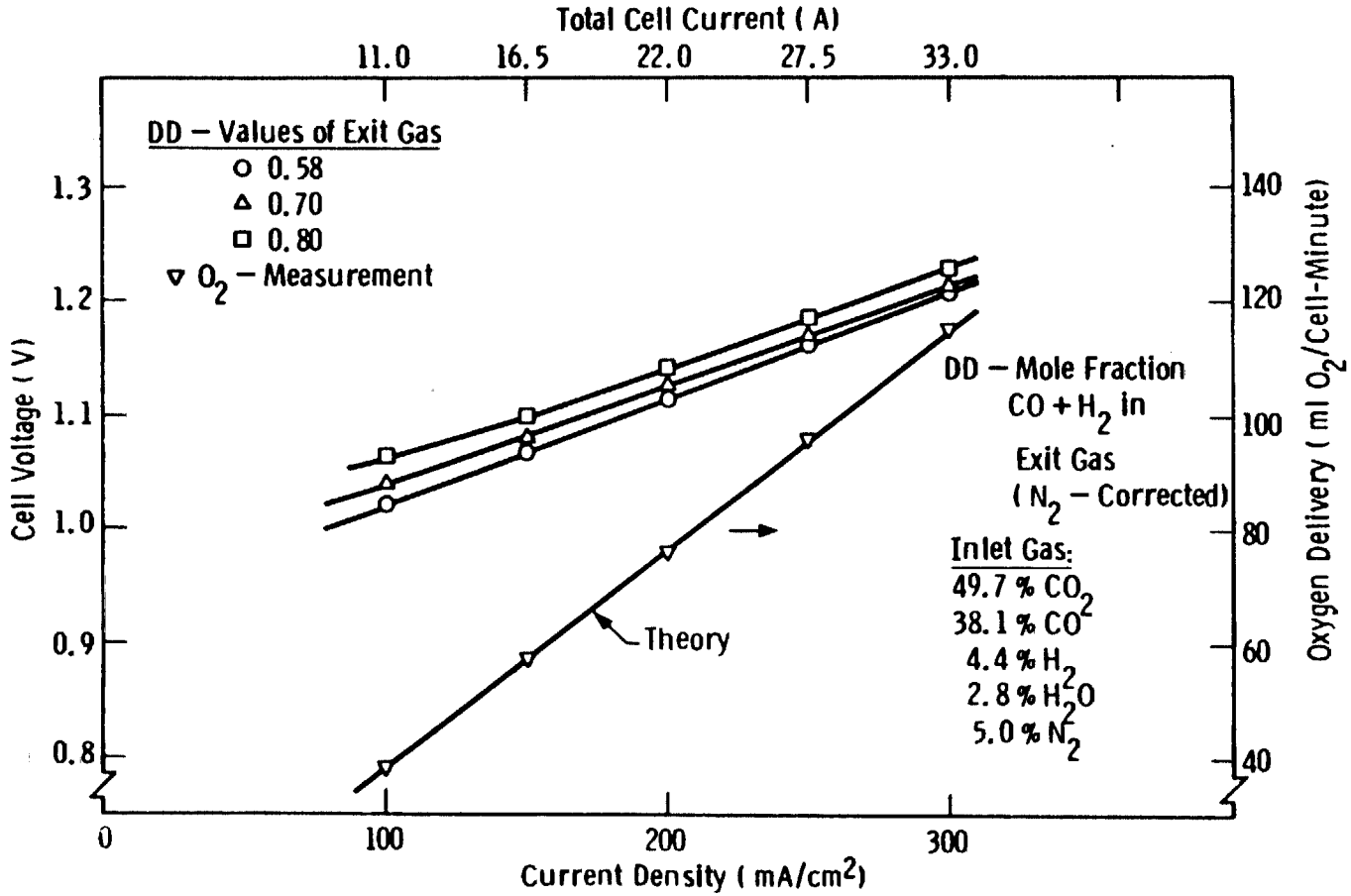

Figure 15. Electrolysis Cell Characteristics at 900°C For Three Constant Degrees of Decomposition (DD) of Carbon Deposition Reactor Recycle Feed Gas Cell Type B Cell No. 2

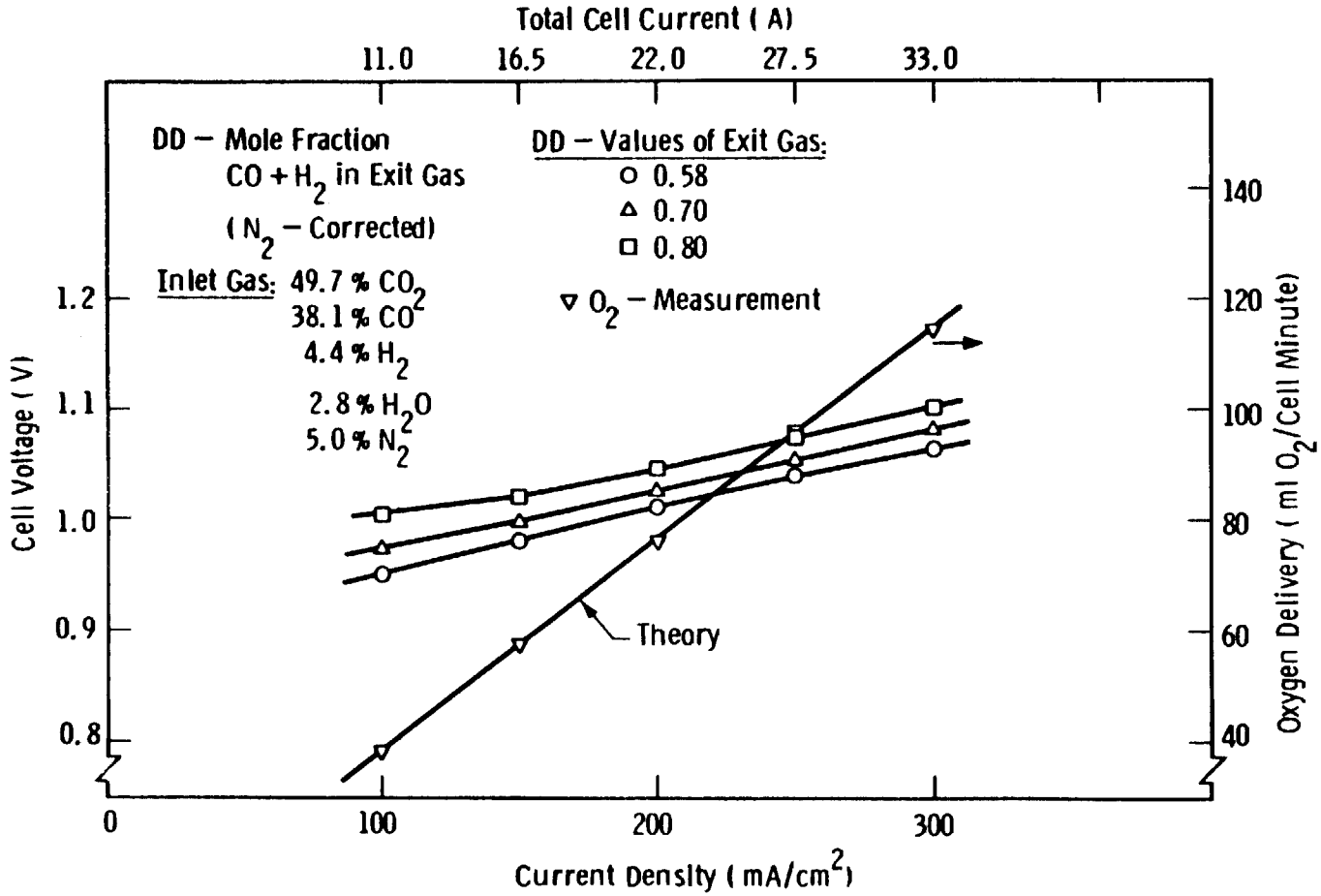

Figure 16. Electrolysis Cell Characteristics at 1000°C For Three Constant Degrees of Decomposition (DD) of Carbon Deposition Reactor Recycle Feed Gas Cell Type B Cell No. 2

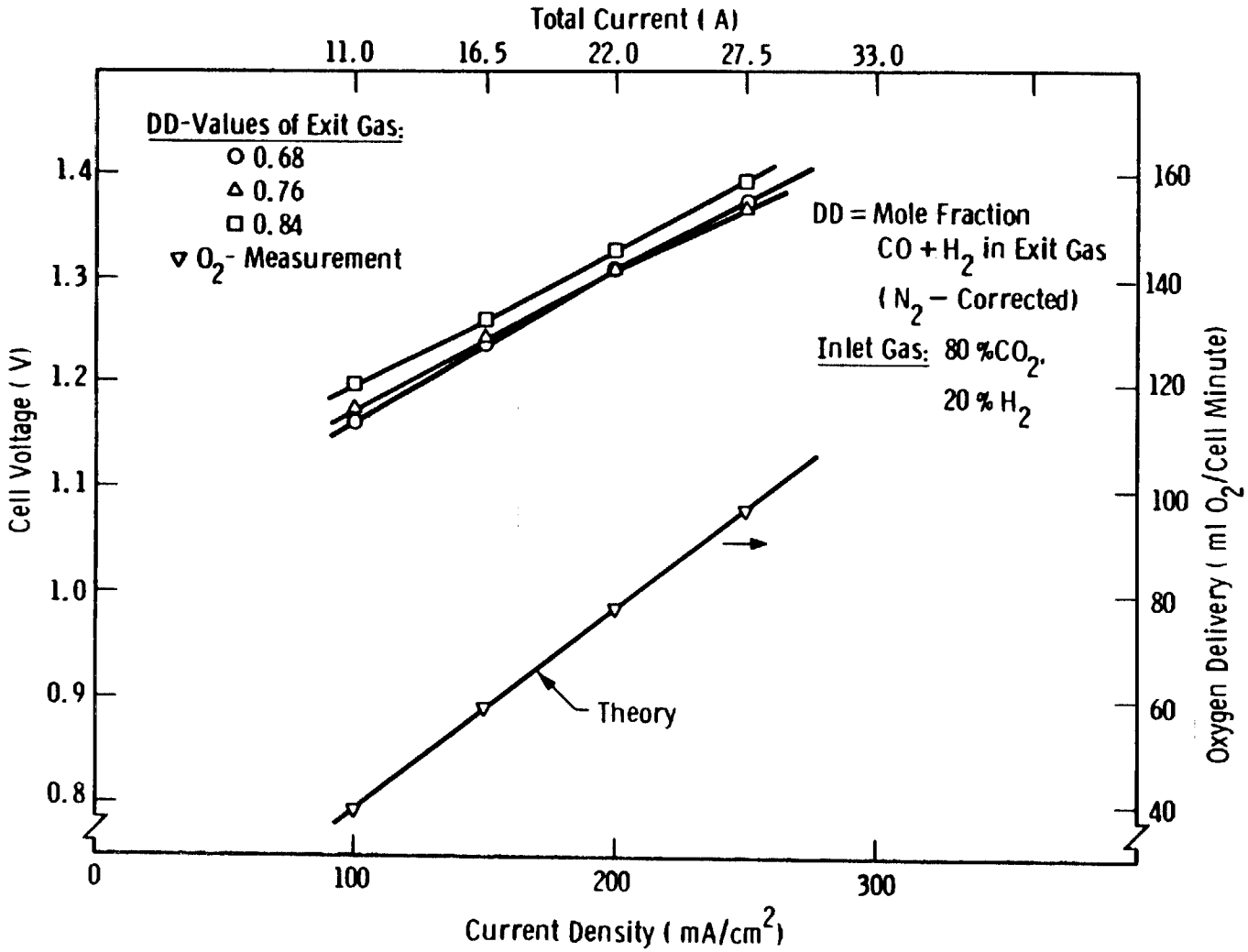

Figure 17. Electrolysis Cell Characteristics at 800°C For Three Constant Degrees of Decomposition (DD) of Carbon Deposition Reactor Recycle Feed Gas Cell Type B Cell No. 2

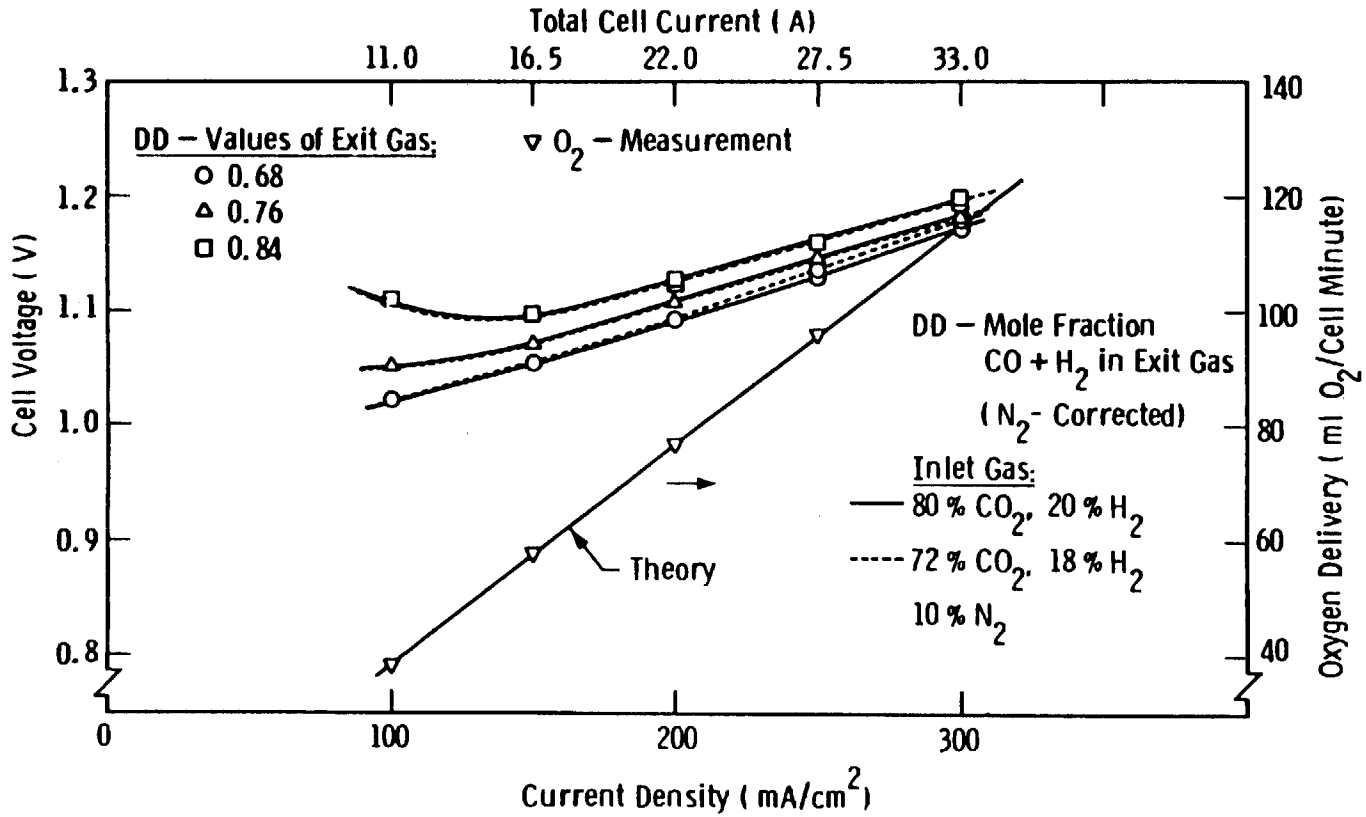

Figure 18. Electrolysis Cell Characteristics at 900°C For Three Constant Degrees of Decomposition (DD) of Carbon Dioxide - Hydrogen - Nitrogen Inlet Gas, Cell Type B, Cell No 2

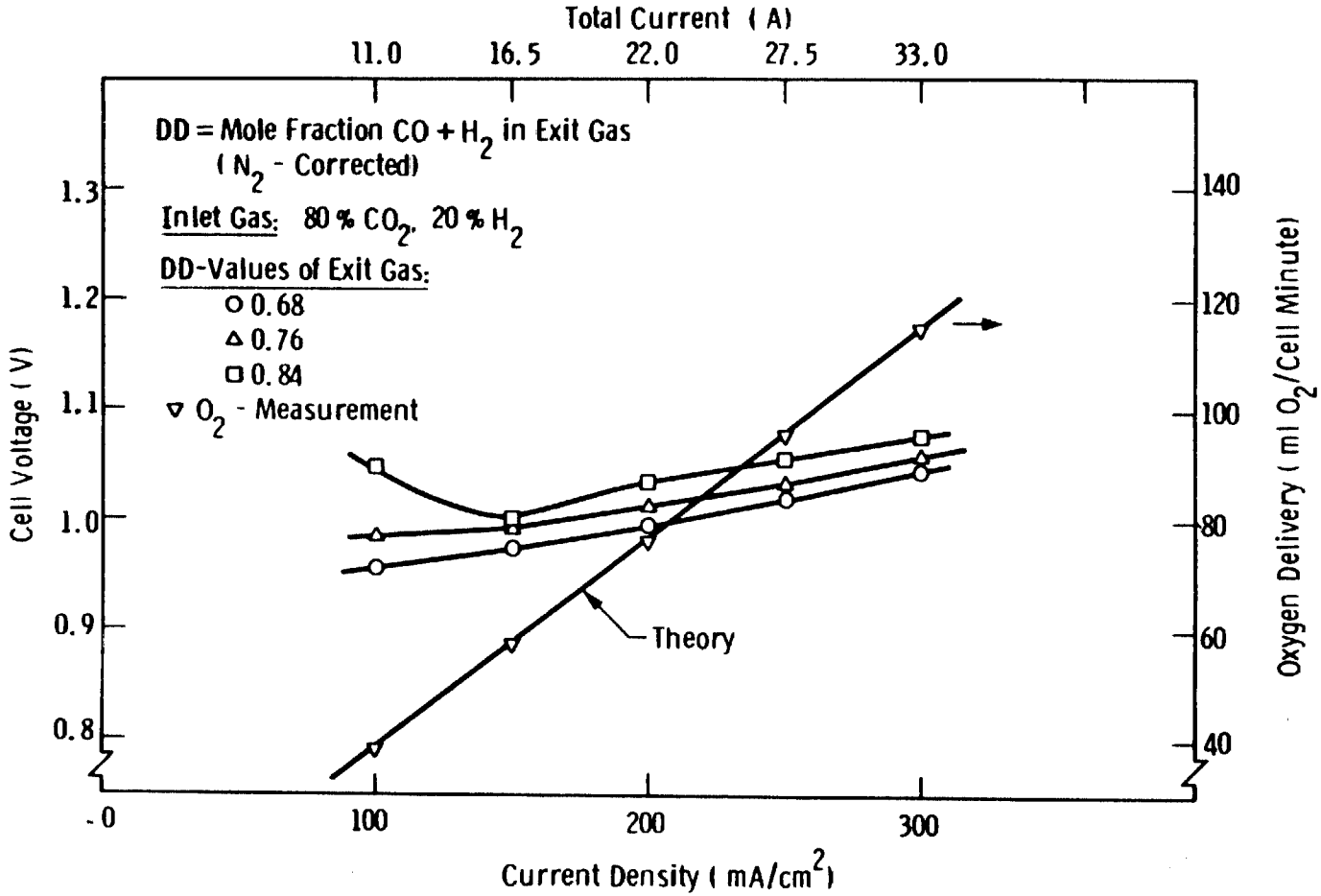

Figure 19. Electrolysis Cell Characteristics at 1000°C For Three Constant Degrees of Decomposition (DD) of Carbon Dioxide - Hydrogen Inlet Gas, Cell Type B, Cell No. 2

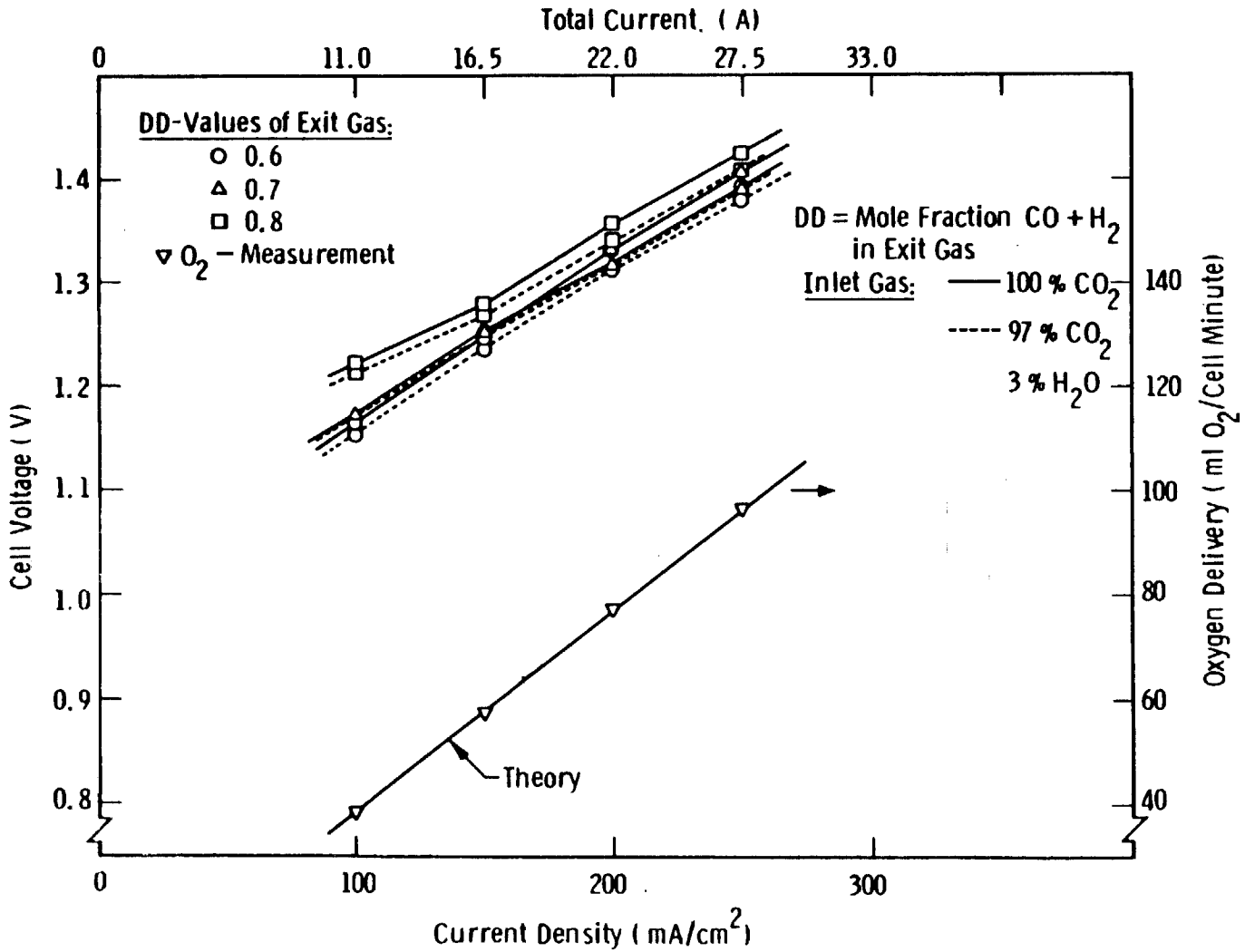

Figure 20. Electrolysis Cell Characteristics at 800°C For Three Constant Degrees of Decomposition (DD) of Carbon Dioxide - Water Vapor Inlet Gas, Cell Type B, Cell No 2

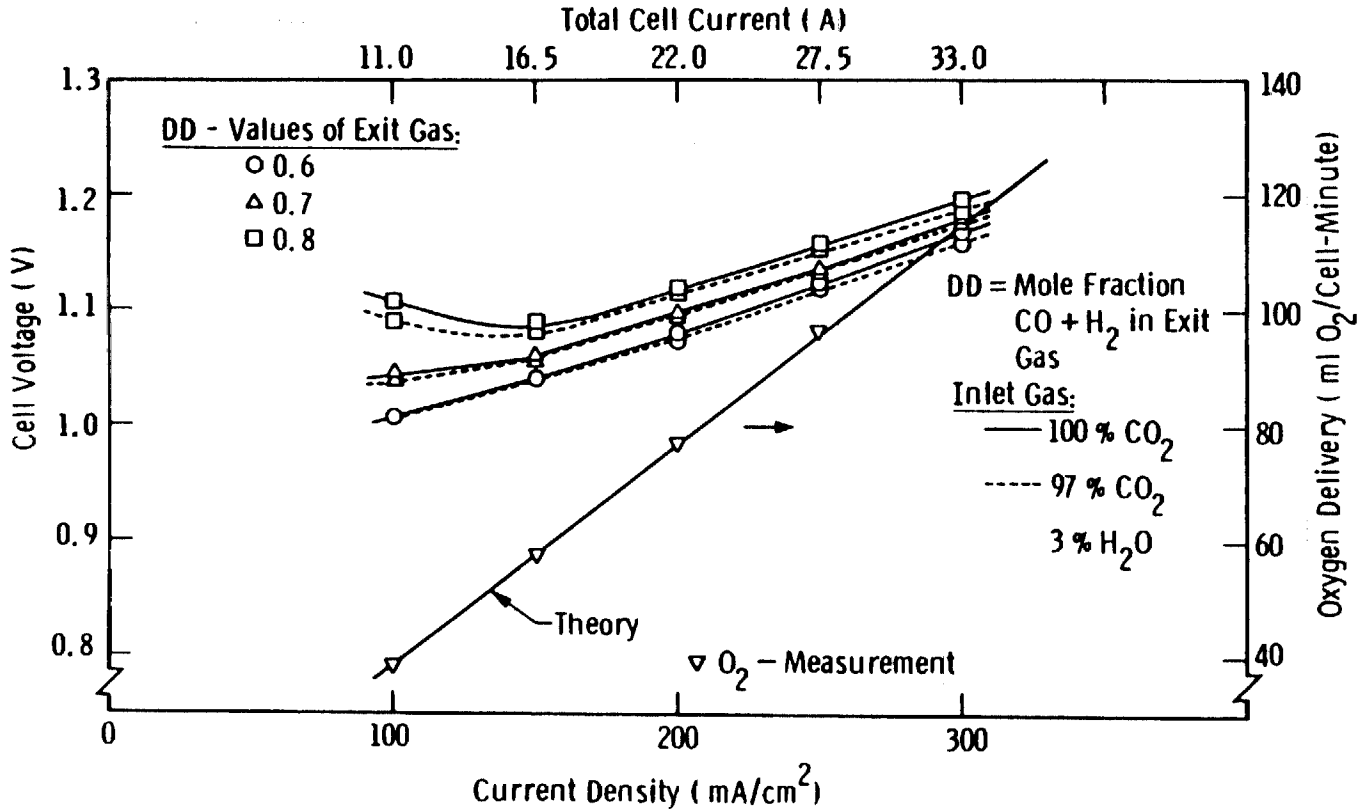

Figure 21. Electrolysis Cell Characteristics at 900°C For Three Constant Degrees of Decomposition (DD) of Carbon Dioxide - Water Vapor Inlet Gas, Cell Type B, Cell No. 2

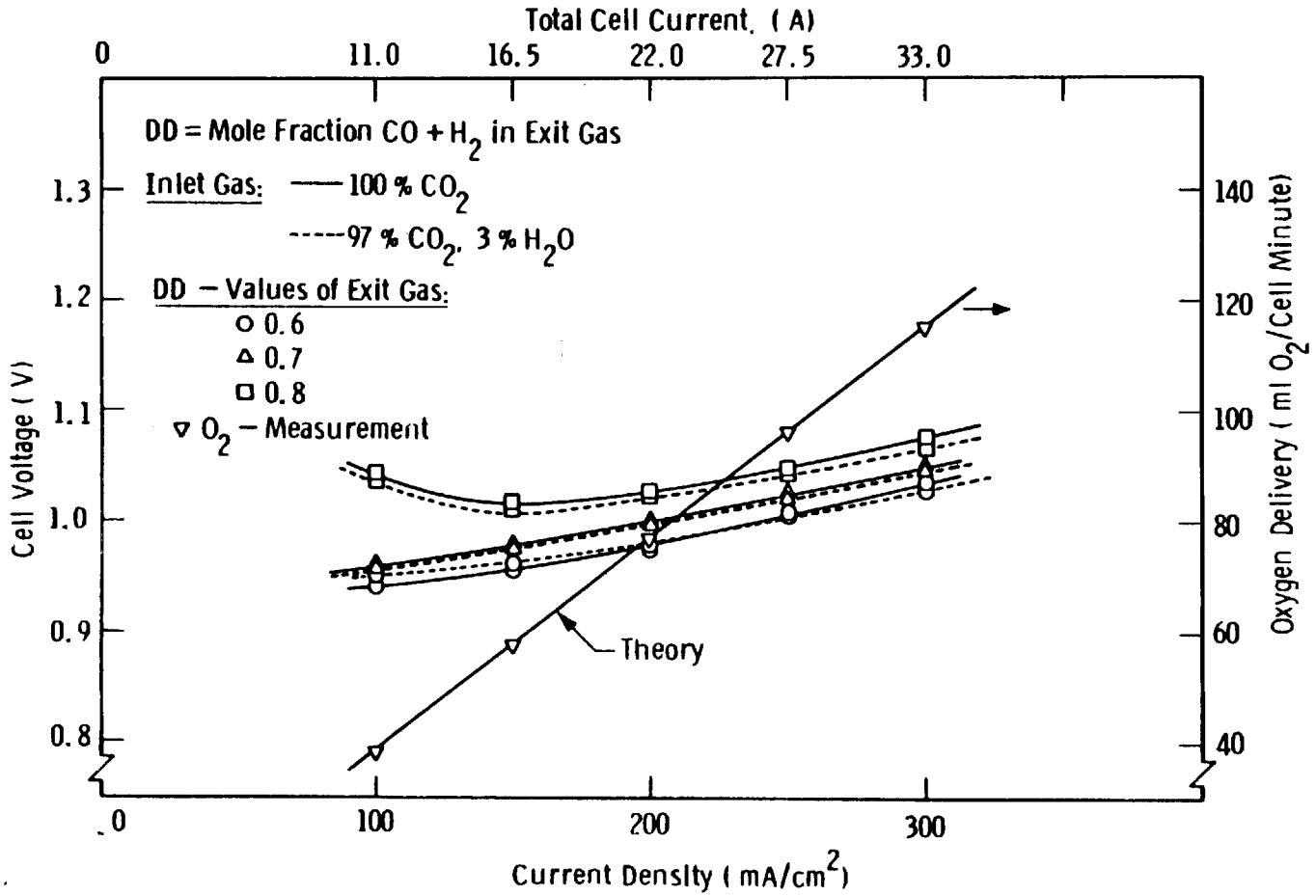

Figure 22. Electrolysis Cell Characteristics at 1000°C For Three Constant Degrees of Decomposition (DD) of Carbon Dioxide - Water Vapor Inlet Gas, Cell Type B, Cell No. 2

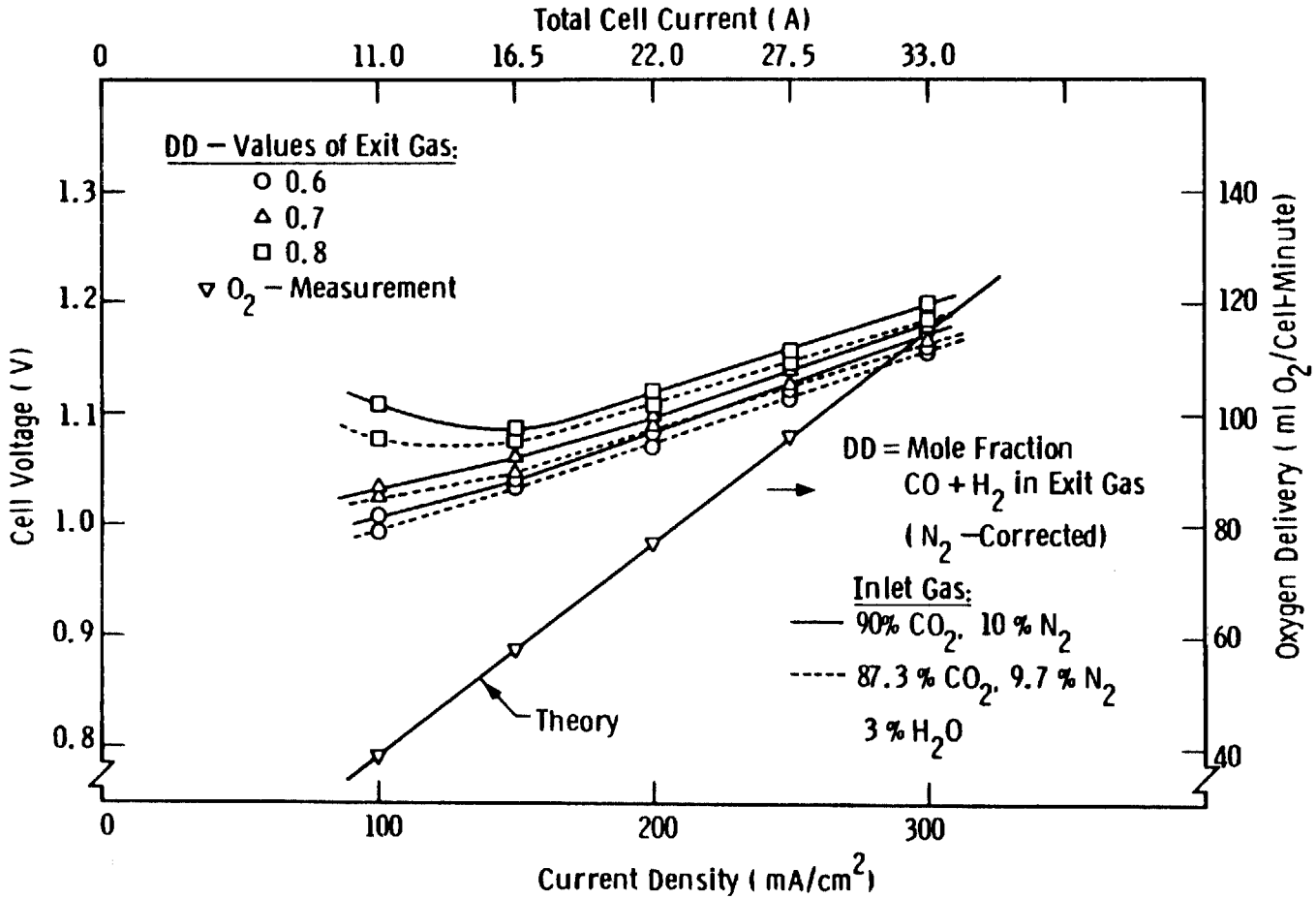

Figure 23. Electrolysis Cell Characteristics at 900°C For Three Constant Degrees of Decomposition (DD) of Carbon Dioxide - Nitrogen Inlet Gas, Cell Type B, Cell No. 2

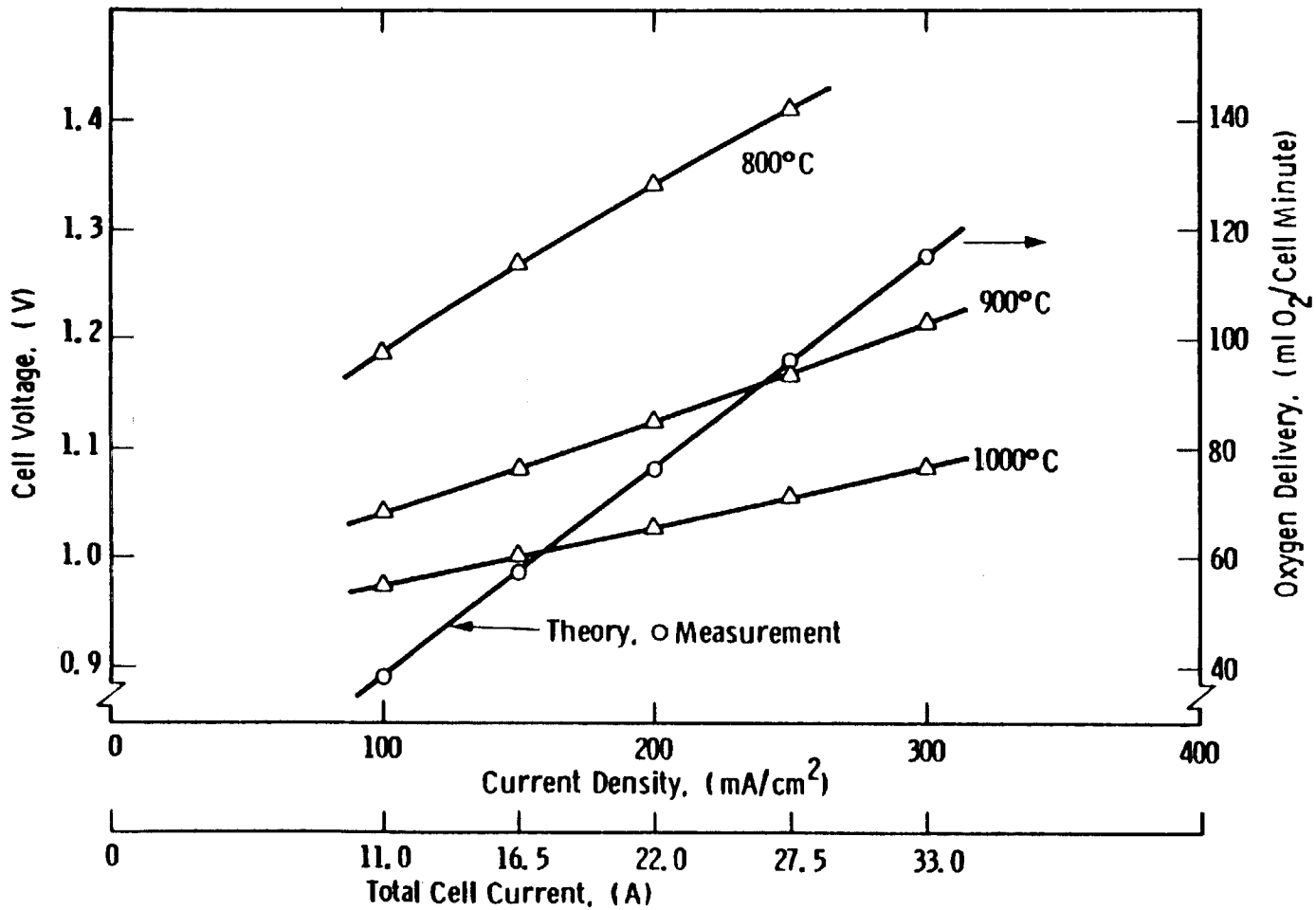

Figure 24. Electrolysis Cell Characteristics at Three Temperatures; Carbon Deposition Reactor Recycle Feed Gas. DD = 0.70, Cell Type B, Cell No. 2

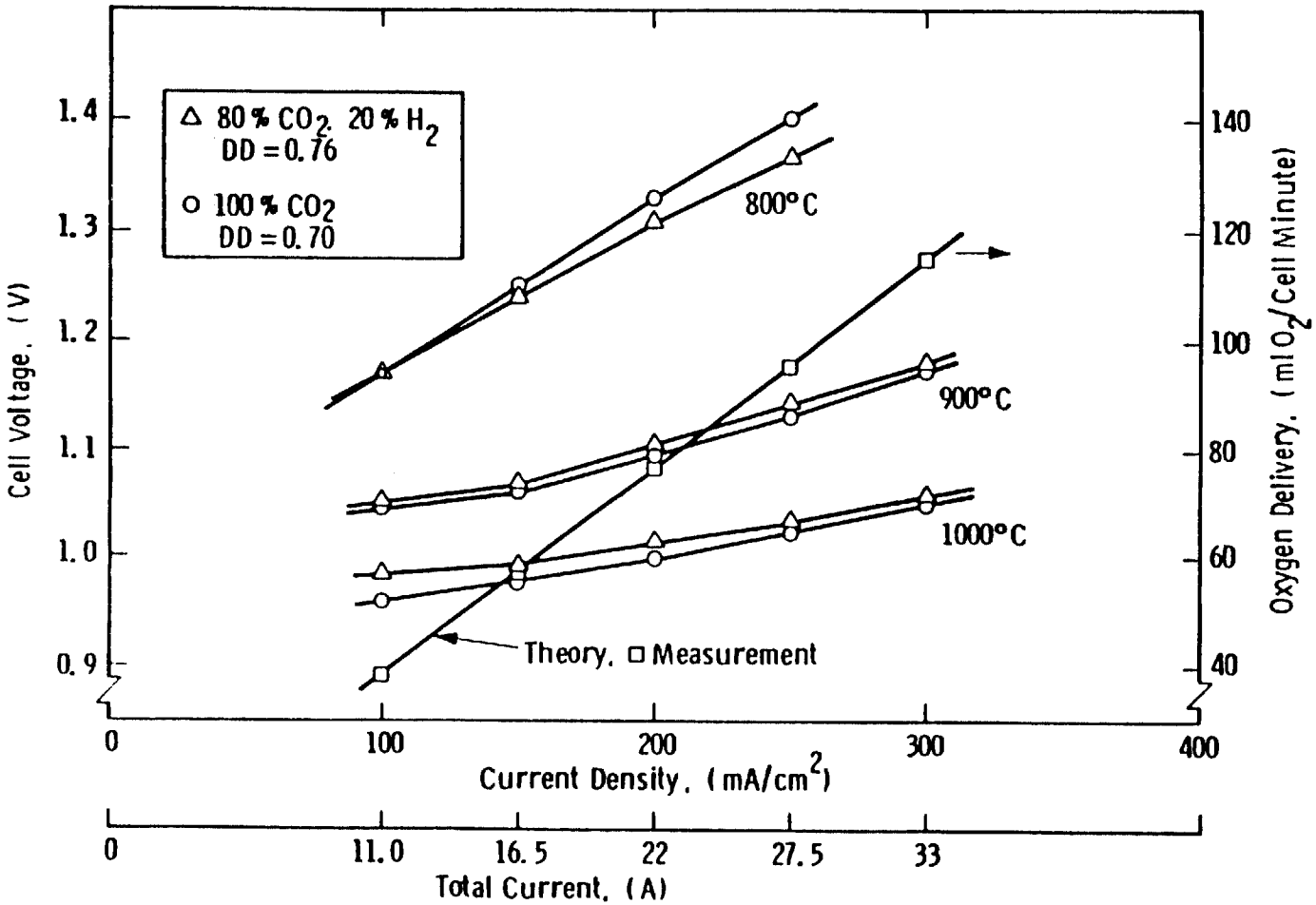

Figure 25. Electrolysis Cell Characteristics At Three Temperatures; Carbon Dioxide Concentrator-Type Feed Gas, Cell Type B, Cell No. 2

3.4.3 Endurance Test of Test Cell No. 2

Figure 26 shows the life performance of this cell. During 1100 hours of operation the electrolysis voltage increased by nearly 4%, which is assumed to be due to the increase in cell resistance which is caused by a minor loss of electrode contact. Throughout cell life the current efficiency was 100%. The CO_2 content in the oxygen was 70 ppm at the beginning of the test and rose to 360 ppm during the course of the test. This indicates the presence of a minor leak from the anode side of the electrolysis cell into the cathode side. There is no danger of CO-poisoning of breathing gas to a crew, because carbon monoxide is oxidized reliably to CO_2, which can be removed by the CO_2-removal system.

The conclusions of these tests are that the numerous test data on the cell performance between 800 and 1000°C and for most cathode gas composition and degrees of decomposition can be extrapolated. The formation of oxygen is, within experimental error, and 100% efficient.

For the endurance testing of cells, a temperature of 900°C was selected and an inlet gas composition of CO_2 + 20% H_2 contaminated with 10% N_2 was chosen. Similar conditions are recommended for the operation of a breadboard module.

3.4.4 B-Type Cell (Self Supported), Test Cell No. 5

A self-supported B-type cell was fabricated in an attempt to reduce cell resistance by using a lower resistance oxide anode tube which simultaneously serves as cell support (see 2.3.2). The anode (tube wall) of this cell is 2 mm thick as compared to 1 mm in the zirconia tube supported standard B-type cell. The chosen cathode was a cobalt-zirconia cermet electrode, identical in structure to nickel-zirconia and using the same processing parameters.

Cell characteristics are shown in Figures 27 and 28. The two feed gas compositions that are most meaningful for breadboard operation,

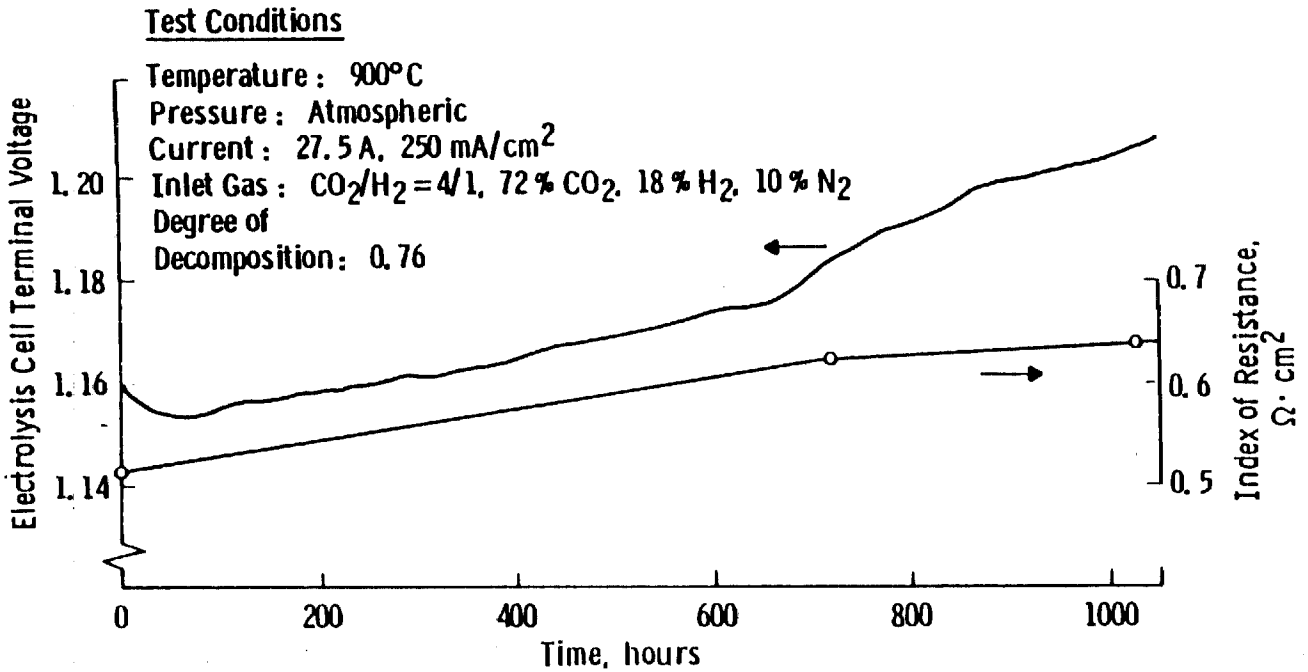

Figure 26. Life Performance Characteristics of Carbon Dioxide Electrolysis Cell B-Type Cell No. 2

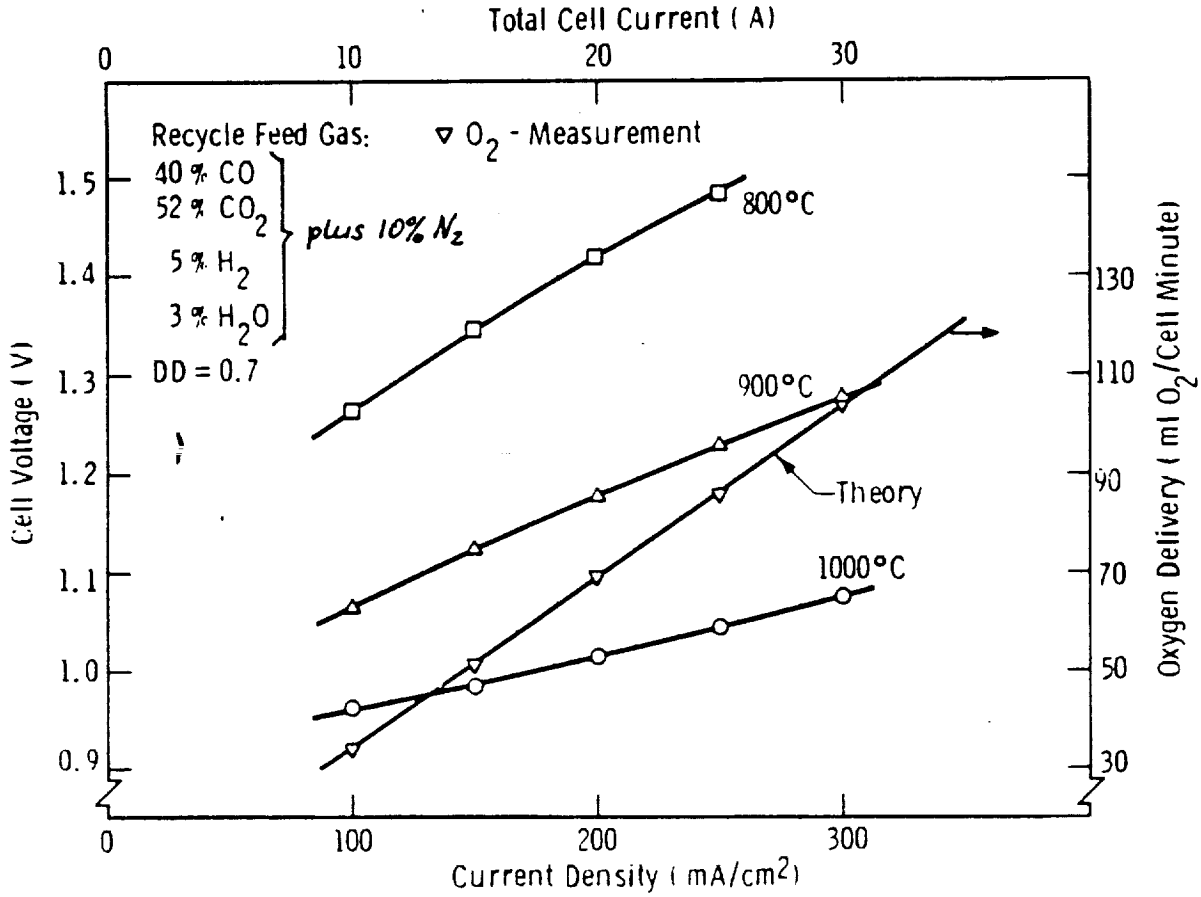

Figure 27. Temperature Dependence of Electrolysis Cell Performance Self Supporting Cell Type B, Test Cell No. 5

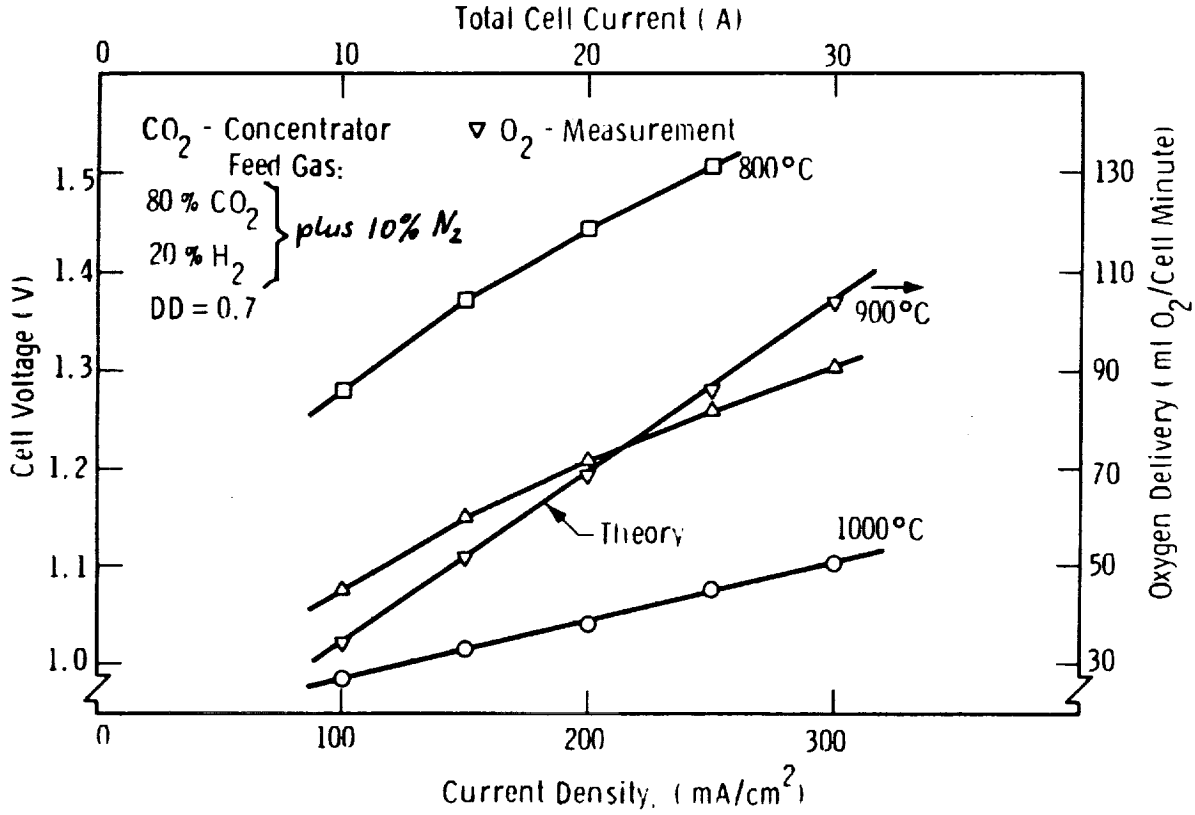

Figure 28. Temperature Dependence of Electrolysis Cell Performance Self Supporting Cell Type B, Test Cell No. 5

namely, recycle gas and CO_2 + 20% H_2 contaminated with 10% N_2 were used in these tests.

The initial cell resistance of 0.6 Ω cm^2 is much higher than the expected one (0.4 Ω cm^2). The reason for this is not understood. Only few cells of this kind have ever been built (for fuel cells), and the development of this cell type is not yet advanced enough for this application. The rate of oxygen delivery corresponds to a current efficiency of near 100%. An independent gas chromatographic analyses of cell exit gases also showed a 1:2 ratio of oxygen delivery to carbon monoxide production, when a near 100% CO_2-cathode feed gas was used.

This experimental cell shows great promise for developing low resistance cells. This capability, however, must be demonstrated. The reduced complexity in cell fabrication, and quite acceptable performance behavior during cell testing (100% current efficiency) are remarkable. The anode material, made into the support tube, has the potential for a higher temperature shock resistance than calcia stabilized zirconia supports due to a better heat conductivity of lanthanum manganite. The elimination of one cell component (zirconia support) makes this cell potentially more reliable. Lack of performance life data, as well as lack of production experience are the reasons for not considering this cell for the breadboard electrolyzer.

3.4.5 C-Type Cell, Test Cell No. 3

This C-type cell was the first of its kind to be tested electrically. The cell mounting and electrical contacting in the test envelope was considerably more complex than originally anticipated. The same cell test envelope, used for B-type cells, was also employed here. The bus bars of the test cell had to be applied to the cell, as shown schematically in Figure 13. The difficulties which resulted in testing the cell are because of not achieving reliable contacts. The electrical contact rods tend to shift and the cell rotates when it is not properly aligned in the test envelope.

Electrical insulation of the two contacts was still another problem which was overcome with an arrangement of insulation pads of alumina felt shown in the lower part of Figure 29.

A further difficulty was wire wrapping and spot-welding the cell without causing damage to the cell structure.

The initial test results were disappointing because the cell showed a very high internal resistance index of 1.4 Ω cm^2 which was more than five times the expected one. This fact cannot be explained by the resistance of cell components, because component resistance values are expected to be similar to those of the standard B-type cells. The high resistance, therefore, must be due to contact resistance between the wire wrapping and the anode and cathode contact surfaces. Also cell performance deterioration (increased cell resistance) was observed during the first few days of operation. Initial cell operation characteristics were:

Cell Active Area:	102 cm^2
Temperature:	900°C
Inlet Gas:	70% CO_2, 20% H_2, 10% N_2
Current:	25.5 A
Resistance Index:	1.40 Ω cm^2 (start)
Cell Voltage:	1.41 V (start)
O_2 Delivery:	74.4 ml O_2/min
Current Efficiency:	85%

The test cell No. 3 was taken off test after twelve days of operation. The high initial cell resistance index of 1.4 Ω cm^2 rose to 3.7 $\Omega \cdot cm^2$ during the course of the test. It was obvious that the initial high resistance was due to contact resistance. During the test, the operating cell voltage rose from 1.41 V to 2.09 V. Upon disassembly it was noted, that the cathode, which was identical to the one in test cell No. 2 (B-type) had developed "blisters" on some cell segments. These areas showed severe separation of the cathode from the electrolyte, causing the rapidly increasing cell resistance. It was concluded from a structural analysis of test cell No. 3, that cathode separation from the electrolyte is the most probable cause

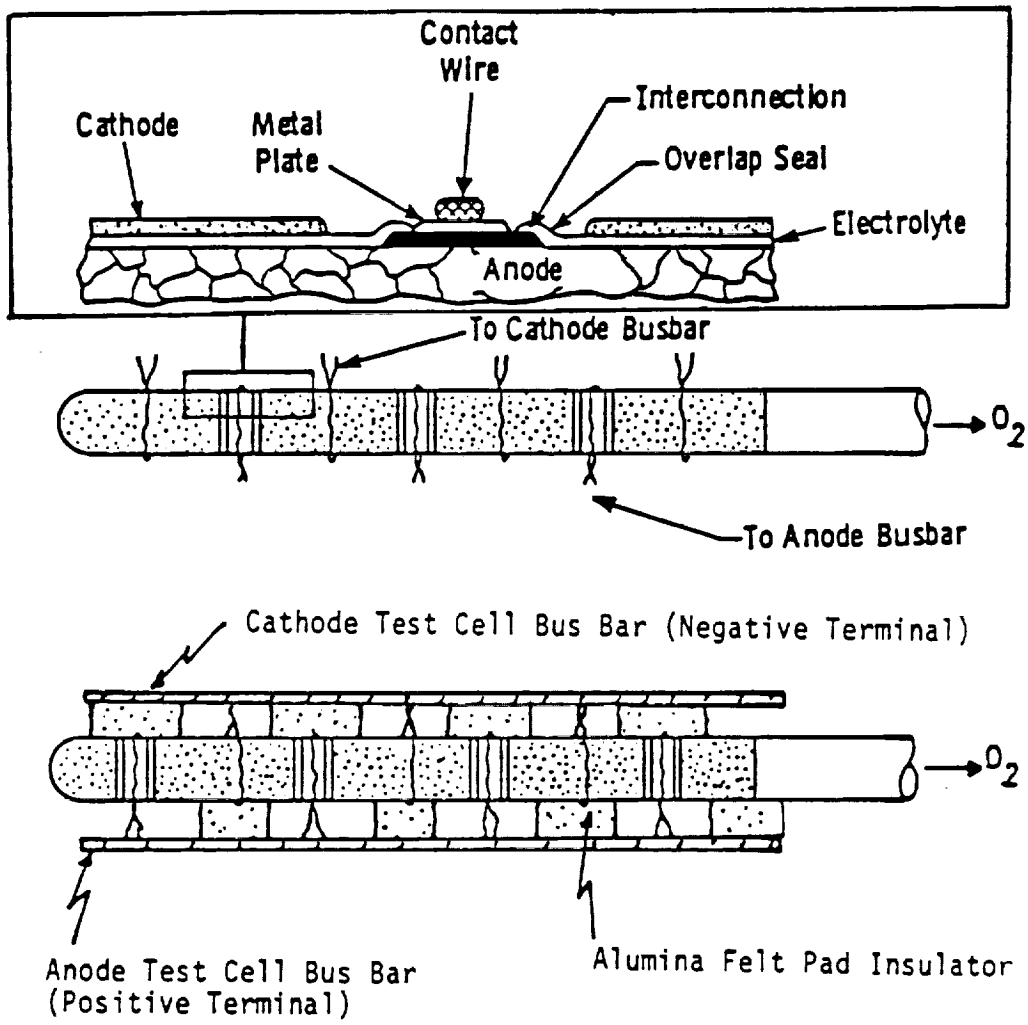

Figure 29. Schematic Showing the Electrical Contacts for a C-type CO_2-Electrolysis Test Cell

of cell performance deterioration. This condition must be improved by better cathode bonding.

The conclusions from this cell test are that wire contacting of C-type cells is problematic and irregular electrical contacts can lead to non-uniform current distribution in the active cell area and electrode deterioration at high current points. The low current efficiency of 85% as related to oxygen delivery could not be adequately explained but it is suspected that the diminished current efficiency was caused by a partial electrical short.

3.4.6 C-Type Cell, Test Cell No. 4

Based on the information obtained from test cell No. 3 the establishment of reduced wire contact resistance and a better electrode bonding to the electrolyte was attempted in test cell #4. The improved electrode bonding was achieved by longer fixation of a more porous cathode nickel layer with a stabilized zirconia skeleton by vapor deposition (see Appendix 1). The improved contacting was achieved by coating the cermet electrode with a thin layer of nickel powder, which was applied by spraying, since the location of the contact resistance was suspected between nickel wires and the cermet cathode structure. The cell resistance measurements indicated a considerable reduction of cell resistance in comparison with the first C-type cell (0.82 Ω cm^2 vs. 1.4 Ω cm^2); however, the low anticipated resistance index (<0.5 Ω cm^2) was not achieved.

Test cell No. 4 was tested parametrically with two feed gas compositions which are most meaningful for breadboard operation, namely, recycle gas and CO_2 + 20% H_2 contaminated with 10% N_2. The cell characteristics are shown in Figures 30 and 31. The oxygen production was close to theoretical (97 to 99%), which showed that the low current efficiency of test cell No. 3 was probably due to a partial electrical short but certainly not related to the cell structure.

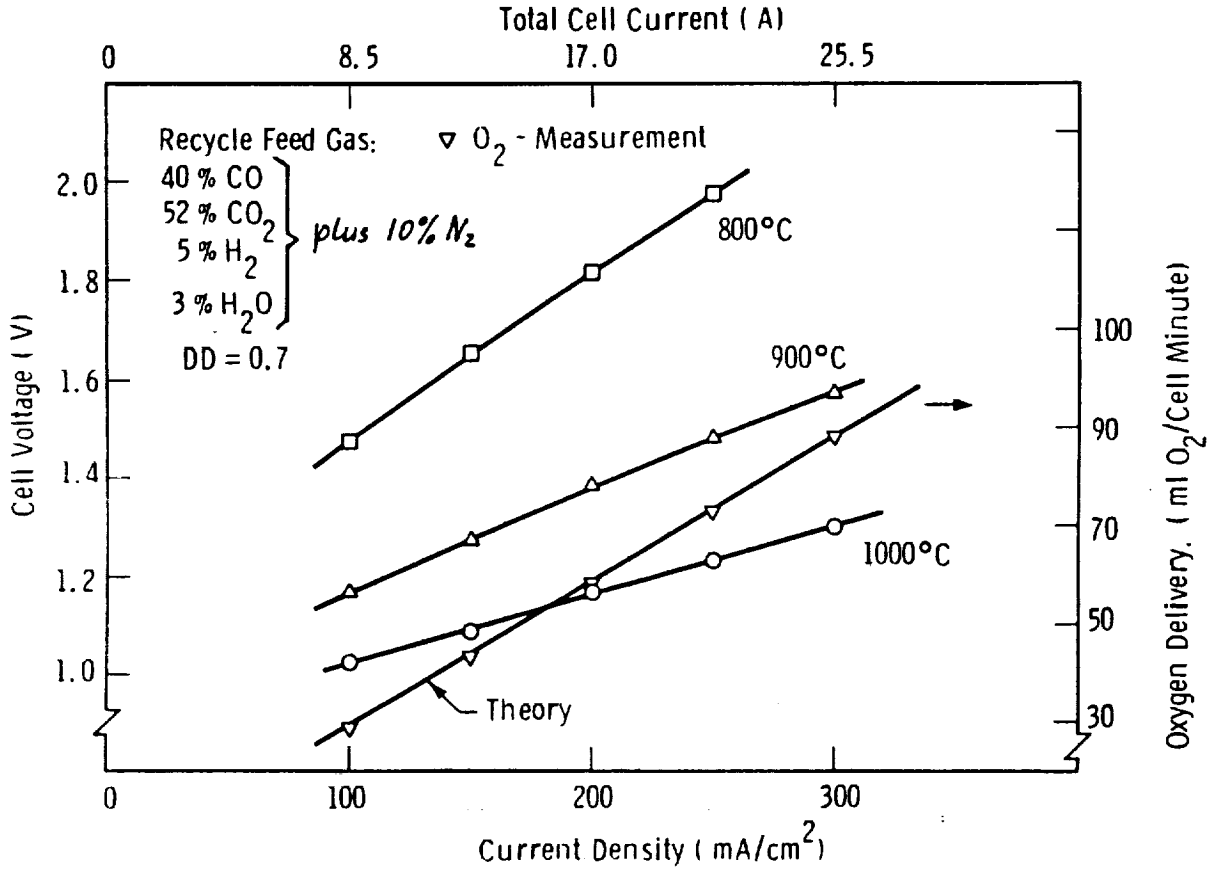

Figure 30. Temperature Dependence of Electrolysis Cell Performance Cell Type C, Test Cell No. 4

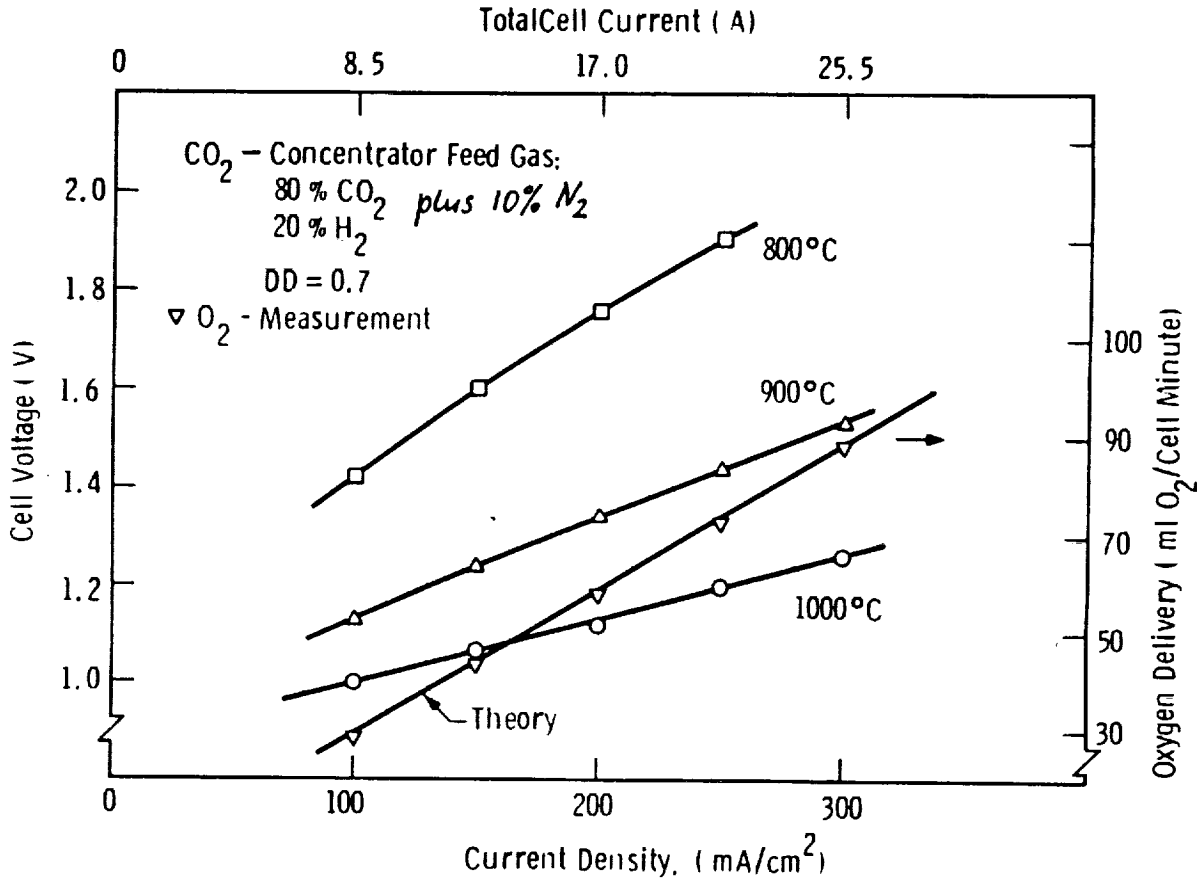

Figure 31. Temperature Dependence of Electrolysis Cell Performance, Cell Type C, Test Cell No. 4

3.4.7 Endurance Test of Cell No. 4

The cell was life tested for 1600 hours and the life characteristics are shown in Figure 32. It was observed that the cell resistance remained nearly constant, which attests to the better cathode bonding. The increase of the electrolysis voltage was due to an increase in concentration overvoltage. The diffusion of CO_2 was probably inhibited by the densification of the nickel powder layer which was applied over the cathode to achieve lower contact resistance to the contacting wire. Microscopical analysis seems to support this assumption. Also, the decreased rate of voltage increase with time supports this view because the rate of nickel layer densification by sintering will slow down with time. To observe this effect, the cell was tested for a longer time than originally planned (1600 hours).

It was evident from test cells 3 and 4 that the potential of C-type cells for low internal resistance could not be demonstrated because the multiple wire contacts introduced more resistance (probably due to contact restrictions) than expected. The application of a contact-enhancing nickel layer over the cathode improves contact but introduces additional gas diffusion resistance which leads to a higher electrolysis voltage. The cell endurance test demonstrated, however, that improved stability of cell resistance of nickel/zirconia cermet electrodes can be achieved through better fixation of cathodes by vapor deposition.

3.5 Conclusions from Cell Fabrication and Cell Testing

Problems in the fabrication and testing of new cell structures clearly showed their limitations. A-type cells could not be completed into test cells due to problems which were caused by materials incompatibility during EVD processing.

The fabrication of zirconia supported and self supported B-type cells, however, was virtually free of problems during fabrication and testing.

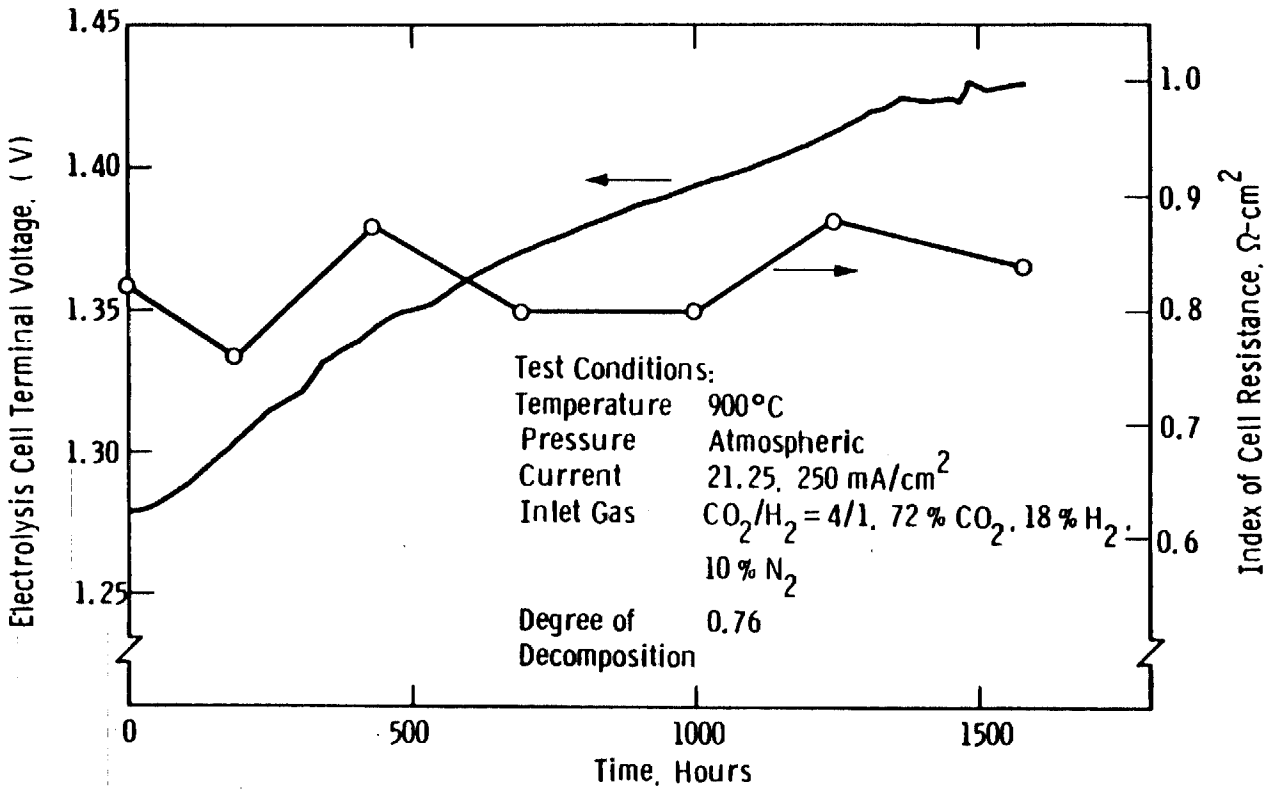

Figure 32. Life Performance Characteristic of Carbon Dioxide Electrolysis Cell C-Type Cell, No. 4

A zirconia supported B-type cell showed the lowest electrolysis voltage and the least voltage deterioration during a 1000 hour performance test.

C-type cells presented fracture problems in manufacturing which are related to residual stresses in the cell structure. However, two cells were completed and tested. Additional problems with this cell type lie in the electrical contacting method which causes higher than anticipated resistance losses. On the basis of these problems in cell fabrication and because of high electrical resistance, this cell could not be recommended for incorporation in the planned breadboard electrolyzer.

The information on electrolysis cell fabrication and electrical performance of different types as obtained throughout Phase I of this program, allowed a clear choice for the candidate breadboard cell, namely, for the zirconia-tube supported B-type cell. In the following paragraphs this cell will only be referred to as the breadboard electrolysis cell.

4. PHASE II OBJECTIVES AND TASKS

The choice of cell type for the breadboard electrolysis unit allowed the program to progress into the phase for breadboard design, fabrication, and testing. The detailed objectives of the second program phase were:

- design of cell stack
- design of hydrogen removal system
- design of cell stack containment and product gas handling
- design of auxiliary gas supply system
- design of auxiliary electrical equipment
- selection of IBM-PC compatible data handling system
- structural integration of all subsystems into a compact breadboard ready for delivery

The objectives for electrolyzer performance characteristics were, that cells would operate at 900°C, and at a current density of 250 mA/cm^2. An individual cell voltage of 1.2V was expected including a minimum current efficiency of 85%. The two selected design cathode feed gases were 100% CO_2, and a gas mixture of 80% CO_2 with 20% H^2.

4.1 Design of Cell Stack

The cell stack containment, and the related structural components are shown in horizontal and vertical cross sections in Figures 33 and 34, respectively (legend to both figures is given in Figure 34). It was decided to arrange the 16 electrolysis cells electrically in series in order to minimize the DC current. A higher current would be required for parallel connected cells which would lead to heavier current collectors and to increased heat losses by conduction. In addition, a weight penalty would be paid not only by the heavy contact bus bars but also by the increased weight of the power leads from the DC-power source.

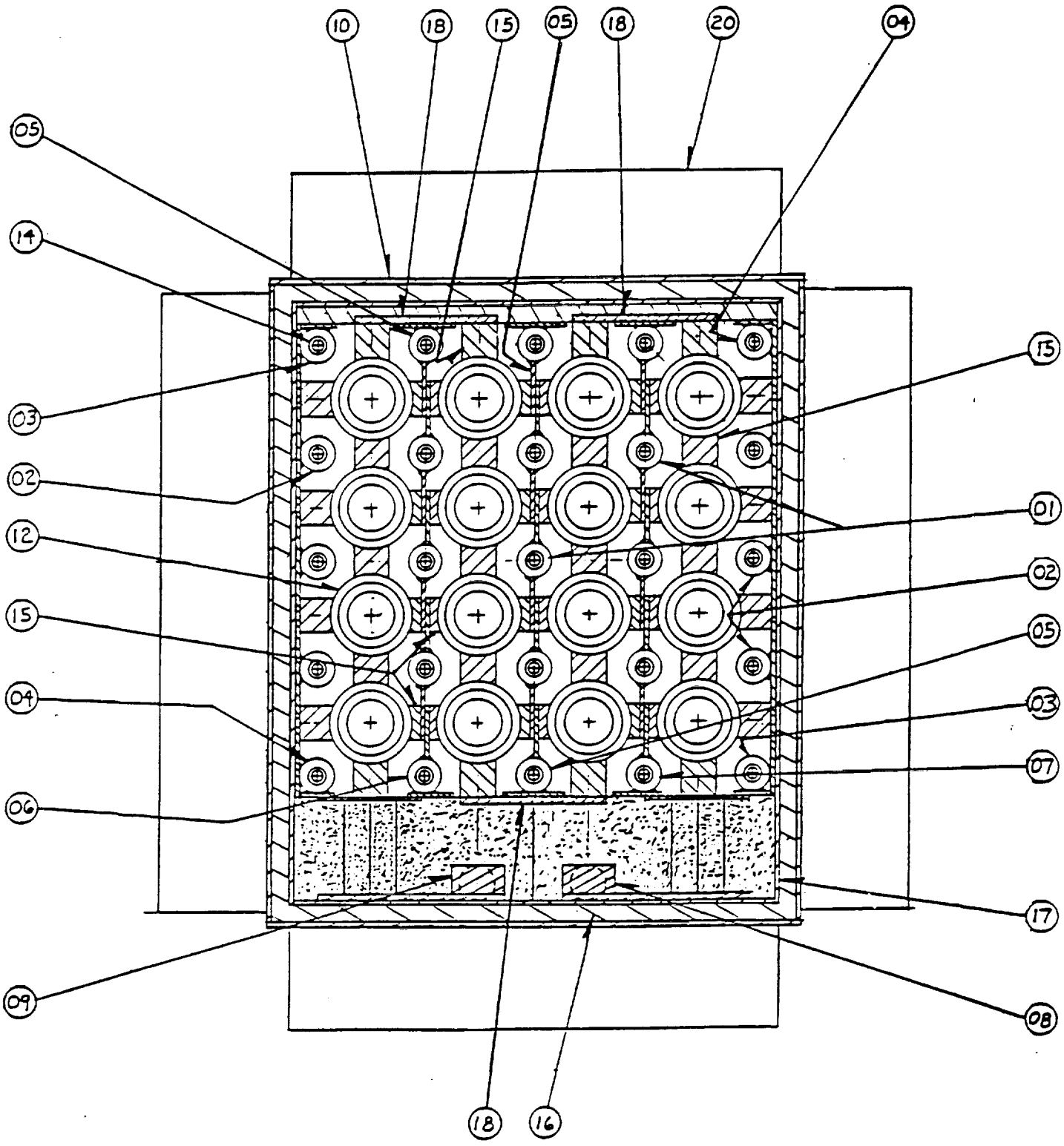

Figure 33. Horizontal Cross Section of Electrolysis Cell Stack

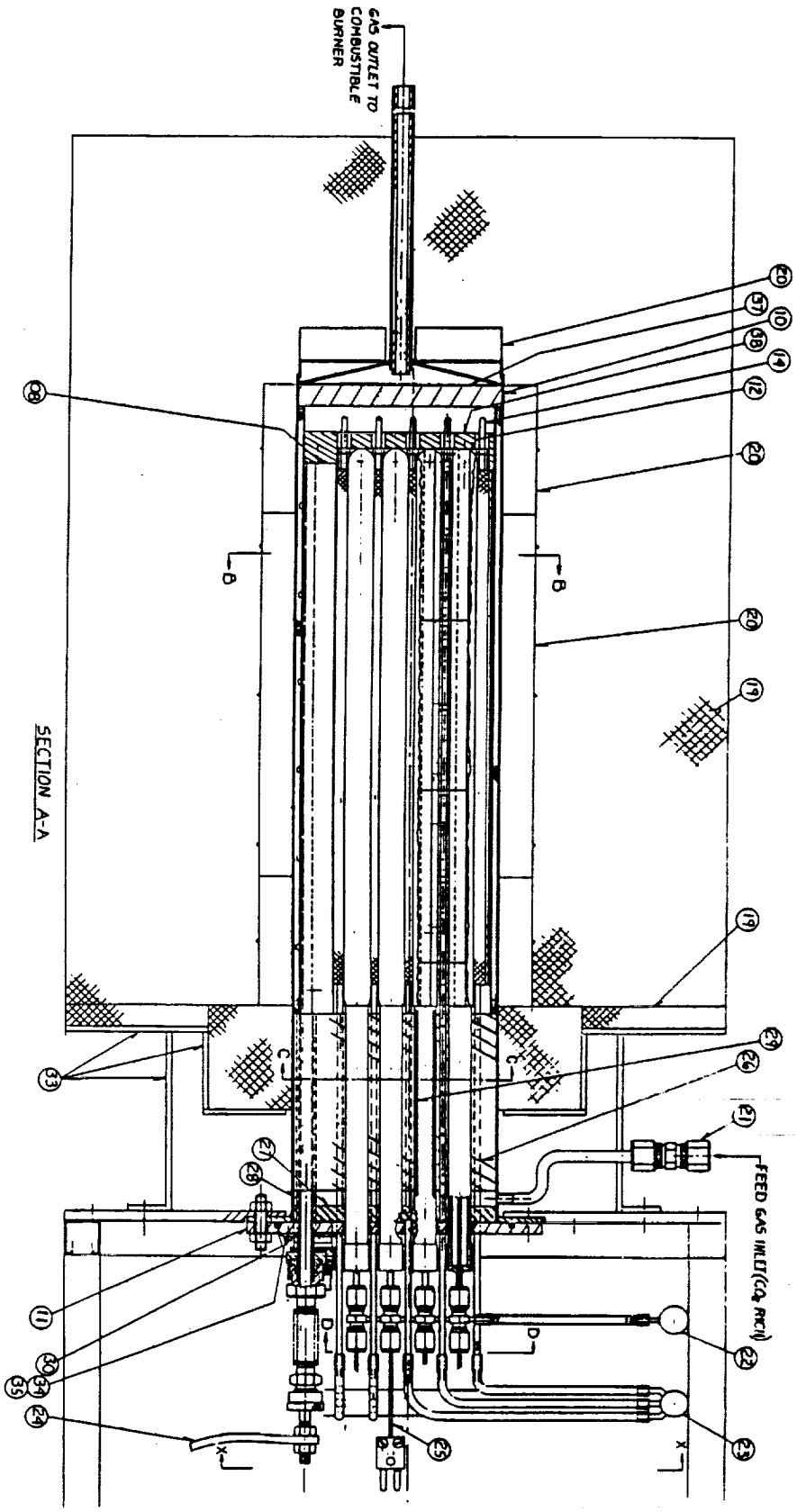

01	Ct. Pd. Tube Support
02	Border PD tube support-straight
03	Corner PD tube support-left
04	Corner PD tube support-right
05	Border PD tube support-T type
06	Border PD tube support-T type
07	Border PD tube support-T type
08	Right hand power lead
09	Left hand power lead
10	Cannister
11	Bottom flange
12	Cell
13	O_2 exhaust fitting
14	Palladium tube
15	Nickel felt
16	Alumina fiber insulation
17	Alumina plates
18	Cross over connectors
19	Alumina fiber insulation
20	Heaters
21	Feed gas inlet
22	Oxygen manifold
23	Hydrogen manifold
24	Power lead strap
25	Sliding thermocouple
26	Alumina insulation
27	Silicon rubber seal
28	Power lead support
29	Feed gas duct
30	O-ring
31	Flexible tubing
32	Flexible tubing
33	Support structure
34A	Voltage lead feed thru
35A	Voltage lead feed thru plug
36	SCR
37	Alumina board insulation
38	Alumina insulation

Figure 34. Vertical Cross Section of Electrolysis Cell Stack

4.1.1 Electrolysis Related Stack Components

Referring to Figures 33 and 34, items 1 through 7 are dual-function Pd tube holders made from high purity alumina. Their function as holders is described in Section 4.1.2.2. Their second function is to act as electrical insulators between the vertical rows of cells (Figure 33) as well as to prevent any electrical contact between Pd tubes and cells. Legend #8 and #9 are the DC-power leads; #12 are electrolysis cells; #15 are felts of nickel fibers; and #18 are segmented electrical cross-over connectors from one cell row to the adjacent one. Figure 33 shows the actual size of the cell stack, stack canister, and other structural members (see section 4.1.3).

4.1.1.1 Electrolysis Cells

The dimensions of the breadboard electrolysis cell are shown in Figure 35. The processing steps in the fabrication of the cells are described in section 3.1 and 3.2.2. Since component fabrication processes do not result in a 100% yield, we processed 48 cells. The 48 cells were prepared in four batches of 12 cells each, because the vapor deposition reactor (see section 3.1.2) is sized for the parallel processing of 12 cells. Sixty porous support tubes were extruded and sintered to provide a sufficient number for the 48 cells. All 48 cells were successfully passed through the various processing steps except for the last two steps which include cathode activation (section 3.1.4) and nickel plating of the interconnection contact surface. The quality control of individual cells is followed throughout the fabrication processes via visual-, electrical-, dimensional-, and leak rate-inspection.

Visual inspection is used to insure the quality of the masking and demasking steps for vapor deposition, making use of a low magnification (10-50X) microscope.

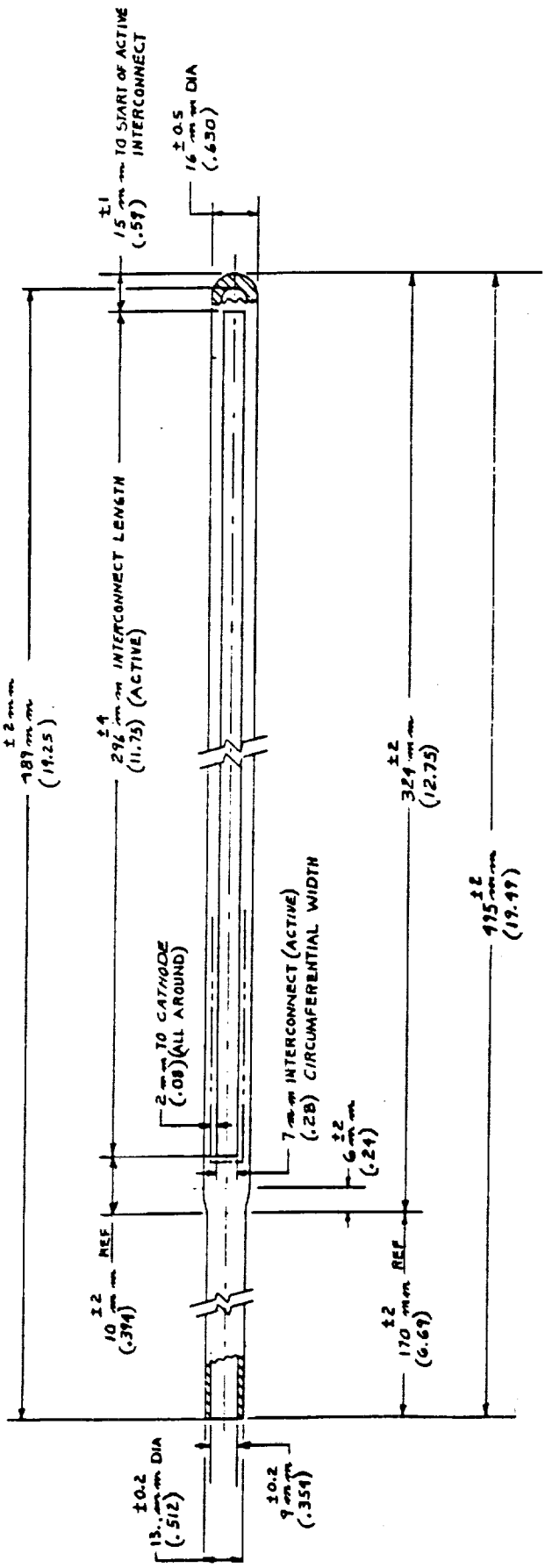

Figure 35. Individual Electrolysis Cell Dimensions

ORIGINAL PAGE IS
OF POOR QUALITY

Electrical tests are made to measure the resistance behavior of electrodes. Figure 36 is a typical example of an electrical induction-loss measurement over the length of an anode after sintering. The anode is pushed at a controlled speed through a calibrated induction coil at room temperature and the induction losses are measured. This measurement is sensitive to hidden structural flaws like hairline cracks. The electrode sheet resistance is measured with a conventional four-probe measurement, and measured room temperature values can be extrapolated to the operational electrolyzer temperature by simple factoring as seen on the computer printout. A similar four probe measurement is made for the cathode. The sheet resistance control values at 900°C are 0.2 Ω for the anode and 0.05 Ω for the nickel/zirconia cermet cathode.

Dimensional inspection includes measuring length, diameter and thickness of components. The vapor deposited oxide layers that are grown over masking materials are used to measure layer thicknesses by microscopy. The scales can be removed by scraping after the electrolyte and interconnection deposition steps. Both layer deposits are controlled to within 20 to 50 μm.

The leak measurements involve the evacuation of the cell tubes, which can only be done after the interconnection and electrolyzer layers have been deposited as gas-tight structures. The maximum permissible leak rate of cells was controlled to 3×10^{-6} mole air per minute and was measured in the pressure range of 10^2-10^4 pascal on the cell inside and atmospheric air on the outside (cathode side).

Cells which did not fall within the established limits were not eliminated from further processing, because their deviation from the control values did not endanger the quality of sibling-cells during EVD processing. Of the 48 processed cells 24 cells did meet all the specifications of which sixteen of the cells were used for the breadboard. The first batch of 12 cells did not contribute candidate breadboard cells because of irregularities during EVD processing. The electrical performance of electrolysis cells of the other batches was evaluated through the electrical testing of a single cell from each batch as a representative qualification cell.

CELL IDENTIFICATION

ENTRY: 322 (AIRDATS)
DATE:21 Jan 1988
CELL NUMBER:13-41
GROUP NUMBER: 0

ELECTRODE SHEET RESISTANCE DATA

PROBE RESISTANCE,CLOSED END: 0.655 OHMS
PROBE RESISTANCE,MIDDLE: 0.694 OHMS
PROBE RESISTANCE,OPEN END: 0.729 OHMS
PROBE RESISTANCE, AVERAGE: 0.693 OHMS
SHEET RESISTANCE, AVERAGE, @ 22°C: 2.875 OHMS/SQUARE
SHEET RESISTANCE, AVERAGE, @ 1000°C: 0.192 OHMS/SQUARE

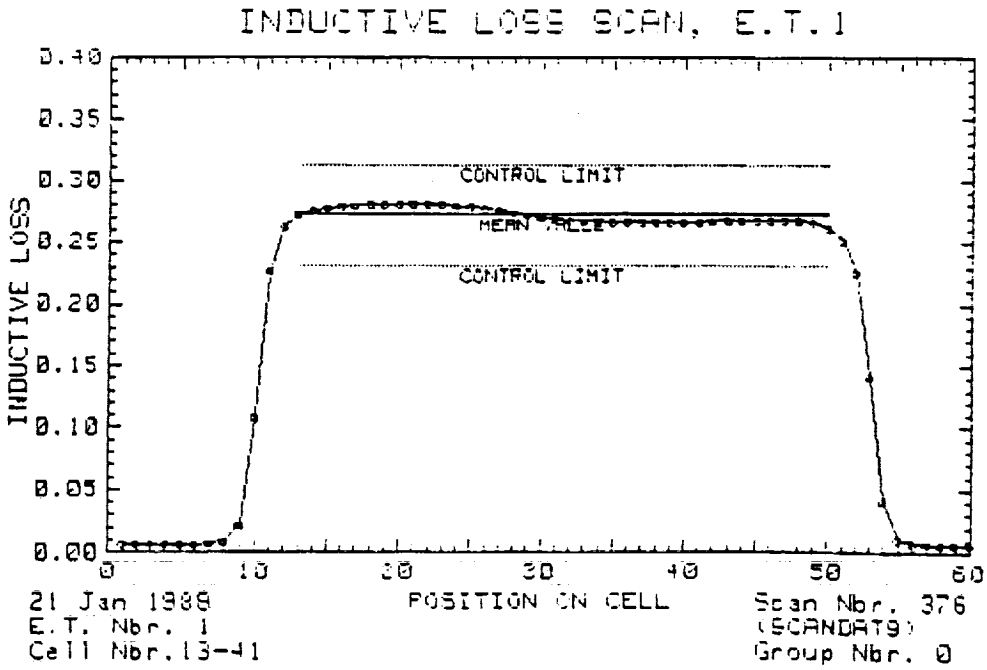

Figure 36. Resistance Profile of a Strontium-Doped Lanthanum Manganite Anode

Twenty candidate cells were equipped with six alumina tubes (100mm by 1.2mm O.D., 0.4mm I.D.) each, which were arranged in a hexagonal axial position on the inactive part of the cell tube. They served as the cathode feed gas channels through the cold end insulation of the cell stack. The tubes were attached temporarily with an epoxy glue for assembly purposes only. Later, during cell stack operation, they are held in position by the firmly packed insulation. The glue burns off near the hot zone of the active cell. Another purpose of the tubes is to achieve uniform cathode gas preheating, while it flows toward the active cell stack zone. Figure 37 shows the individual cells on a stand. The alumina tubes are seen on the lower cell portion.

4.1.1.2 Cell to Cell Electrical Contacts

Figure 33 also shows the nickel felt strips which are placed between the cells as electrical series connections in the vertical direction and as spacers in the horizontal direction. The felts are made of ~100 μm size nickel fibers. The fiber loading is approximately 750 mg/cm^2 for the thicker felts and 250 mg/cm^2 for the thinner felts, which are in contact with the Pd tube holders. The felts are made by a paper-making process in 200 mm by 200 mm pads, which are sintered in a reducing gas mixture. They are partially compressed and subsequently cut by a laser beam into 6.4 mm wide and 145 mm long strips.

Two of the nickel felts are bonded to the interconnection and two to the cathode, at 180° opposing axial positions of the cell. The bonding medium is a creamy paste of fine nickel powder (1-10 μm) in an aqueous solution of polyvinyl alcohol (8 wt%). The nickel felts and cell contact areas are painted with this paste and the painted faces are placed against each other, compressed, and air dried.

Four cells are connected to each other in a row by placing the cells in a holder that provides for the precise positioning of the tubes with respect to felts and to each other. Figure 38 shows the cell holder for felt

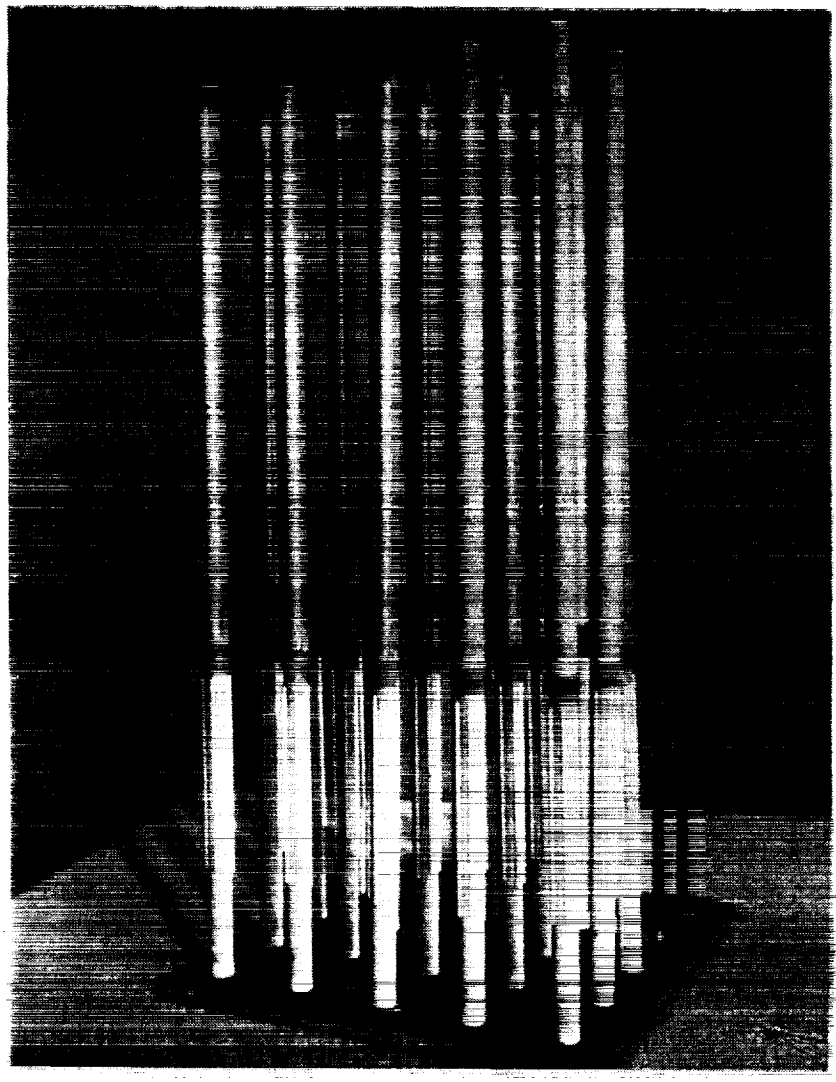

Figure 37. Candidate Breadboard Cells With Attached Alumina Tube Feedgas Channels

Figure 38. Holder and Electrolysis Cells for Electrical Series Contacting and Nickel Felt Bonding

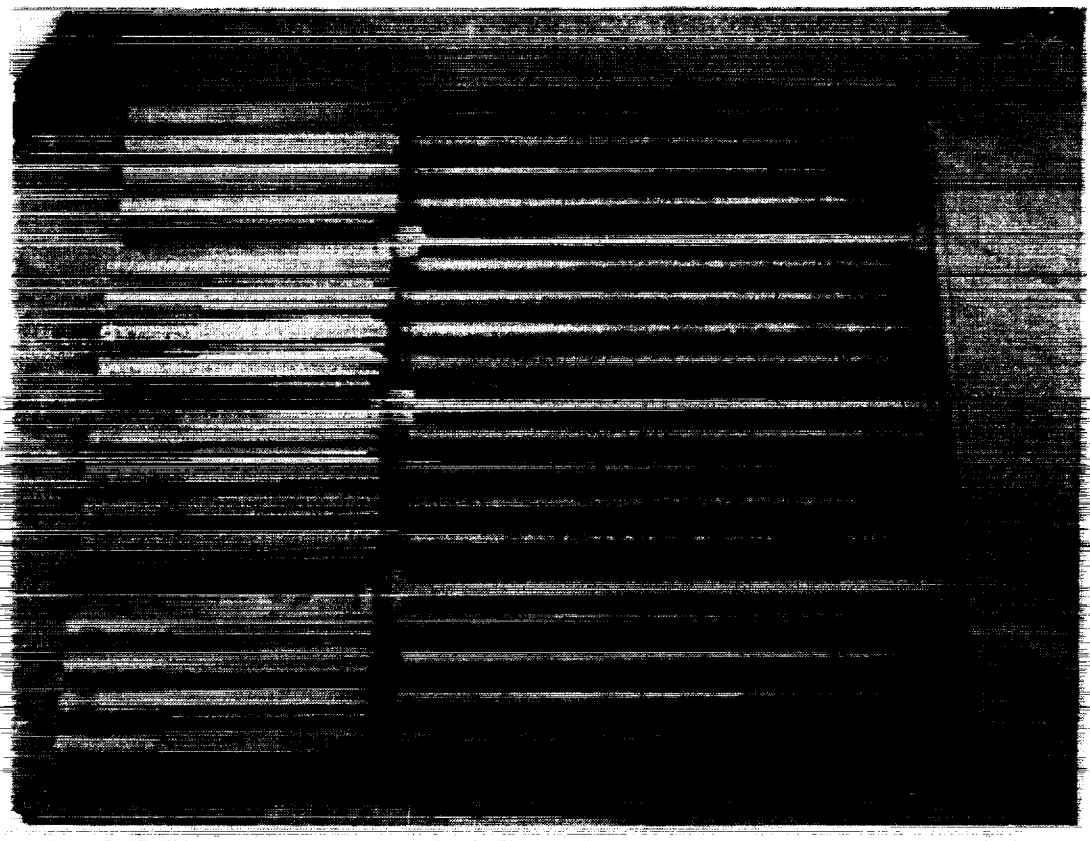

Figure 39. Four Cell Rows Made by Nickel Felt Bonding

attachment. Figure 39 shows the four rows of four cells each, that make up the cell stack, prior to their assembly into the cell stack.

The cross-over connectors between rows of cells (item 18 in Figure 33) are made in six segments of nickel plates having the dimensions, 48mm by 30mm by 0.5mm. They are arranged along the nickel felts of two adjacent cell rows to accomplish the electrical series connection of all sixteen stack cells. The bonding of the nickel felts and nickel plates is accomplished by sintering during stack operation.

4.1.1.3 End Cell Current Power Leads

The D.C.-power leads are shown in Figure 33 as legend #8 and #9. Figure 40 shows a single power lead, stripped from its surrounding insulation. The electrical contact surface is segmented like the cross-over contacts (section 4.1.1.2) in order to avoid stresses due to mismatch in thermal expansion between the nickel plates and the electrolysis cells. The segmented contact plates are connected to a second set of segmented nickel plates by a multitude of 30 mil nickel wires. The second set of nickel plates is welded to a solid rectangular nickel bus bar which ends in a round rod. The segmented nickel plates are separated by alumina fiberboard, which surrounds the large number of nickel wires. This flexible and thermally insulated D.C. power contacting scheme accomplishes the task of obtaining a low stress, low loss, low temperature gradient busbar. The 6.4mm (1/4") round end of the nickel busbar is plasma-spray coated with an aluminum oxide layer for electrical insulation. This insulation is required in the areas where the busbars penetrate the metal flange plate (legend #11 Figure 34) and the expansion bellow seal. The ends of the nickel busbars are bare and threaded for screw connection to the flexible D.C. power supply cables.

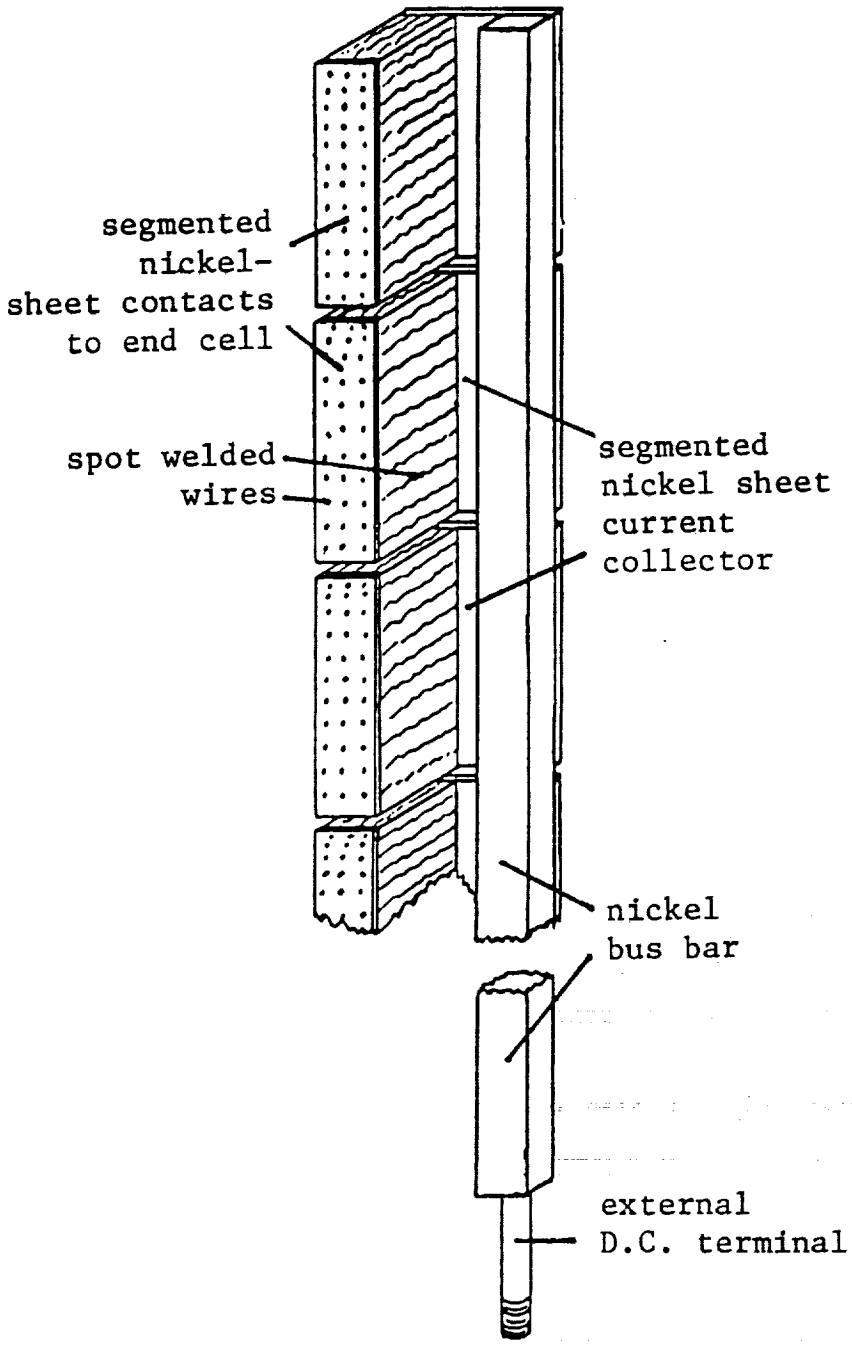

Figure 40. Schematic of End Cell D.C. Current Collectors

4.1.2 Hydrogen Removal Stack Components

In section 1 it was explained that H_2 will accumulate in the cathode gas of a closed loop O_2 recovery system, which, requires continuous H_2 removal. In order to achieve a compact H_2-removal system Pd diffusion tubes were incorporated into the cell stack as shown in Figure 33.

4.1.2.1 Palladium Diffusion Tubes

The maximum number of Pd tubes (25) that could be integrated into the cell stack was determined by the number of channels between the electrolyzer cells in the cell stack. Pure palladium was chosen for achieving the maximum permeation rate for H_2. A wall thickness of 10 mils (0.25mm) was selected to increase tube strength. A thinner wall size (5 mils) had been tested before[1] and had shown signs of collapsing under vacuum at 900°C. A tube size of 1/8" O.D. (3.2mm) was selected for an easy fit into the stack channels which are formed between the cells, as well as between cells and the stack periphery.

The Pd tubes are 457mm (18") long and are gold-brazed to 130mm (5.12"), long 304 stainless steel tubes for achieving mechanically strong ends for reliable cold end seals and attachments to a common vacuum manifold.

A single candidate Pd diffusion tube (Johnson Mathey Co.) was performance tested with respect to hydrogen diffusion at 900°C. The Pd tube was placed into a quartz glass tube of a cross section similar to that of a stack channel. The assembly was heated in an electrical furnace to 900°C. A gas mixture of 80% N_2 and 20% H_2 was flown over the evacuated Pd diffusion tube. The H_2 diffusion rate was measured with calibrated mass flow meters on the vacuum side as well as on the atmospheric-pressure-delivery side. The delivery rate is primarily dependent on the differential pressure of hydrogen, the tube wall thickness, and temperature. While much literature data exist on hydrogen diffusion through palladium, an actual rate can only be achieved by direct

measurement since metal purity, mechanical working and mixed gas atmospheres can affect H_2 diffusion rates considerably.[3] Figure 41 shows the test results for the individually tested Pd tube.

4.1.2.2 Palladium Tube Holders

Items 1 through 7 in Figure 33 show the location of the different Pd tube holders. The holders are shown also in Figure 42 in a perspective view which depicts the structure more clearly. They are made from high purity alumina substrate plates of 30 mil (0.76mm) thickness. The plates (4" by 4") are cut into strips which are bonded at 1500°C to alumina rings (1/8" long, 1/4" O.D., 1/8" I.D). The bonding cement (49 wt% Al_2O_3, 49 wt% CaO, 2% SiO_2) is melted between the slotted rings and alumina plates, which are positioned firmly toward each other during the cementing operation. Seventy-five holders were made. The overlapping parts of adjacent holders in the completed stack can slide over each other even at 900°C because of their excellent surface smoothness and cracking during transient temperature conditions is minimized in the stack. The surfaces of the holders that are in contact with the nickel felts are made into high-friction-surfaces which form a firm bond to the nickel felts of the cells. Therefore, the holders remain in a fixed position with respect to the cells. In this arrangement the Pd tubes are sufficiently separated from the cells and are accessible to the cathode gas over the entire length. Only a small portion of the Pd tubes is covered by the alumina rings of the three axial holders for each tube.

The high friction surface of the holders was made by sandblasting the surface first and attaching a 1/4" wide very thin nickel felt strip (~120mg N/cm^2) with an alumina cement (Cerama Bond 600) to the sandblasted areas. The cement had been tested before use at 900°C in contact with nickel felt and in a gas atmosphere containing 80% CO_2 and 20% H_2. No deleterious interaction had been detected over several days of testing. Figure 43 shows the drawings for the alumina Pd tube holders.

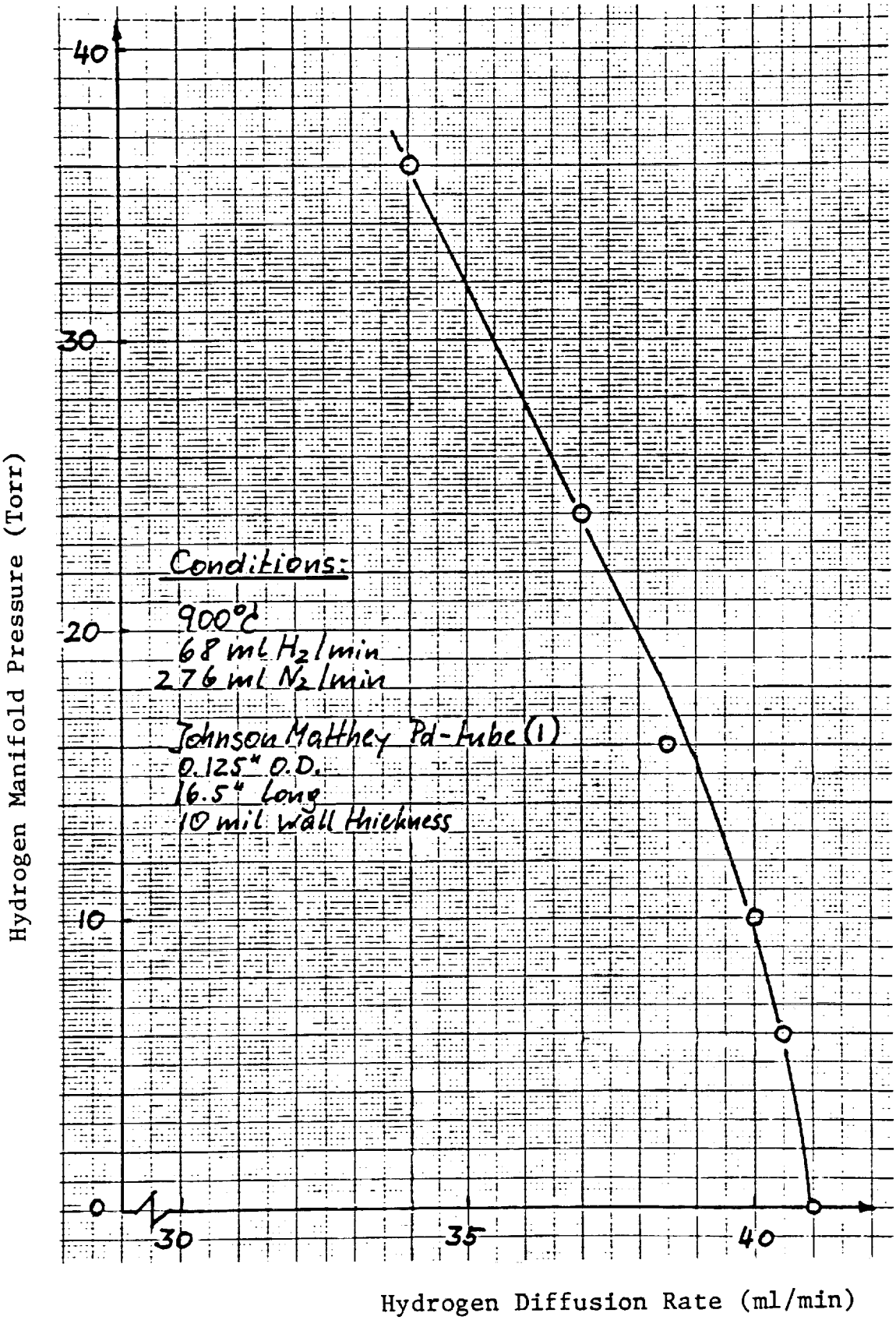

Figure 41. Diffusion Rate of Hydrogen Through a Single Palladium Tube

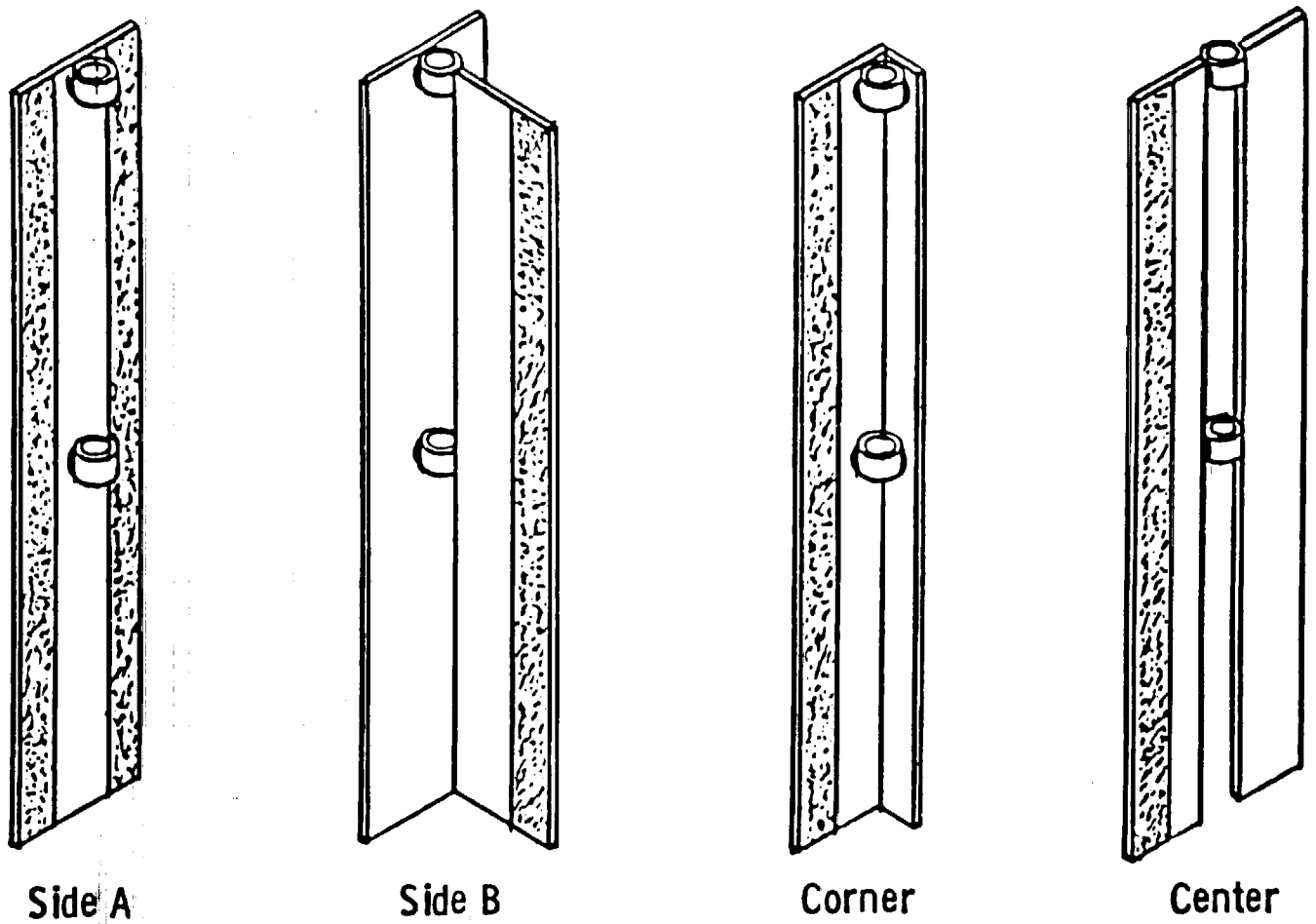

Figure 42. Palladium Tube Holders for Different Locations in Cell Stack

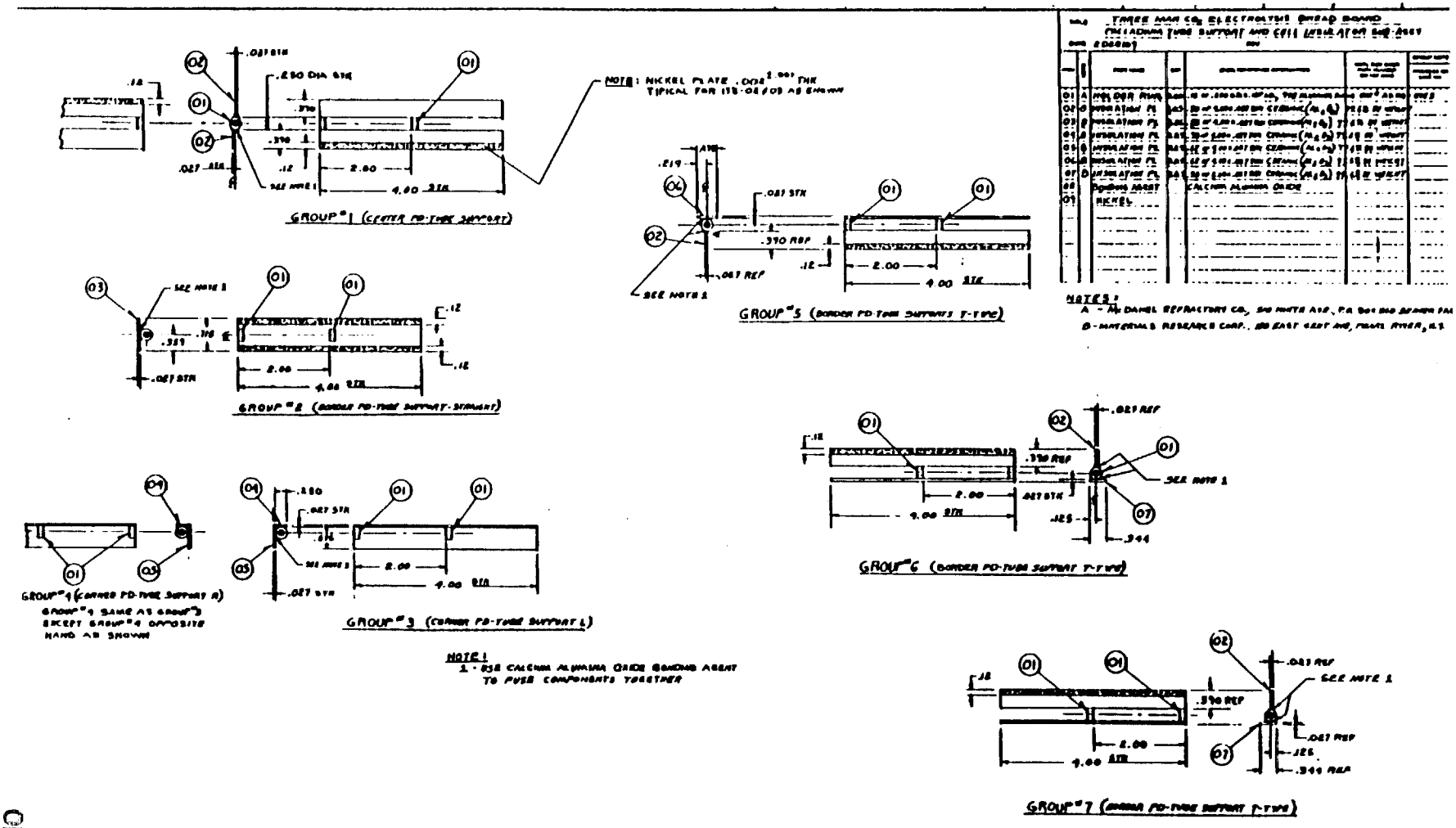

Figure 43. Palladium Holders for the Breadboard Cell Stack

4.1.3 Structural Stack and Containment Components

All essential other stack components are seen in Figures 33 and 34. Figure 33 shows that the stack is surrounded by high purity alumina substrate plates (#17). An Inconel 600 canister (#10) surrounds the cell stack with fibrous alumina insulation (#16) between the steel and the alumina plates (#17). This insulation is more a padding to prevent pressure contacts and plate fracture.

4.1.3.1 Stack Canister

Figure 44 shows the dimensions of the stack canister. A special feature in its design is the internal copper liner of the cathode exit gas tube (legend #5 in Figure 44). This liner is laser-welded to the Inconel 600 pipe toward the hot zone. The copper liner prevents the deposition of carbon from the CO-rich cathode gas when it passes through a temperature zone (400°-800°C) where carbon deposition normally occurs.

4.1.3.2 Flange Plate

The canister flange plate is sealed with viton O-ring against the canister flange. The plate has 25 clearance holes for Pd tube extensions, 16 clearance holes for cells, 2 feed-through holes for D.C. power terminals and one plug hole for electrical contacts to each of the cells. The holes for the cells and Pd tubes are drilled into the plate after assembly of the stack and their position has been accurately established. The positions were identified by making an ink impression of the open ends of the cell tubes on paper.

4.1.3.3 Stack Heaters

It is of importance for good stack operation that the temperature profile along the active cell length is as uniform as possible. In order to

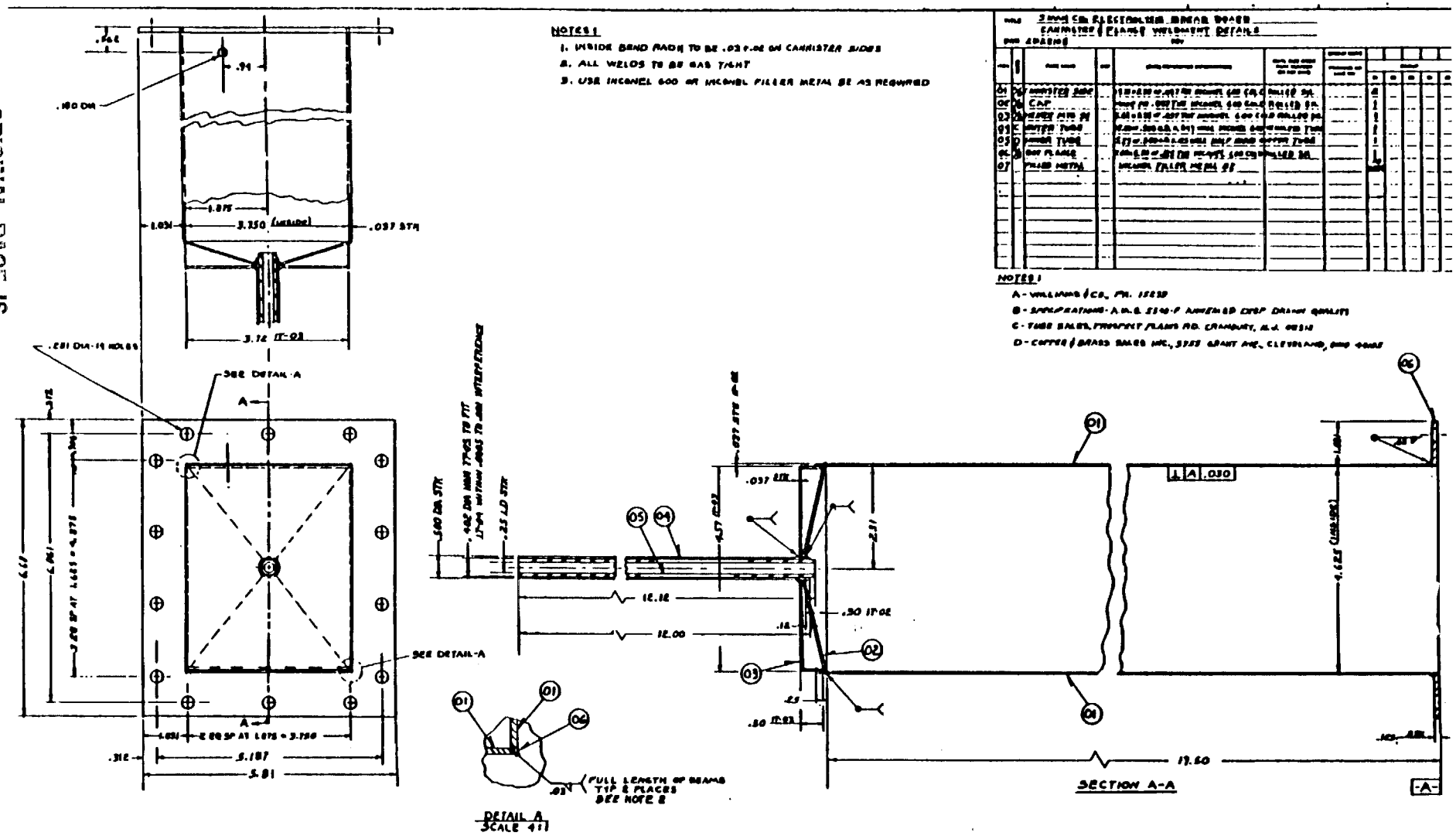

Figure 44. Electrolysis Stack Canister

achieve this, the canister was equipped with custom made heaters. The heaters were attached directly to the canister wall in three separate heating zones. They were made from Kanthal Al wire which is insulated from the canister by alumina insulation tubes. The partially completed heater structure is seen in Figure 45. Figure 46 shows the finished heaters, embedded in alumina cement. The total heater thickness is 1/4" (~6mm) thick. The heater resistance values at 900°C are: 12.0 Ω top heater, 6.6 Ω center heater, and 10.0 Ω bottom heater.

4.1.3.4 Electrolysis Unit Housing

The canister is placed in a housing made of 40 mil aluminum sheet metal with 1/4" (~6mm) thick top and bottom plates. The outside dimensions of the housing are 15" by 15.5" by 24" (381mm by 394mm by 610mm). An insulation of Duraboard 3000 is placed around the stack canister and fills the aluminum outer housing tightly. The Inconel 600 canister penetrates the bottom housing plate and the cathode gas exit tube penetrates the top housing plate. The A.C. power contacts to the heaters are made with stand-off insulators at the top housing plate. Three Pt/Pt 10% Rh thermocouples are inserted through one side wall. They penetrate the insulation and touch the heater face in the middle of each zone.

4.2 Electrolysis Stack Assembly

The cell stack assembly focused on four major tasks, namely, (a) maintaining correct spacing of cells and palladium tube holders; (b) providing for uniform packing of insulation; (c) sealing of the cells and Pd tubes in-place, and (d) making electrical contact for all the cells. This sequence of steps was employed during stack assembly.

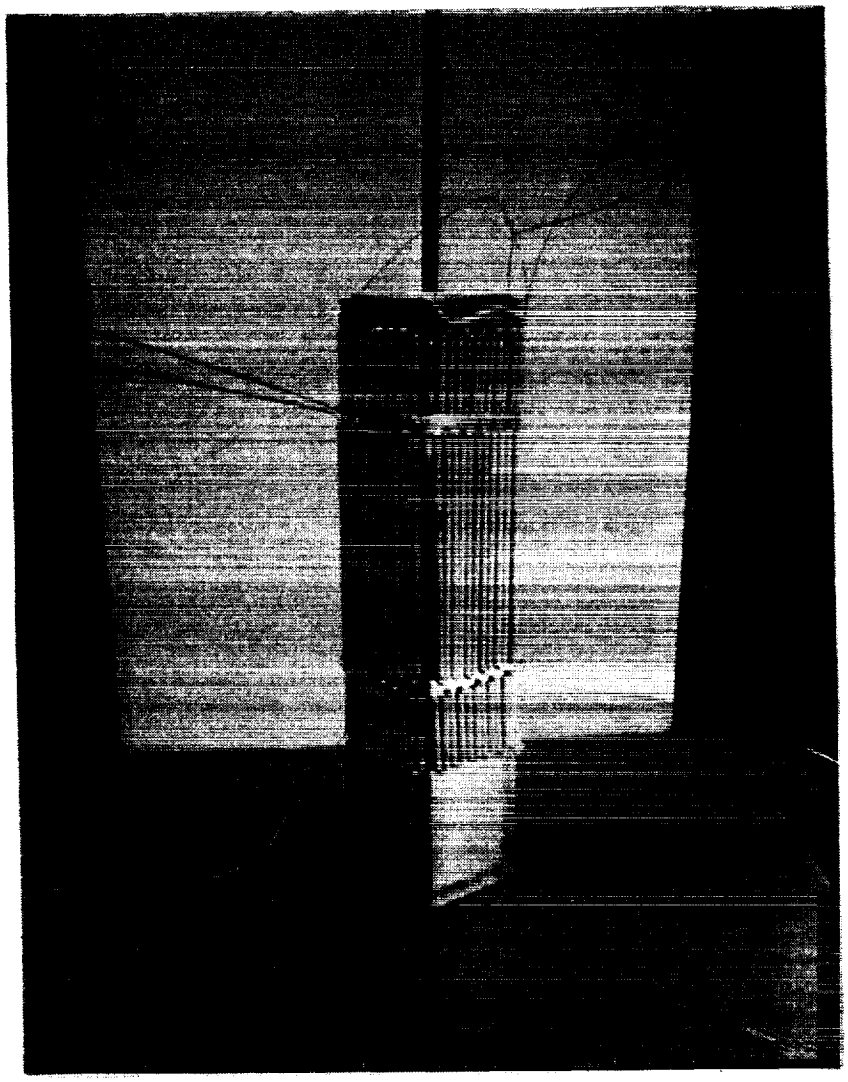

Figure 45. Partially Completed Heater Zones On Stack Canister

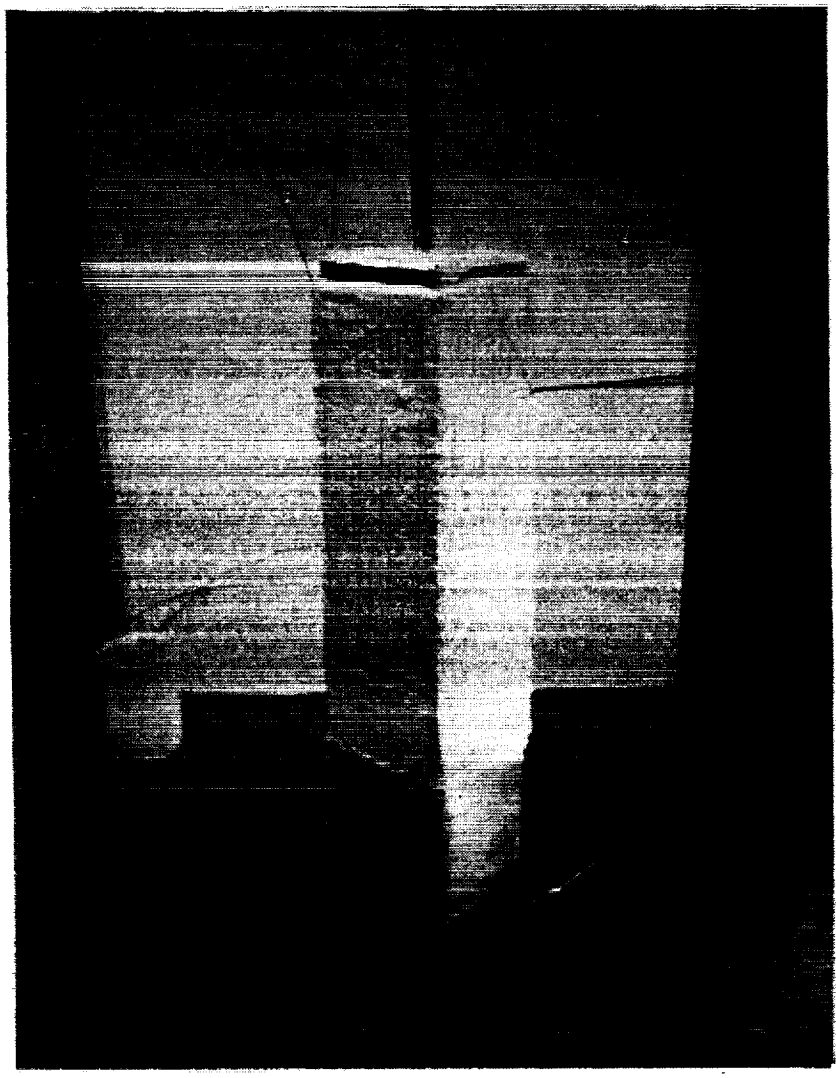

Figure 46. Three Zone-Heaters Completed and Embedded In Alumina Cement

4.2.1 Layering of Cells and Central Palladium Tube Holders

The four rows of series connected cells are shown in Figure 39. Alternating layers of cells and Pd tube holders are placed on top of each other with nickel felts placed between cells and holders. The nickel felts are glued to the cells as described in section 4.1.1.2 while the Pd tube holders were lined up by inserting steel rods in place of the Pd tubes. The overlapping holders were glued to each other with transfer-glue tape to prevent shifting during the layering operation. After a layer of Pd tube holders and felts had been placed between two cell layers, the partial assembly was dried for one hour by blowing dry air through the axial channels. Figure 47 shows the layering of components.

After the layering operation, the cell bundle was slightly compressed by adjustable clamps between heavy Micarta boards to adjust the final spacing dimensions. Rubber sheets are placed between the cells and the compression boards to prevent cell damage while the nickel felts are plastically deformed. Figure 48 shows the state of assembly at this point.

The subsequent operations involved the application of the cold-end insulation and current collector attachment. The insulation was applied by pushing perforated alumina fiber boards (Zircar AL 15) over the inactive cell ends to form a solid insulation block. The current collectors were attached to the nickel felts of the end cells by nickel powder paste and subsequent drying as described above. Figure 49 shows the cell stack in a vertical position after completion of these tasks. This position was also used to line up and square the flange plate (bottom of Figure 49) with the stack.

Further assembly operations included the attachment of the peripheral Pd tube holders (see Figure 50); the application of the closed-cell-end positioning board, Zircar, AL 30 (Figure 51); and the attachment of the outside alumina tiles on the stack periphery as shown in Figure 52. The alumina tiles were temporarily glued to the peripheral Pd tube holders by transfer glue-tape. The cell stack was placed in front of the stack

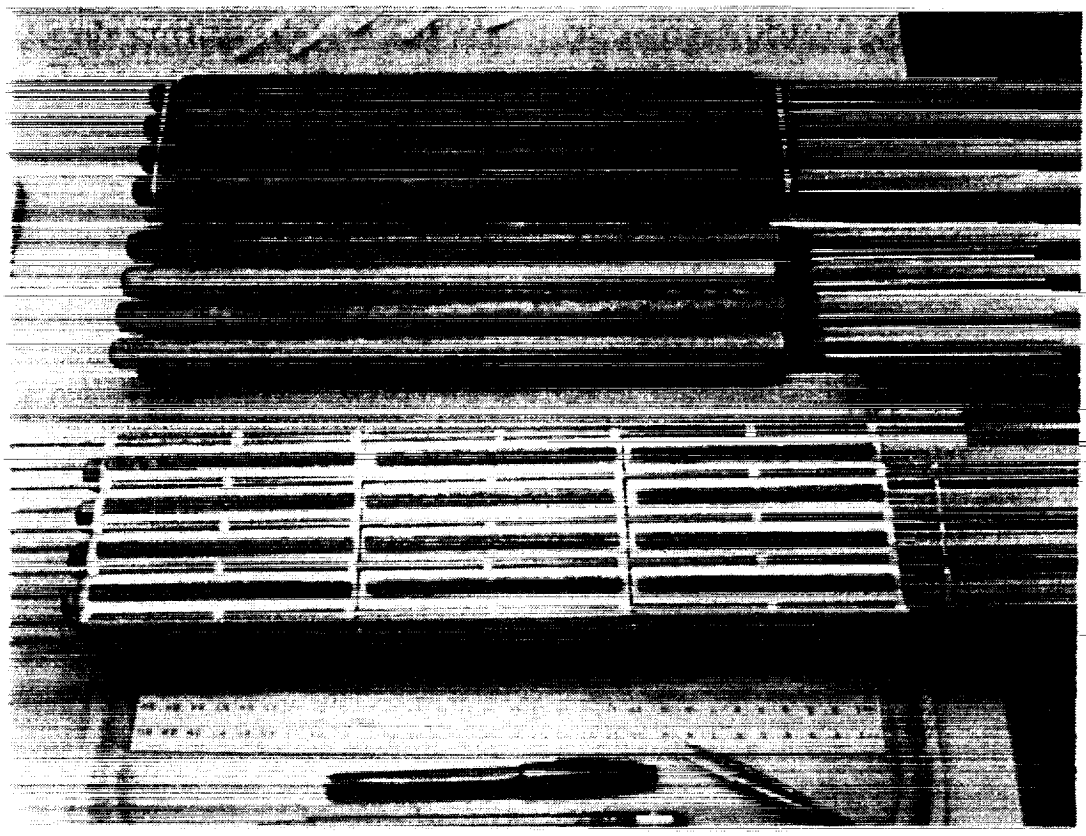

Figure 47. Assembly of Stack Components By Layering

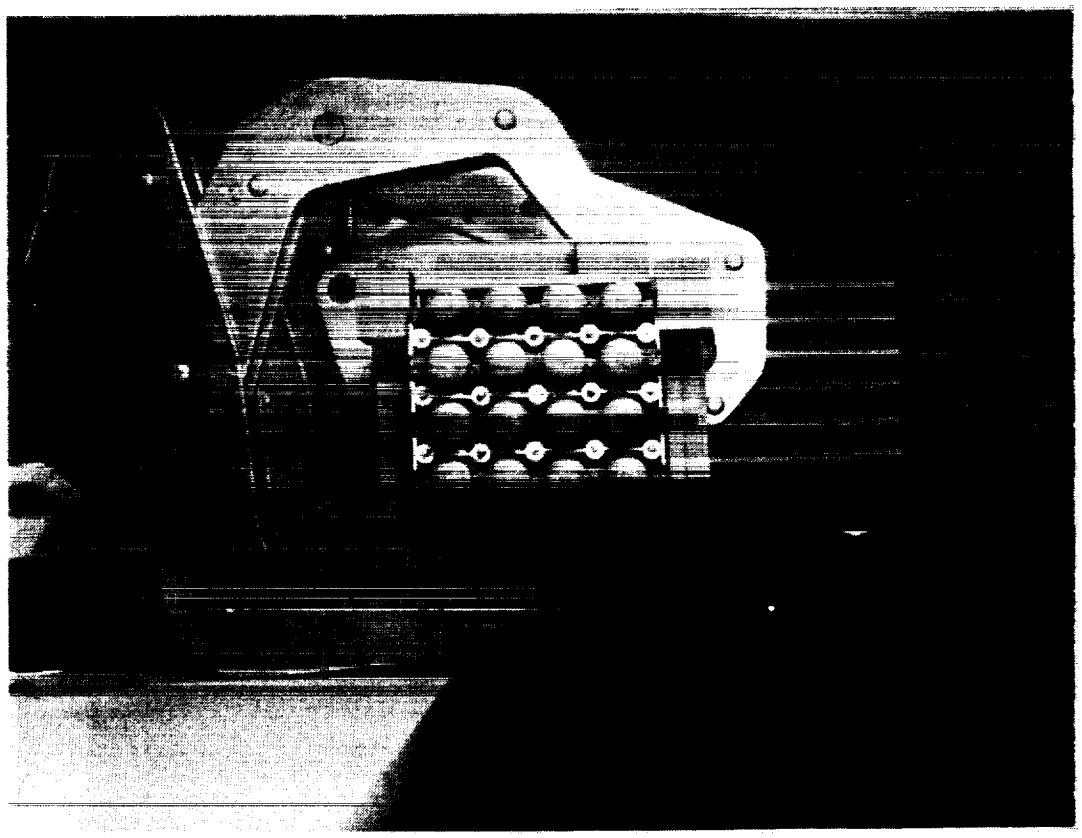

Figure 48. Compression of Cell Bundle To Correct Dimensions During Assembly

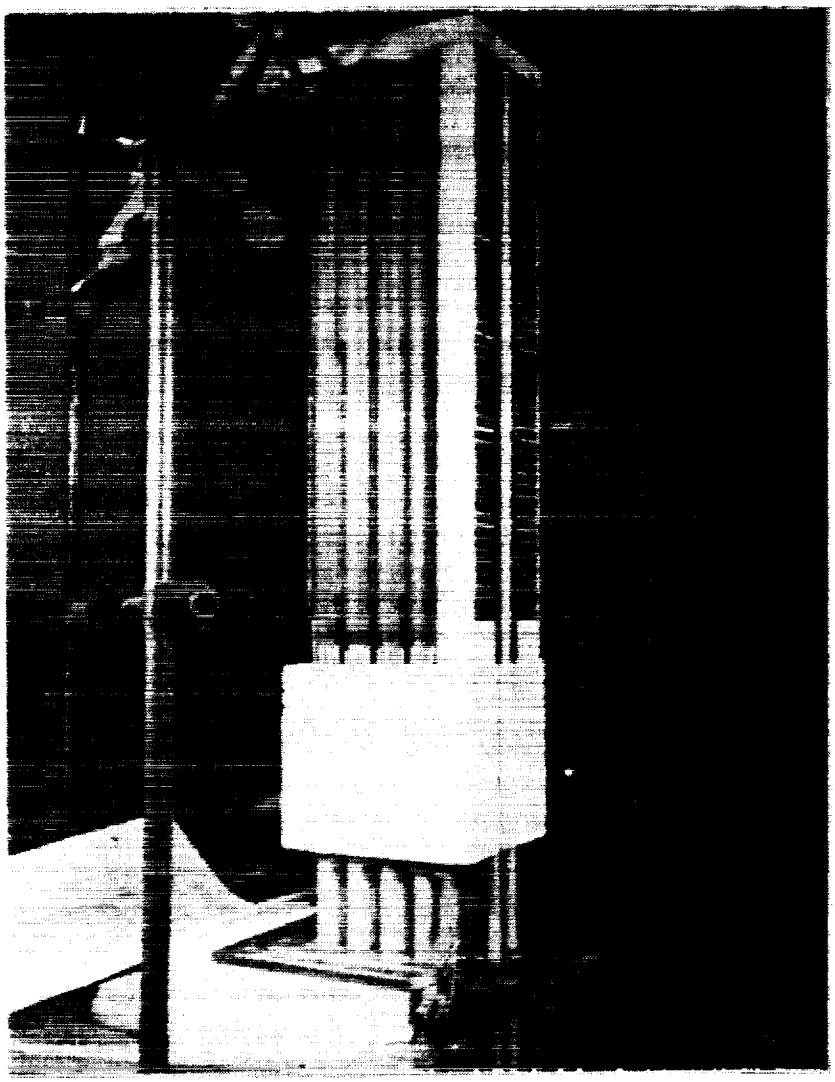

Figure 49. Cell Stack After Current Attachment and Cold-End Insulation Application

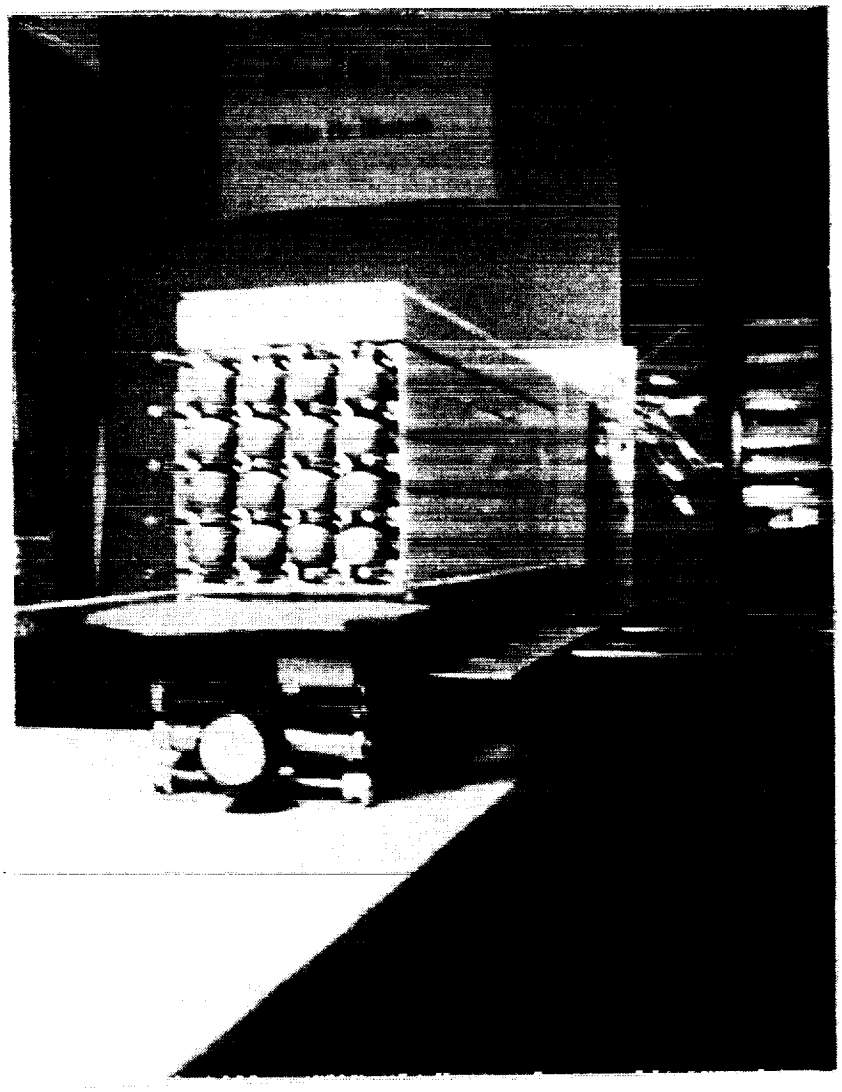

Figure 50. Stack Appearance After Application of Peripheral Palladium Tube Holders

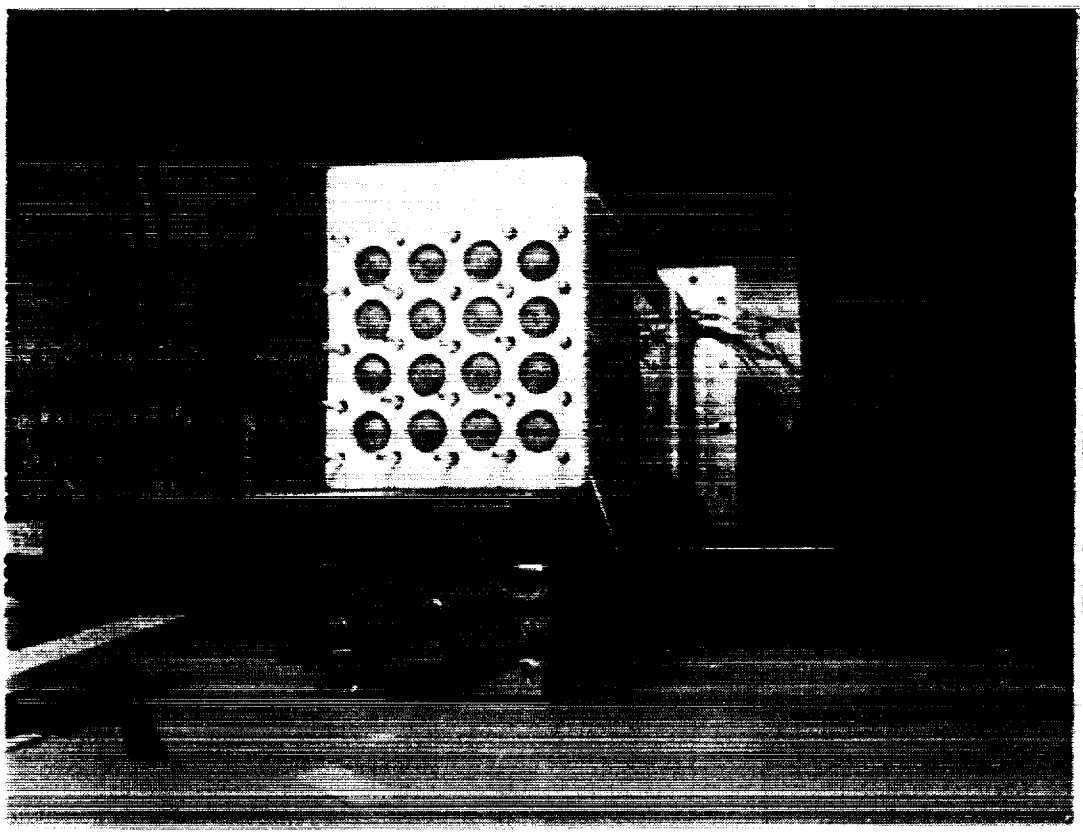

Figure 51. Positioning Board Installation of Stack Cell Ends

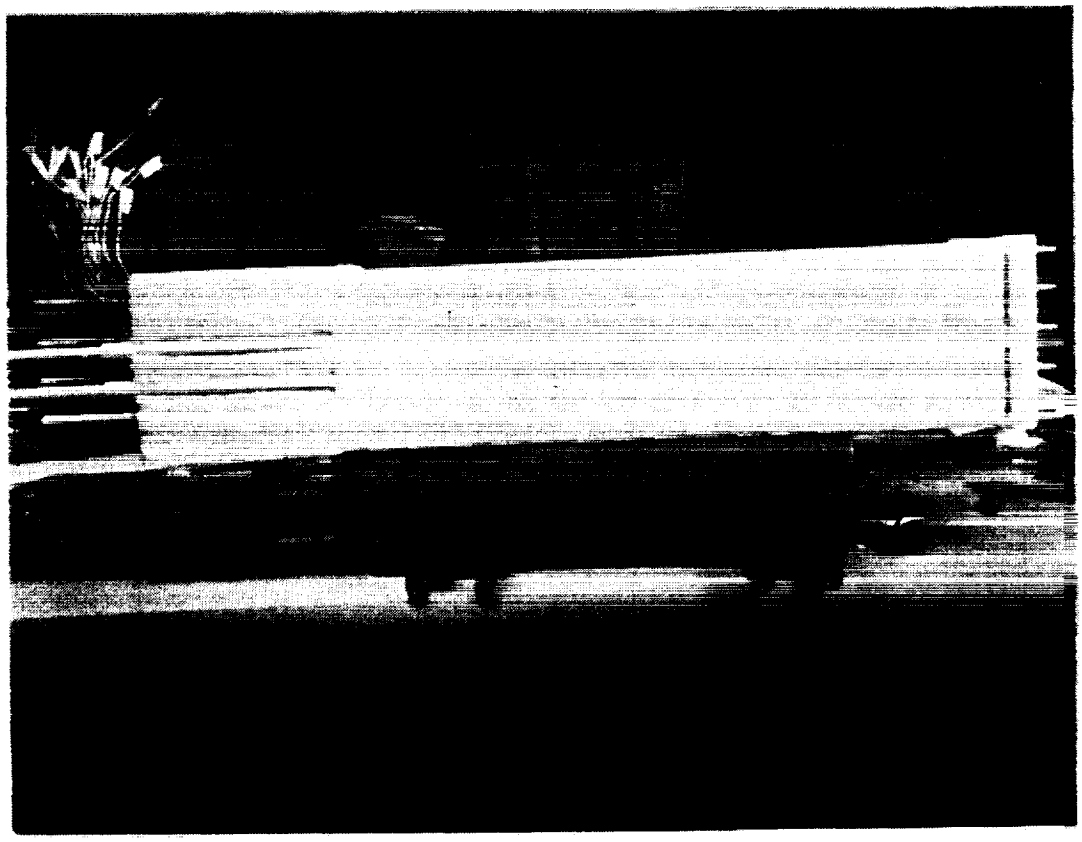

Figure 52. Stack External Appearance After Alumina Tile Application

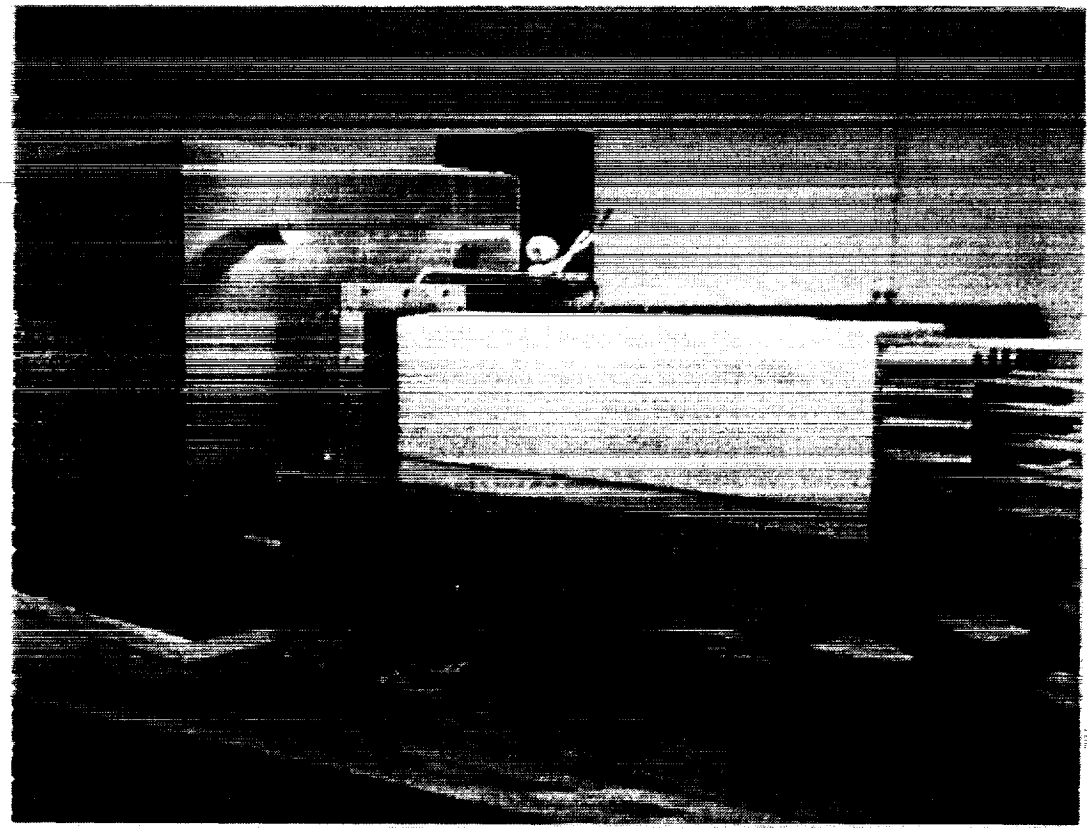

Figure 53. Stack Before Insertion Into Inconel 600 Canister

canister as shown in Figure 53 to determine the required thickness of Saffil alumina felt for the padding between the alumina tiles and canister wall. After applying a thin layer of alumina felt on each of the four stack sides, the cell stack was pushed into the canister. To facilitate guiding the cell stack into the canister, all the metal surfaces had been sprayed with a graphite coating (Aquadag) and nickel guide sheets (5 mil) were placed onto the four sides of the stack during insertion, in order to prevent the alumina felt from crumbling during the process of insertion. These sheets were withdrawn after the completed operation. A very snug fit between canister and cell stack was achieved. The insertion pressure, required to slide the bundle into the cannister was approximately 30-40 lb. (2-3 psi) which was applied uniformly to the open ends of the sixteen cell tubes.

4.2.2 Sealing and Contacting of Cell Stack

After stack insertion into the canister, the electrolyzer unit was positioned vertically so that the flange region faced upward. A 1/4 inch thick perforated silicon rubber sheet was pushed snugly over the cells and steel rods (see Figure 54). After this operation the perforated flange plate was placed over the cell tubes, steel rods (still positioned in place of the Pd tubes), and over the contact busbars. Also, seventeen 15 mil size insulated nickel wires, each of which contact one cell, were bundled together and placed through a hole in the flange plate. After this alignment operation the steel rods were withdrawn and replaced by the palladium tubes.

A moldable silicon rubber compound (RTV) was poured around the cells and the Pd tube extensions. The rubber penetrates the gaps around each tube and slightly bonds to the silicone rubber sheet behind the flange plate. Figure 55 shows this state of assembly. This method of sealing also insured the elimination of "hard" contact points between brittle ceramic and the steel flange plate.

The completion of the cold end of the cell stack included the epoxy-bonding of the metal adapters, which are shown in Figure 56, to the

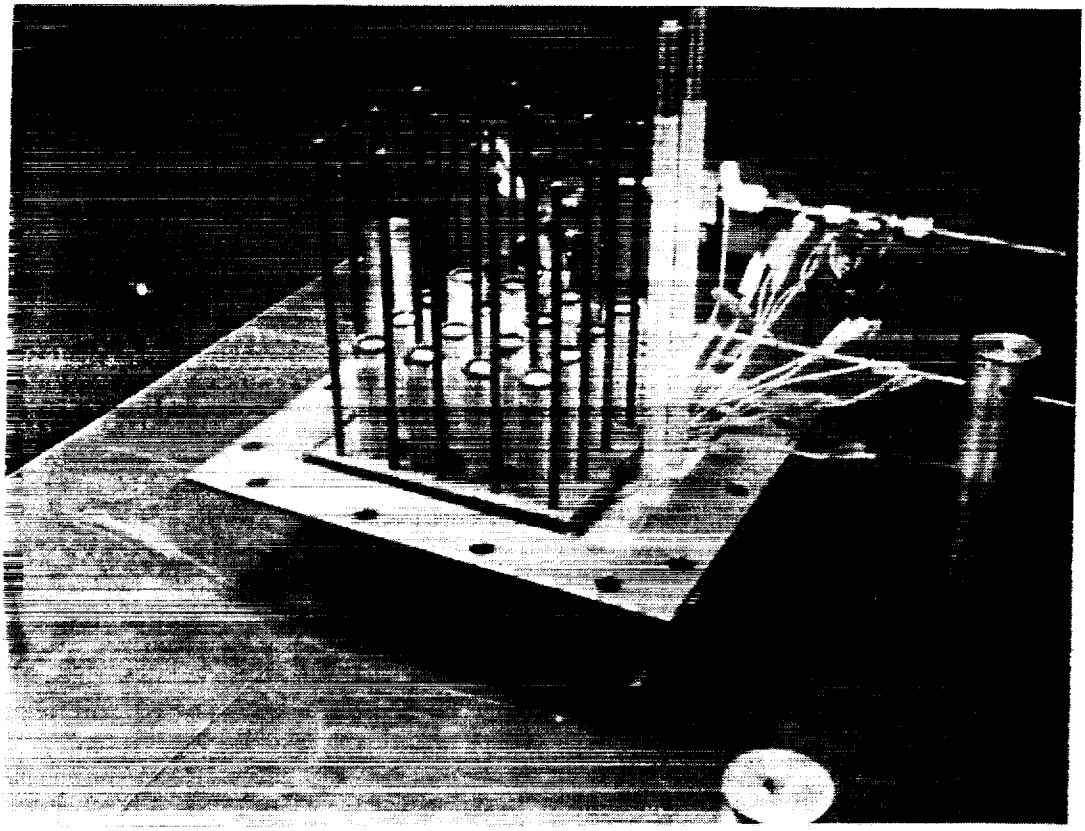

Figure 54. Stack End Appearance After Installation of Silicon Rubber Internal Seal

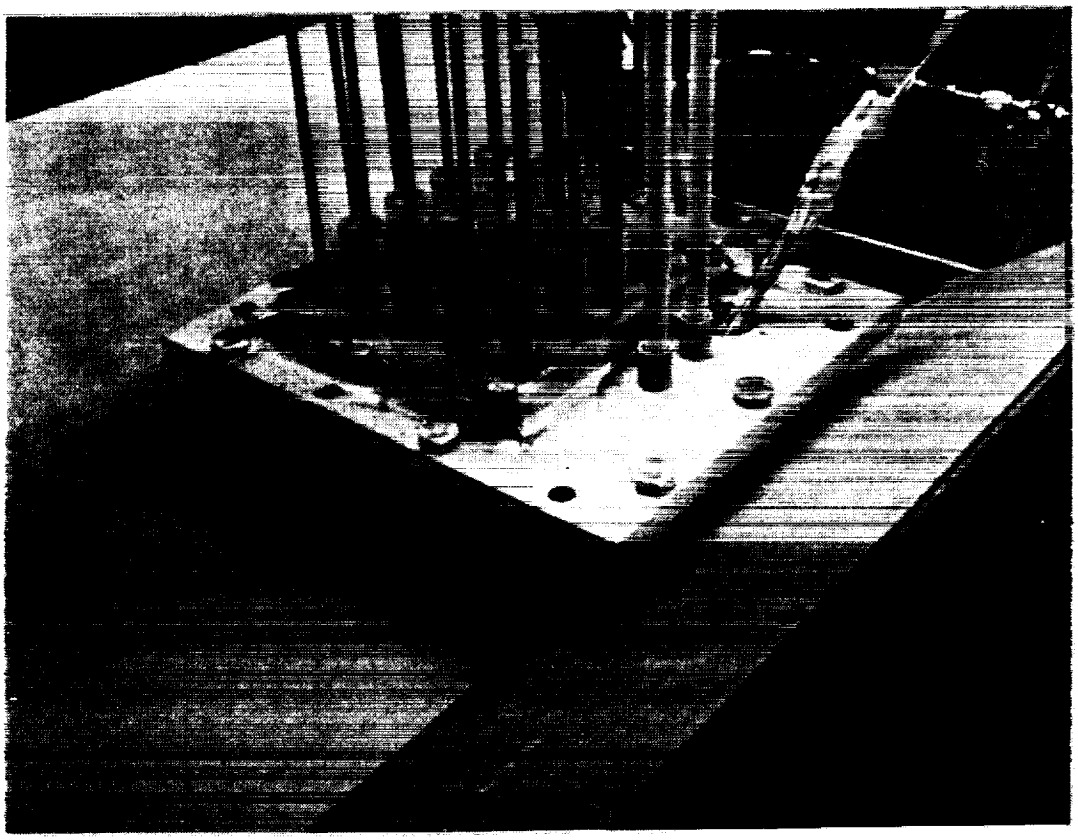

Figure 55. Application of External Silicon Rubber Seals

TITLE THREE MAN CO_2 ELECTROLYSIS BREAD BOARD
O_2 EXHAUST FITTING

DWG 4290B24 REV 1

ITEM	NOTE	PART NAME	DEF	(SIZE) REFERENCE INFORMATION	MATL SIZE CODE PART NUMBER OR REF DWG (N) R & D STK NO	GROUP NOTE / PROCESS OR LINE NO	GROUP 01	02	03	04	05
01		SLEEVE		1.15 OF .625 DIA SST TYPE 304	7305-1601		1				
02	A	TUBE	BOS	.75 OF .093 O.D. x .020 WALL 304 SST	TUBING		1				
03	B	UNION TUBE FITTING	BOS	SWAGELOK CAT NO SS-3-200-6			1				

NOTES:
A - PITTSBURGH VALVE & FITTING CO., PGH, PA
B - TUBE SALES, PROSPECT PLAINS RD. CRANBURY, N.J. 08512

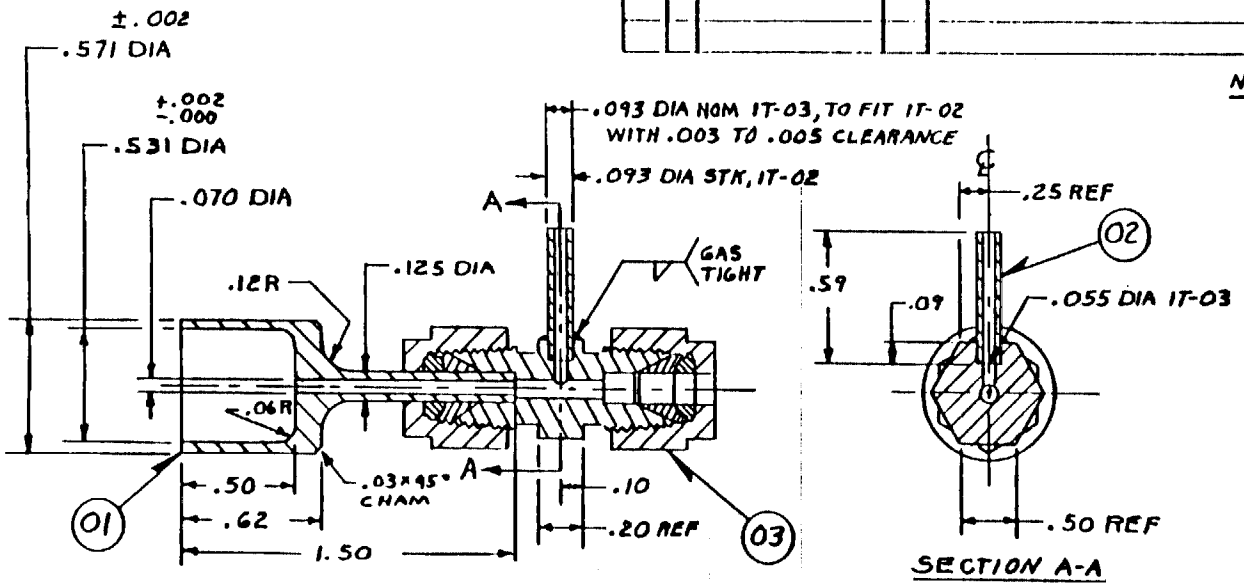

Figure 56. Metal Adapters For Oxygen Collection From Cell and For Insertion of Thermocouple Into Cell

NOTES:

1-MACHINE .375 NOM. DIA. (REF.) OF TUBE FITTINGS (ITEMS-01 & 021 TO GIVE A DIAMETRAL CLEARANCE OF .001 TO .002 TO BORE OF BELLOWS (ITEM-031 PRIOR TO JOINING.
2-BRAZE JOINTS TO BE GAS TIGHT.
3-REMOVE "O"-RINGS FROM FITTINGS (ITEMS-01 & 021 DURING BRAZE OPERATION.

TITLE THREE MAN CO_2 ELECTROLYSIS BREAD BOARD
POWER LEAD EXPANSION SEAL
DWG 4290B04 REV 1

ITEM	NOTE	PART NAME	DEF	(SIZE) REFERENCE INFORMATION	MATL SIZE CODE PART NUMBER OR REF DWG	GROUP NOTE / PROCESS OR LINE NO.	GROUP 01	02	03	04	05
01		TUBE FITTING	DWG.		4290B03H01		1				
02		TUBE FITTING	DWG.		4290B03H02		1				
03		BELLOWS	DWG.		4281B03H01		1				
04	A	SILVER BRAZE		EASY-FLO			AS REQ'D				

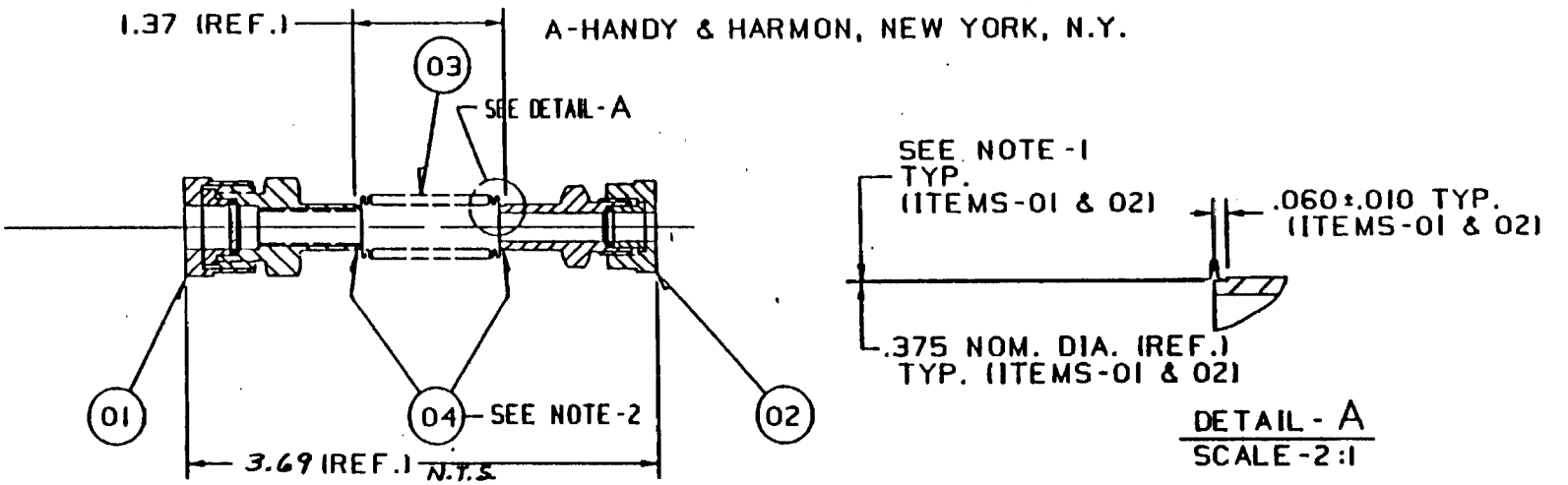

Figure 57. Power Lead Expansion Seals

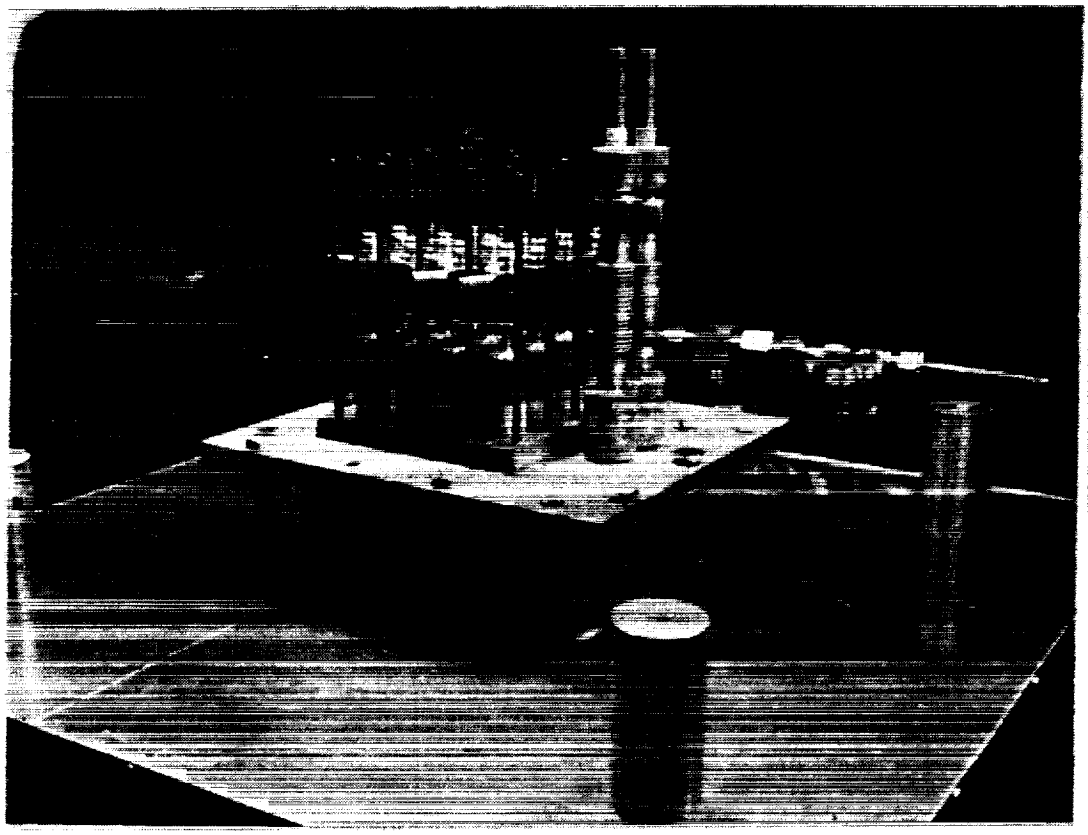

Figure 58. Electrolysis Stack Cold End Appearance After Completion of Sealing

open end of the cell tubes for oxygen manifolding; the sealing of the busbars against the flange plate with metal bellows, seen in Figure 57; and the insertion of the sealed connection plug into the flange plate. Figure 58 shows a photograph of the completed cold-end assembly.

4.2.3 Mounting of Electrolysis Stack

The electrolysis unit was lifted into the breadboard enclosure and secured on an alumina support plate in such a way that the cold flange plate as well as the 2 inch long legs of the outer insulation housing rested on the same support surface. The stack flange plate was fastened to the alumina plate with fourteen nuts and bolts. Figure 59 shows a photograph of the breadboard assembly, showing the electrolysis unit on the left side.

The electrolysis unit was then connected to the A.C. control unit, as well as to the D.C. power terminals. The feedgas connection was attached with 1/4 inch Swagelock compression seals via a flexible (bellow) metal hose. The oxygen outlet of each cell was connected via silicone rubber hoses to a metal tube manifold that is connected to a mass flowmeter; the Pd diffusion tube outlets were connected via tygon tubing to a metal tube manifold that is connected to a mass flowmeter on the low pressure side of the vacuum pump. The installed and manifolded cold end assembly is seen in the photograph of Figure 60.

4.3 Auxiliary Breadboard Subsystems and Components

The following sections deal with the breadboard subsystems that are required to operate the electrolysis unit in reliable, simple, and safe fashion, and which allow also the testing of the unit under off-design operational conditions. Function, equipment, data handling (DHS) interfacing, and malfunction response of the subsystems are described and shown in schematic block diagrams. The total breadboard systems overview is shown in Figure 61.

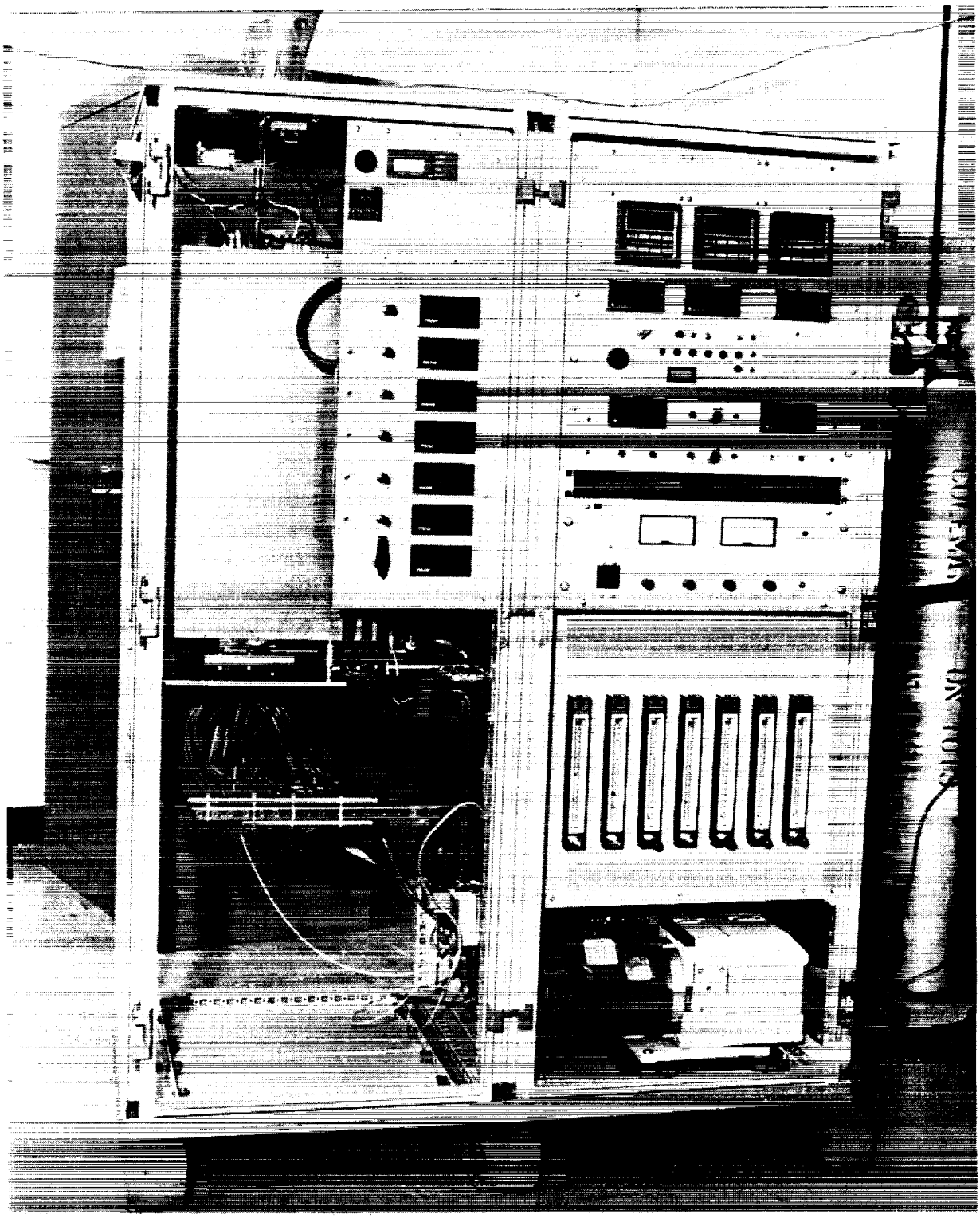

Figure 59. Electrolysis Unit Mounted in Breadboard

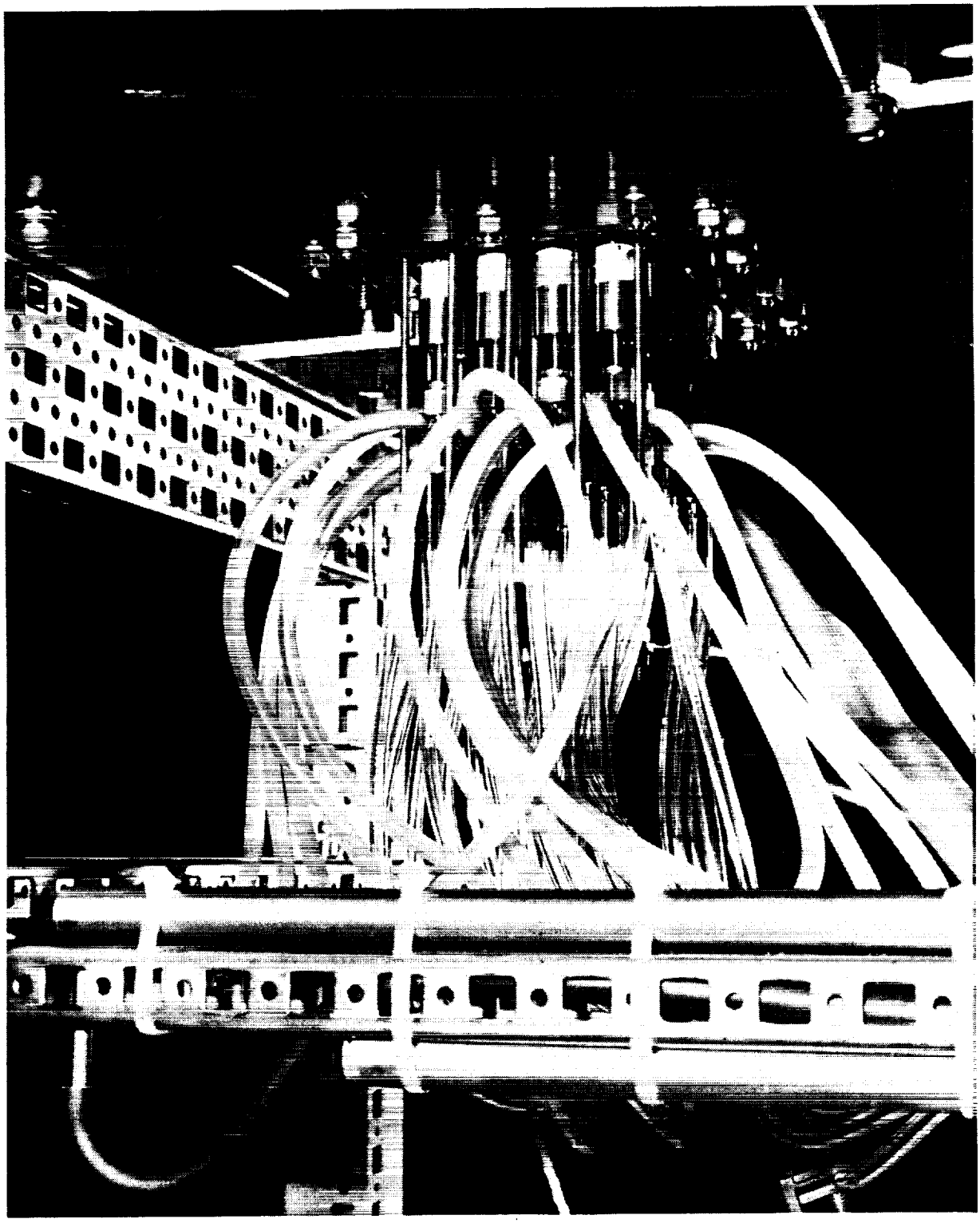

Figure 60. Electrolysis Cell Oxygen Manifold and Palladium Tube Hydrogen Manifold View

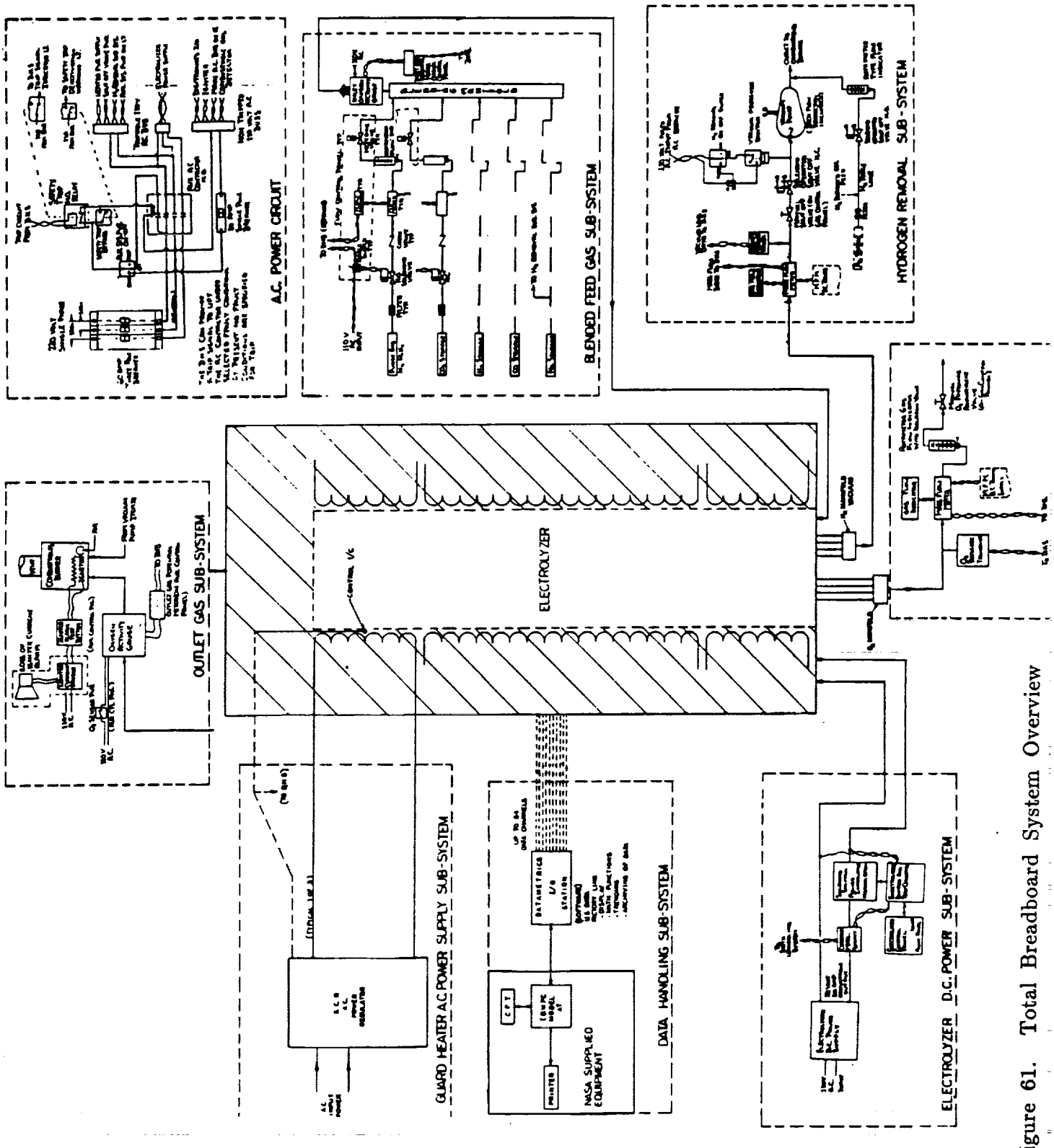

Figure 61. Total Breadboard System Overview

ORIGINAL PAGE IS
OF POOR QUALITY

4.3.1 Electrolyzer D.C. Power Subsystem

Figure 62 shows the schematic arrangement of components in this subsystem, which is characterized as follows:

Function:	Supplies and regulates the dc power required by the electrolyzer.
Equipment:	This subsystem includes an H.P. dc power supply (25 volts - 30 amperes - controllable for either constant voltage or current), a 24 volt dc current interrupter, a 50 amp shunt and control and meter interfaces.
DHS Interface:	The dc output current and voltage is recorded by the DHS.
Malfunction Response:	Should the dc power supply system fail, the electrolyzer will automatically be open circuited and the electrolyzer current trip light will come on.

4.3.2 Oxygen Product Subsystem

Figure 63 shows the schematic arrangement of components in this subsystem, which is characterized as follows:

Function:	Oxygen product collection subsystem.
Equipment:	The subsystem includes the tubing, manifolds, mass flow meter, valving and pressure transmitter needed to collect, meter, and pressure-regulate the product O_2 stream.
Interface:	The O_2 pressure transducer and mass flow meter ties in the the DHS for data recording.
Malfunction Response:	When the O_2 pressure rises or falls out of a preset range the DHS can initiate a trip of the experiment, sound an alarm and display a message pertaining to the fault or the CRT.

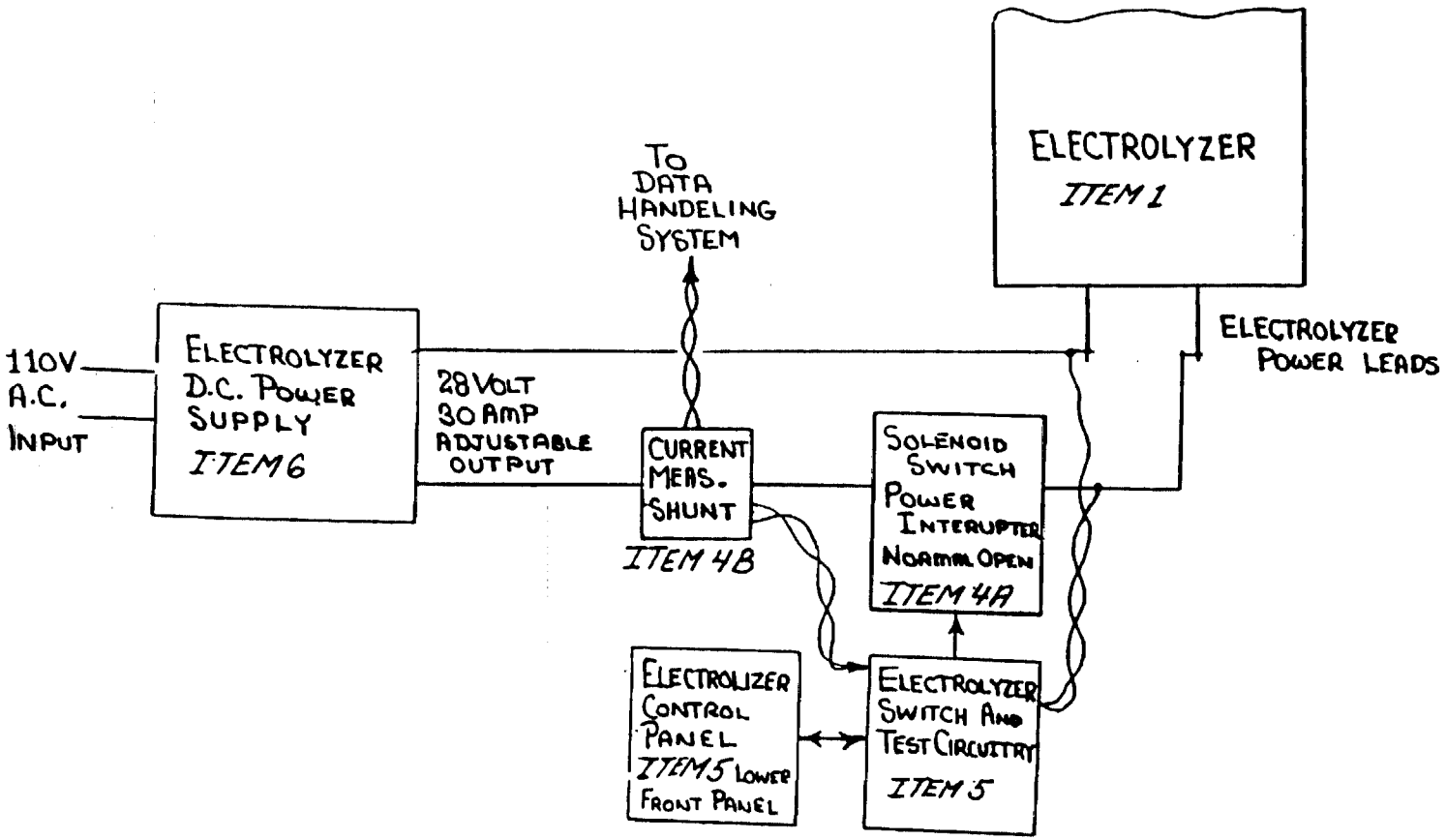

Figure 62. Electrolyzer D.C. Power Subsystem

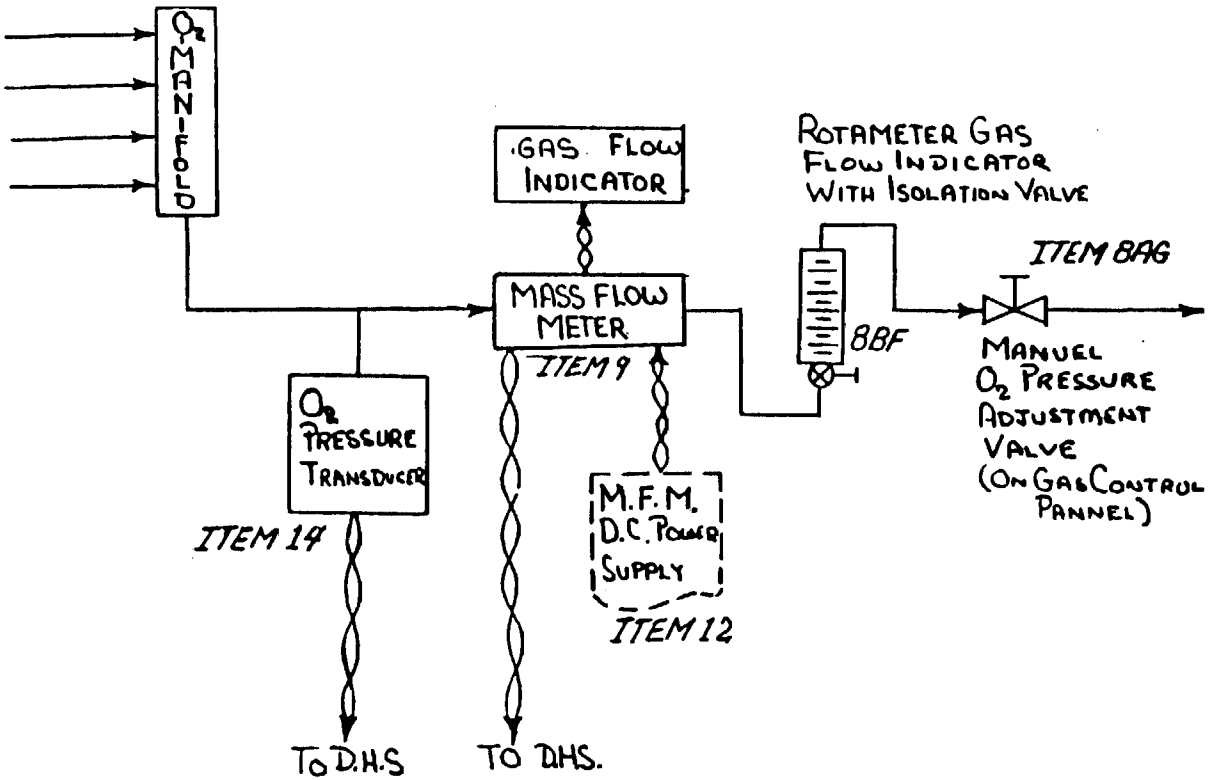

Figure 63. Oxygen Product Subsystem

4.3.3 Blended Cathode Gas Subsystem

Figure 64 shows the schematic arrangement of components in this subsystem, which is characterized as follows:

Function:	Provision of blended cathode feed gases (CO_2, CO, H_2 and N_2) to the electrolyzer, supply purge gas (N_2) to the electrolyzer system, and delivery of reducing cover gas for the electrolyzer cathodes, (N_2/H_2).
Equipment:	Each gas specie flow stream is provided with a mass flow meter, and a small rotameter in series for visual flow rate inspection. Each flow stream is connected to a common manifold and is controlled by a manually operated metering valve. Each flow stream contains a 110 volt a.c. solenoid valve for emergency shutdown. All gas species can be supplied from storage cylinders through a pressure regulator, (~30 psig).
DHS Interface:	All flow meter outputs (0-5 V d.c.) are recorded in DHS and are continuously displayed on digital panel meters in engineering units (liter per minute).
Malfunction Response:	Nominal operation for each gas flow will be programmed into the DHS. Anomalous outputs will trigger visual alarms and in the case of irregularities in the CO_2 flow, the DHS will initiate a shut down of the equipment. The reason for any alarm will be displayed on the CRT for all situations.

4.3.4 Outlet Cathode Gas Subsystem

Figure 65 shows the schematic arrangement of components in this subsystem, which is characterized as follows:

Function:	Conduct exhaust gas out of the electrolyzer and safely burn any reducible by-products (CO and H_2) of the experiment.

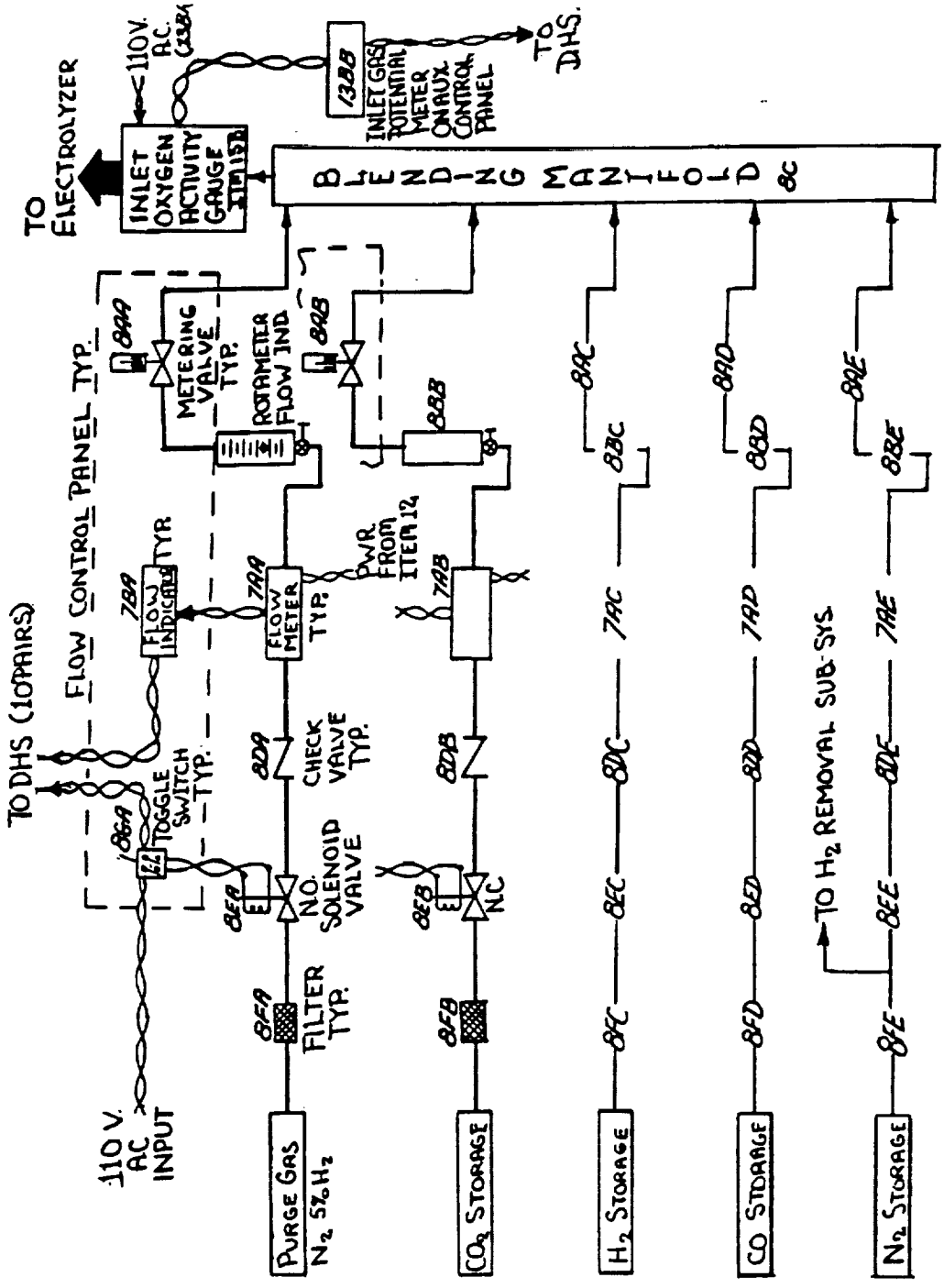

Figure 64. Blended Cathode Gas Subsystem

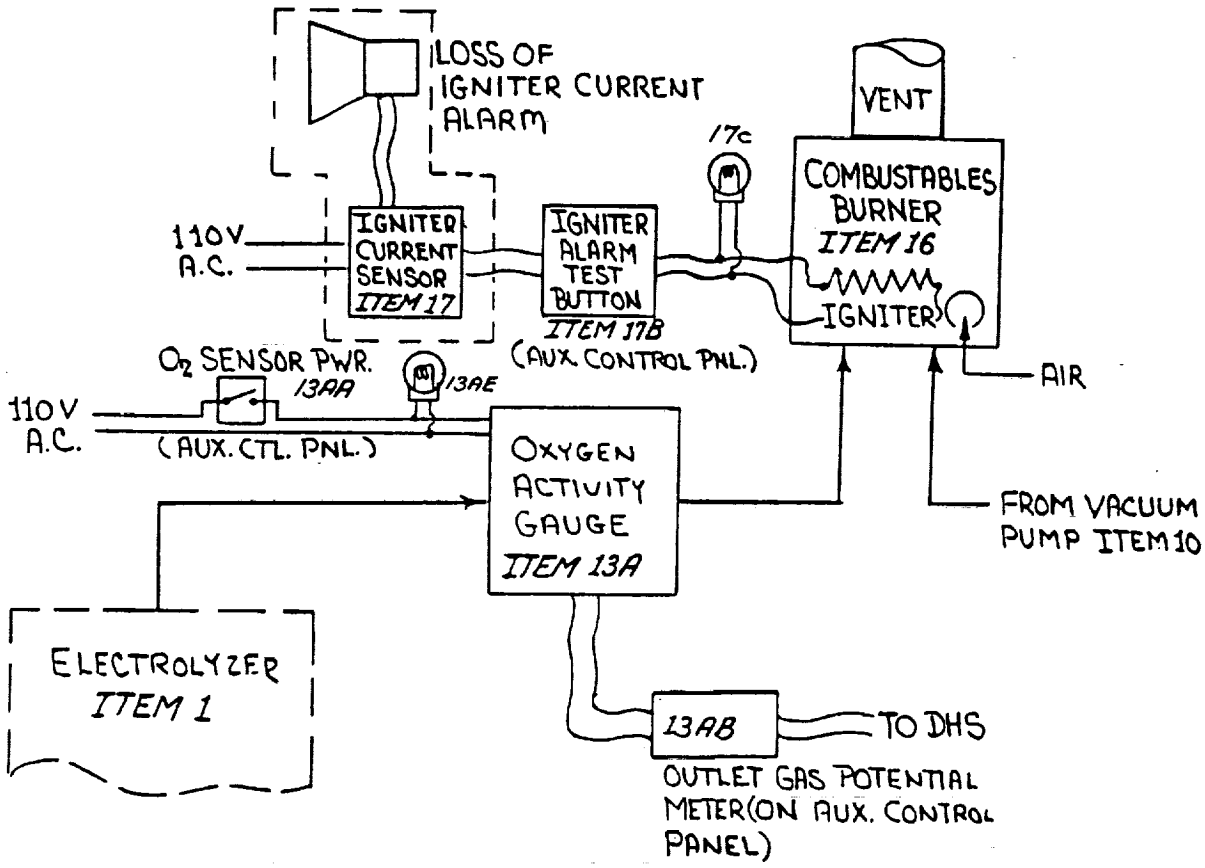

Figure 65. Outlet Cathode Gas Subsystem

Equipment: Plumbing, and burner with an electric ignitor (silicon carbide). An oxygen activity gauge measures a small side stream of the exit gas before combustion.

DHS Interface: The signal from the oxygen activity gauge, which indicates the degree of cathode gas conversion is displayed by a millivolt reading on the front panel meter. The millivolt signal is transmitted to the DHS for a permanent record.

Malfunction Response: Ignitor failure will cause an alarm to sound, to indicate that combustibles can be emitted should the combustibles content of the exit cathode gas be low and be insufficient for a self-sustaining flame.

4.3.5 Hydrogen Removal Subsystem

Figure 66 shows the schematic arrangement of components in this subsystem, which is characterized as follows:

Function: Continuous hydrogen gas removal from the active region of the electrolyzer.

Equipment: Evacuated palladium tubes are positioned in between the electrolysis cells (25 in number). Vacuum hoses connect each palladium tube to a vacuum manifold. A vacuum pressure switch is connected to the vacuum manifold piping to shut the system down due to either a palladium tube failure or a failure of the vacuum pump. A Tylon mass flow meter monitors the flow and transmits the information to both a gas flow indicator and to the DHS. The manifold can be isolated from the vacuum pump by both an automatic shut off valve or a manual shut off valve. The manifold pressure is measured and transmitted to the DHS by a vacuum pressure transducer. A supply line from the nitrogen gas supply will provide a purge gas flow on the subsystem for shut down.

DHS Interface: This subsystem will interface with the DHS providing both flow and pressure signals.

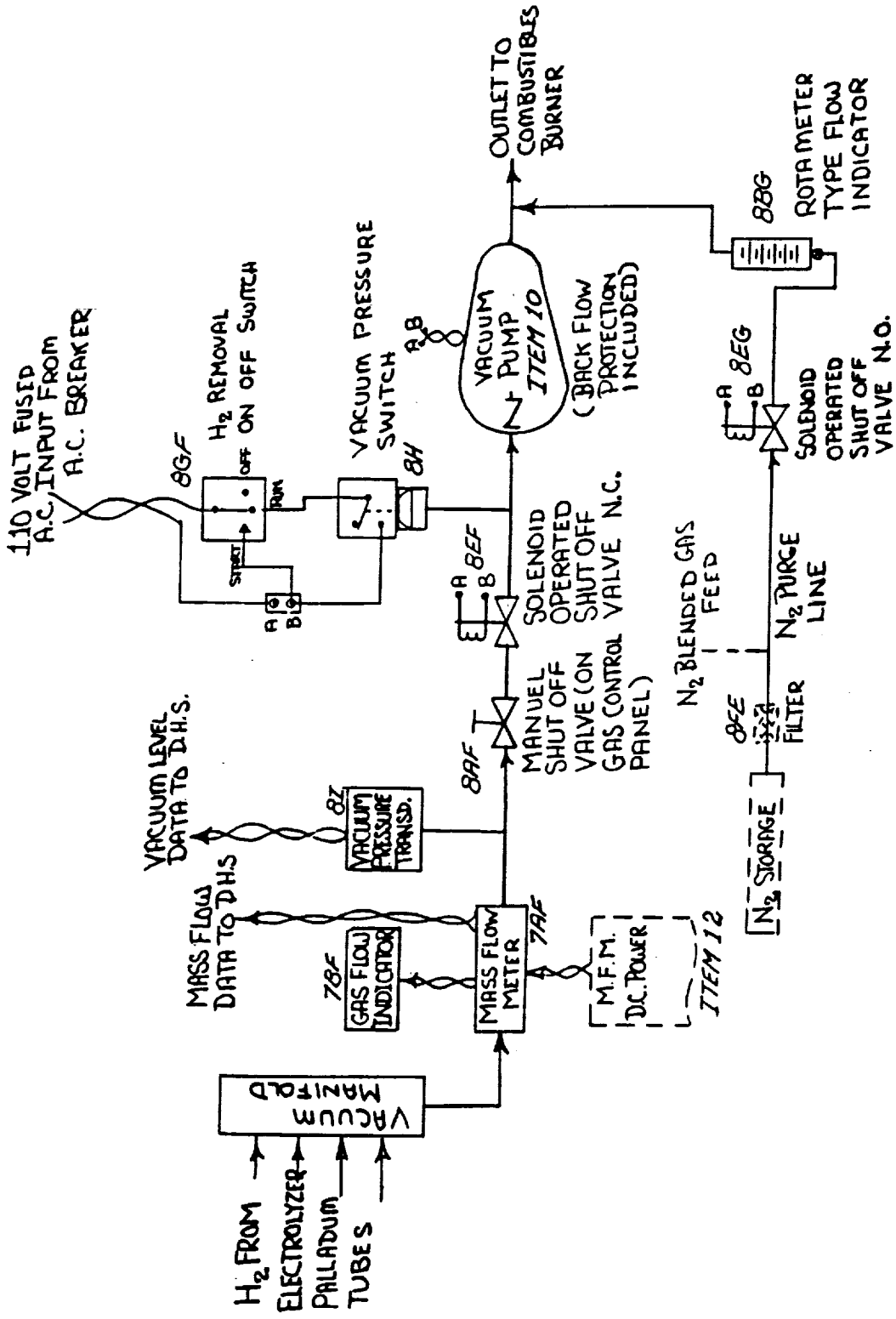

Figure 66. Hydrogen Removal Subsystem

Malfunction: A loss in vacuum (an increase in pressure) beyond a preset value (15mm Hg) will result in shut down of this subsystem. Data on the shutdown from this subsystem is not provided through the DHS.

4.3.6 Electrolyzer Heater Power and Control Subsystem

Figure 67 shows the schematic arrangement and electrical connections of components in this subsystem, which is characterized as follows:

Function: Cell stack heaters on an A.C. power supply.

Equipment: This subsystem includes the 120 V.A.C. power controllers, control thermocouples (Pt/10% Rh-Pt) and light weight resistance heaters which are required to control the three-zone active region of the electrolyzer and supply some heat for the process.

DHS Interface: The control thermocouples are also monitored by the DHS to sense over temperature or an open circuit.

Malfunction Response: The DHS can trip the DC power to the electrolyzer and print out a fault message on the CRT if out or range condition anomalies are encountered.

4.3.7 A.C. Electrical Power Requirements

Figure 68 shows the schematic arrangement and electrical connections of components in this subsystem, which is characterized as follows:

Function: To supply 220 volt A.C. power to run the experiment and to interface with the DHS to provide an interruption (trip out) capability when a significant fault is diagnosed in the experiment by the DHS.

Equipment: A main power circuit breaker and a solenoid operated contactor is wired and switched to trip

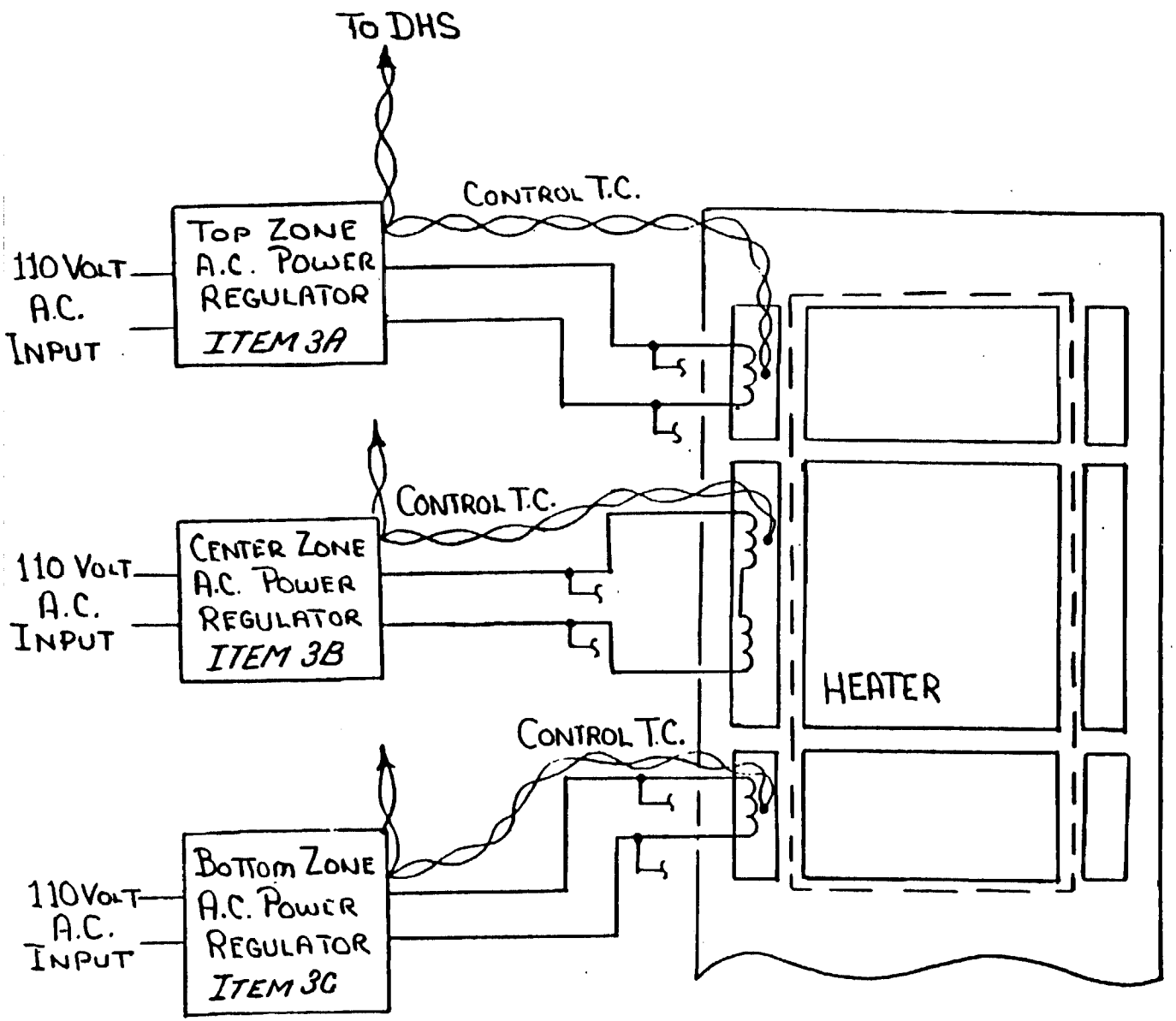

Figure 67. Electrolyzer Heater Power Unit Control Subsystem

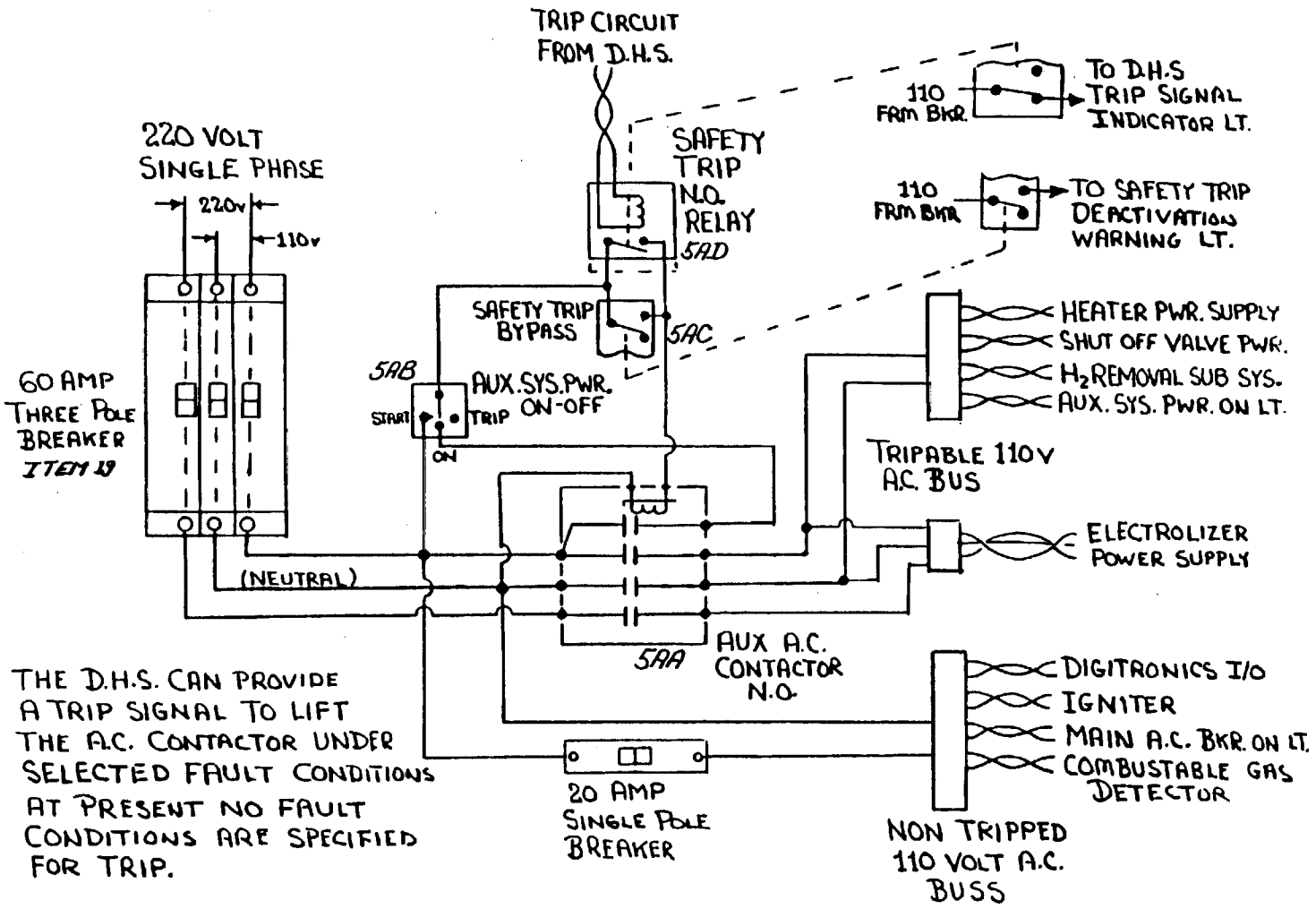

Figure 68. A.C. Electrical Power Requirements

out the A.C. power to selected components on a signal from the DHS.

DHS Interface: The DHS will supply a signal to maintain the contactor in the closed position. In the event of a condition that the DHS determines a serious fault, the signal will be interrupted and the contactor will open, shutting off power to most of the breadboard components and causing it to shut down.

Malfunction Response: This system is not monitored by the DHS. A current draw of over 60 amp will cause the main breaker to open.

4.3.8 Data Handling Subsystem (DHS)

Figure 69 shows the schematic of the DHS components of the subsystem which is characterized as follows:

Function: Data monitoring and acquisition display and storage subsystem.

Equipment: Digitronix compact I/O station coupled to an IBM dedicated PC. This system is configured to handle up to 64 instrument channels. U.S. Data Corp. factory link software for data display and trending is supplied.

DHS Interface: This data system interfaces with all of the other subsystems in the unit.

Malfunction Response: A malfunction of this data handling subsystem will alarm operator to reactivate or replace functional hardware. Breadboard shutdown is not required if the DC power supply shows unchanged voltage and current reading and temperature control is operating. However, the safety trip will be inoperative.

4.3.9 Oxygen Activity Meters for Cathode Gas

Figure 70 shows the oxygen activity meter as it is attached to the side of the electrolysis unit outer housing. The small furnace contains a

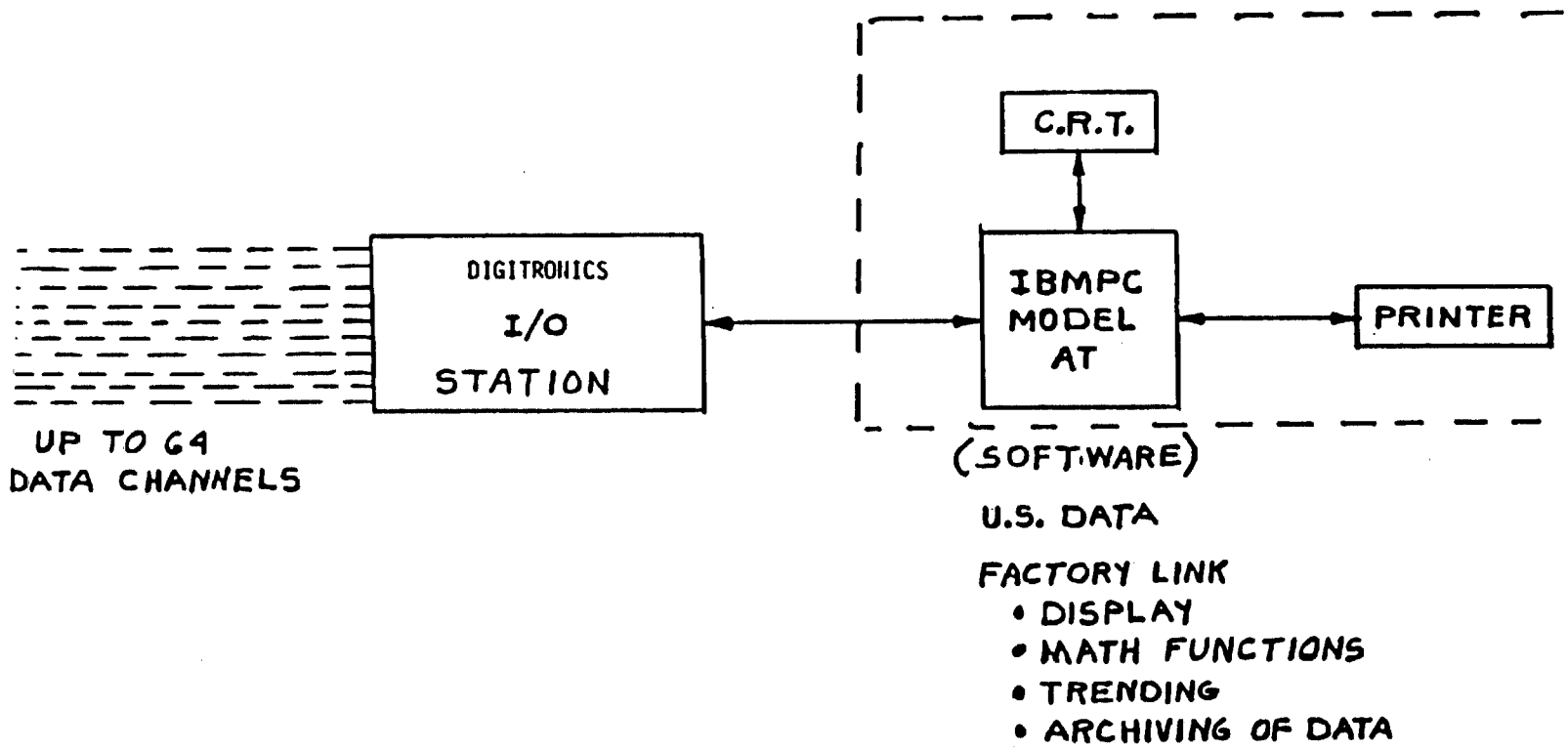

Figure 69. Data Handling Subsystem (DHS)

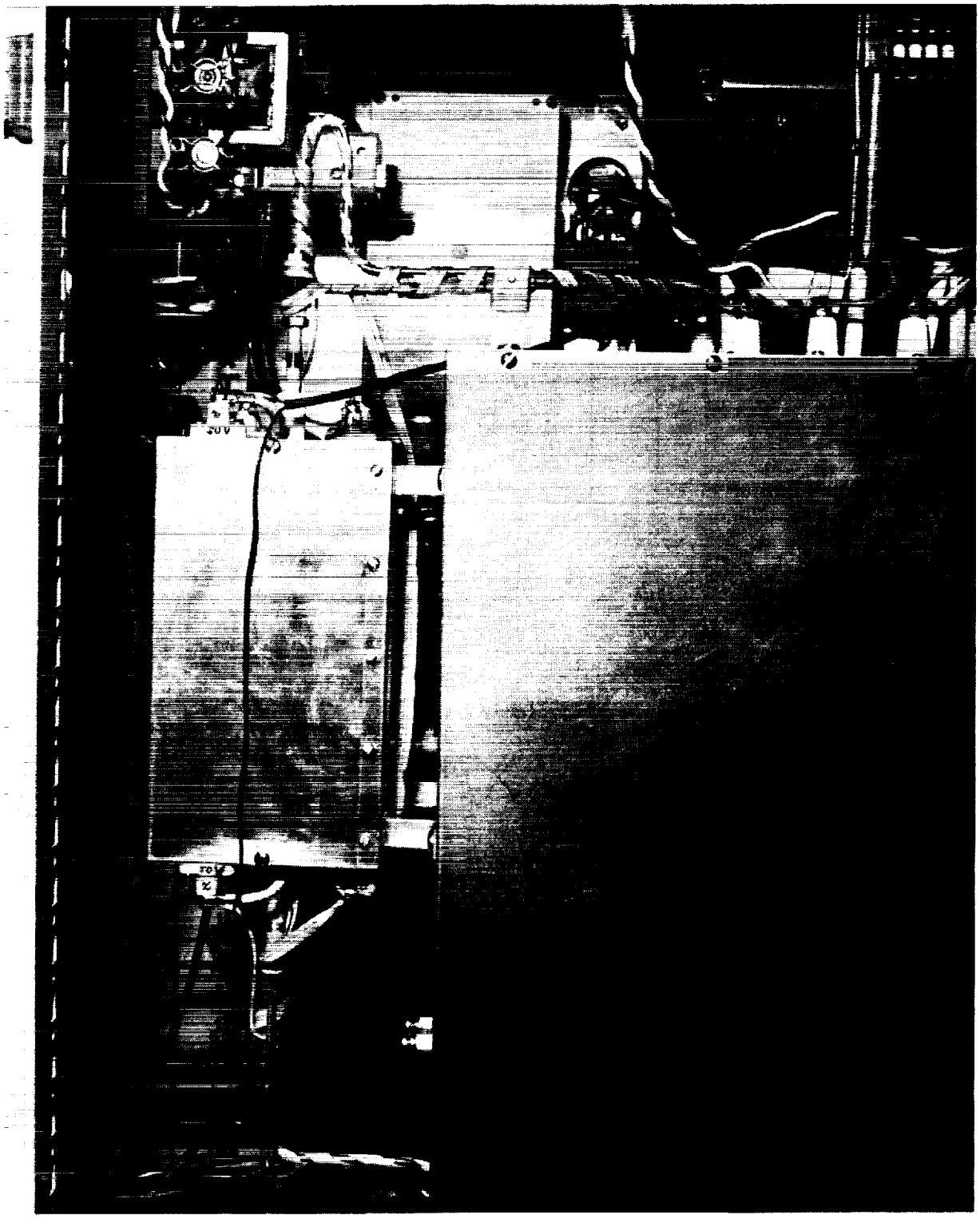

Figure 70. Oxygen Activity Meter For Inlet (Lower Sensor) and Outlet Cathode Gas (Upper Sensor).

1/2 inch diameter single zone heater tube of 5 inch length, which is controlled with a small Omega microprocessor power controller at 900°C. The furnace contains two closed-end tubular zirconia sensing elements of the type:

platinum (cathode gas)/stabilized zirconia/platinum (air)

The two sensor tubes face each other axially in the furnace with the closed ends toward each other. A pair of electrodes each are applied to the inside and the outside end of the zirconia tubes. A small stream of inlet cathode gas flows through one zirconia sensor tube and a small stream of outlet cathode gas flows through the other zirconia sensor tube. The small inlet stream to the sensor is returned to the main stream of the feed gas and is not lost.

The measured electromotive force (EMF) of each sensor is indicated in volts at front panel meters and is transmitted to the DHS. The measured voltage is an independent indication of cathode gas conversion according to the Nernst equation (15):

$$E = \frac{RT}{nF} \ln \frac{[O_2]\ \text{air}}{[O_2]\ \text{cathode gas}} \qquad (15)$$

where E = EMF in volt

R = universal gas constant, 1.9865×10^{-3} kcal x $^{\circ}K^{-1}$ x mol^{-1}

T = temperature in degree Kelvin

n = number of electrons per mole of O_2 (4)

F = Faraday number, 23.06 kcal x $Volt^{-1}$ x mol^{-1}

[ ] = oxygen partial pressure

From equations (3) and (7) one calculates the oxygen partial pressure from the equilibrium constants k of these reactions

$$k_1 = \frac{[CO]^2 x\ [O_2]}{[CO_2]^2} \qquad (16)$$

$$k_2 = \frac{[H_2]^2\ x\ [O_2]}{[H_2O]^2} \qquad (17)$$

In mixtures of H_2 and CO_2 the thermodynamic equilibrium is established at 900°C in the presence of significant amounts of finely divided nickel (cathodes) and that the oxygen activity of the H_2/H_2O ratio is identical to that of the CO/CO_2 ratio. The k-values are tabulated (JANAF-Tables or other).

The oxygen partial pressure in the cathode gas, therefore, becomes an expression for the amounts of the other reactants in the cathode gas inlet- and outlet-steams. The measured EMF is converted into atmospheres of oxygen by the DHS and is recorded as such. The calculation of gas composition must be done separately, using the measured inlet cathode gas flow ratios and equations 15, 16, and 17. Inert gas content in the cathode gas such as nitrogen does not affect the calculations of the equilibrium concentrations of CO, CO_2, H_2, and H_2O.

4.3.10 Completed Breadboard

The completed breadboard is shown in Figure 71. The housing is made of two combined units purchased from RITTAL CO having removable side walls and ceilings. There are two doors at the front and two at the back side. A swing out rack for the data acquisition system (back side) allows easy access to signal wiring boards. All internal plumbing is hard soldered or compression fitted, using soft copper and stainless steel tubing.

Acrylic windows are mounted over the control panels on both front doors which can be locked. In Figure 71 the major breadboard components can be seen. The vacuum pump is mounted on the lower right. The AC-heater control panel is at the top right. The second top right panel shows both oxygen meter outputs and the meter temperature; furthermore, this panel contains switches and indicators for startup and shutdown. Below this panel is the electrolyzer load control, showing current and voltage readouts as well as cut-off voltage selectors, all of which is functionally integrated with the DC power supply below (fourth panel). The group of rotometers above the vacuum pump provide visual flow indication only. They are connected in-series with mass flowmeters, positioned behind the panel. Mass flowmeter readouts are shown on the left side vertical panel of the breadboard, associated with needle valves to regulate gas flows and solenoid valve switches. At the bottom of this panel is a larger ball-valve which connects the palladium tubes to the vacuum. The combustibles alarm and oxygen meter control are at the top of the panel. The space under the electrolyzer unit is free for working on the gas manifolds, cells and for insertion of thermocouples into the cells.

4.4 Breadboard Testing

The test phase duration was 28 days including heat-up and shut-down procedures. This time period can be subdivided into three major activities, namely:

- Heat-up and familiarization with breadboard functions.
- Electrolyzer performance tests.
- Establishment of proper data acquisition and data display.

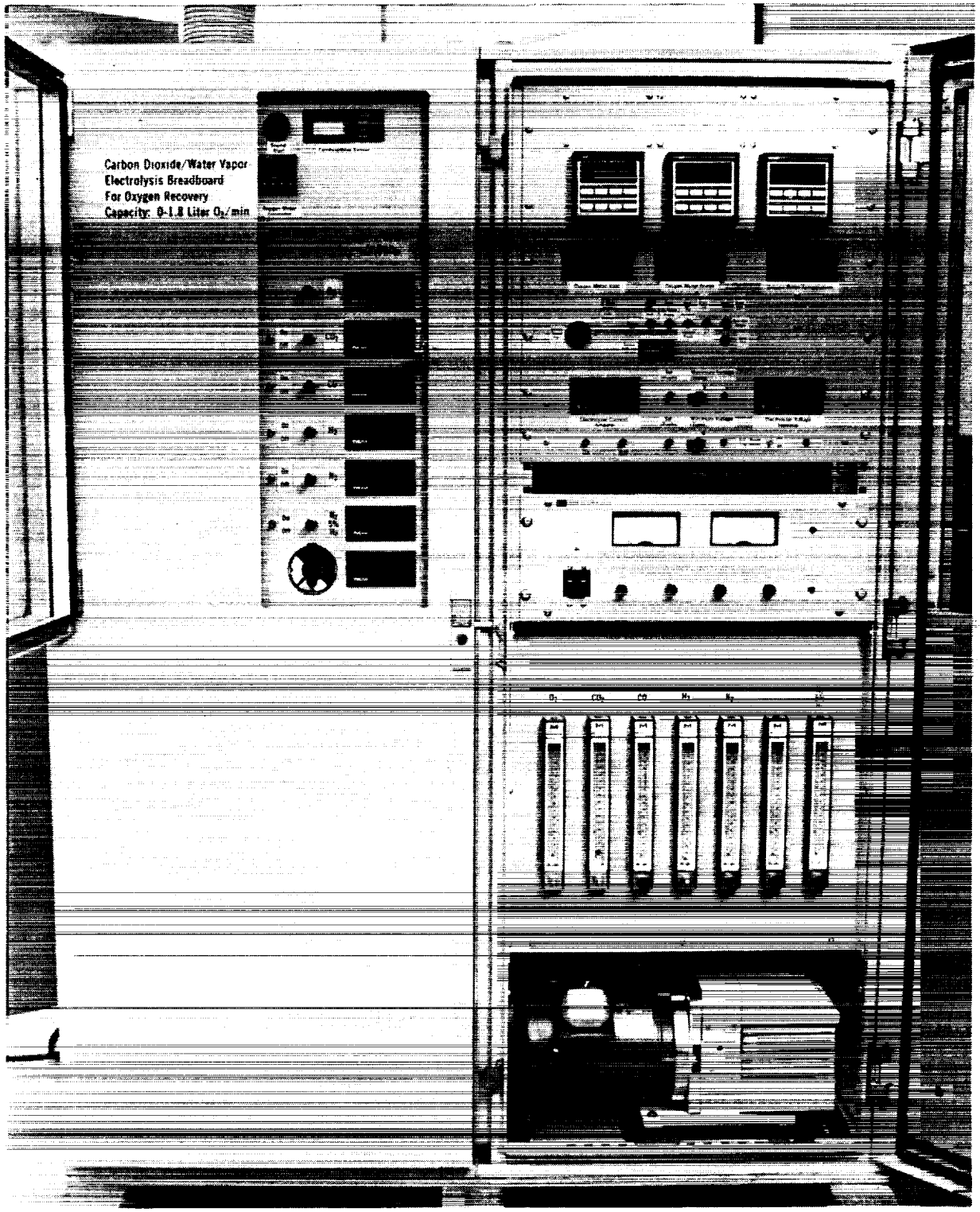

Figure 71. Completed Breadboard.

4.4.1 Start of Breadboard Operation

The first heat-up of the sixteen cell stack was performed with mixed gas flow of N_2, CO_2 and H_2 on the cathode side in order to effectively remove organic residue from temporary adhesives which were used during the assembly of the stack components inside the canister. This included the polyvinyl alcohol (PVA) binder for nickel-felt contacts and binder tapes for alumina tiles on the stack periphery. After all volatile organic material and carbon residues are burned and have oxidized to CO_2 which is complete between 700°C and 800°C, the metallurgical bonding between nickel felts, electrodes, power contacts, and Pd tube holders takes place. This bonding is caused by the sintering of the nickel felts to each other and to the outside cell cathodes which leads to a coherent cell bundle structure.

During heat-up a small current (~250mA) was passed through the cells, starting at 500°C. The current was raised during a four hour heat-up period to 25 ampere at 900°C, while limiting the cell voltages to less than 1.3V per cell as a maximum. The passage of the low current produces a small amount of oxygen at the anode which protects the oxide material of the anode from being slowly reduced by leakage currents of opposite polarity or potential leaks when remaining in the open circuit mode. This is only a precaution and does not imply that reduction is actually taking place in any significant way. The CO_2-concentration in the cathode feed gas mixture was increased in order to sustain the 25 ampere current. The total heat-up time was 6 hours. No major problems were encountered during the heat-up period. The palladium tubes were evacuated during the entire period and the cell stack was maintained at or near 900°C for a 26 day period. Due to an early failure of two controllers, the A.C. power leads were quickly transferred to transformers, (variac), without considerable temperature excursions. The transformers were used for temperature adjustments during a 2-day period until being replaced by functioning controllers. The electrolyzer could be operated during this time period without major difficulties.

After the electrolyzer temperature had reached thermal equilibrium at 900°C, the "design"-cathode gas was introduced, which consisted of 80% CO_2 and 20% H_2. Immediately upon hydrogen reaching the active electrolyzer zone the massflow meter for H_2 indicated the diffusion of H_2 through the Pd tubes. The H_2 flow was not measured before this point since a very low H_2 concentration was used in the cathode feed gas (1-2%) during the heat-up period. The recovery of the H_2 from the cathode gas was 53 percent efficient at a feed gas inlet rate containing 1.0 liter H_2/min. The recovery rate of H_2 depends on the H_2 partial pressure difference between the cathode gas side and the evacuated Pd tube inside. In a preceding independent test (see section 4.1.2.1) the H_2 recovery rate was measured at 900°C for a single Pd tube, having an equivalent flow of a 80/20-N_2 mixture on the outside but with varying H_2 pressure on the inside. The H_2 recovery rate was determined to be 50% at 36mm Hg pressure and 60% at a fraction of 1mm Hg pressure on the Pd tube inside, respectively. The single tube test was executed while having a uniform temperature profile over the entire tube length. The Pd tubes in the electrolyzer unit, however, operate with 20 percent of their length at a nearly linear temperature gradient of 350° to 850°C and a somewhat lower H_2 recovery rate is expected. The measured 53 percent H_2-recovery rate for the electrolyzer stack, therefore, falls well within the expected performance range. After a few hours of observation of the various breadboard functions, the electrolyzer was operated at standby conditions to allow for "break-in" time and safe overnight operation. These standby conditions are indicated in Table 1. During the first standby period leaks developed in the Pd tubes and the vacuum pressure switch, set at 15mm Hg, turned the pump off. The electrolyzer testing, however, continued without further operation of the H_2-removal subsystem.

At this time the failure was poorly understood. The failure also affected the oxygen delivery rate of cells. At the beginning of the test an oxygen delivery of 1.39 l/min was measured at a current flow of 25 ampere. The oxygen delivery corresponds to nearly 100% current efficiency.

Table 1

Summary Of Performance Test Of Three-Person Carbon Dioxide/Water Vapor Electrolysis Breadboard

Date	Time Elapsed (Hours)	Event	Feed Gas	Current Efficiency	Production Of Oxygen		H_2 In (H_2 Out)	Carbon Dioxide Consumption		Current	Voltage	Temperature
					l/m	lb/d	l/m	l/m	lb/day	A	V	°C
12/21/88	0	Heat-up	CO_2+2% H_2	~100%						4.25-25.0	19.9	750-900
	4		0.8 CO_2 0.2 H_2	~100%	1.39	6.31	1.03 (0.53)	4.01	25.0	25.0	19.9	900
12/22/88	20	Run	Same	91.3	1.27	5.76	--	4.00	25.0	25.0	18.74	900
12/23/88	48	Run	Same	91.3	1.34	6.08	--	4.01	25.0	27.5	19.08	900
12/24/88	65	Standby*	CO_2+2% H_2	78.8	0.21	0.95	--	1.00	6.24	5	14.59	900
12/25/88	89	Standby	Same	82.9	0.24	1.09	--	1.00	6.24	5	14.55	900
12/26/88	114	Run	Same	91.3	1.34	6.08	--	4.01	25.0	27.5	18.80	900
12/27/88	139	Run	Same	91.3	1.34	6.08	--	3.99	25.0	27.5	18.93	900
12/30/88	211	Run	Same	91.3	1.34	6.08	--	4.00	25.0	27.5	18.80	900
1/5/89	355	Run	Same	84.3	1.29	5.86	--	4.00	25.0	27.5	18.96	900
1/16/89	619	Run	Same	84.3	1.29	5.86	--	4.00	25.0	27.5	21.48	900
1/17/89	693	Run	0.8 CO_2 0.2 H_2	78.3	1.20	5.44	--	4.07	25.4	27.5	22.75	800

* Standby Conditions:

(CO_2+2% H_2) 1 Liter/min

N_2 3 Liter/min (12/21 - 12/23)

4 Liter/min (12/24 - 1/16)

After the failure the current efficiency had dropped to 91%, which indicated that cells also had developed leaks.

During continuing and uninterrupted breadboard operation it became apparent that the cell leaks had developed near the cathode gas inlet side of the active electrolyzer region. The electrical stack performance stability suggested this condition.

During this initial testing period the auxiliary systems were examined and minor functional inadequacies of electro-mechanical components were corrected. Also, during the first fifteen days of operation, the data acquisition system was tested and refined, therefore, much of the electrical test data on single cells had to be measured manually during this time period until software problems were corrected and data could be collected and displayed through the DHS with confidence.

4.4.2 D.C. Electrical Performance of Cell Stack

A summary of essential data for the electrolyzer operation are given in Table 1.

Since all of the cells were individually accessible for oxygen flow measurement, an O_2-generation efficiency profile of all cells was established by measuring with a soap bubble flowmeter. The results of these measurements are shown in Figure 72. The manifolded oxygen of all cells was analyzed, and it was found to contain 3.6 percent CO_2 which clearly indicated the presence of leaks. Despite the damaged cells, the cell stack generated O_2 at a constant rate of 1.3 l/min with a cathode feed gas flow of 4 l/min of CO_2 containing 2% H_2.

An important aspect in the operation of electrolyzers is the temperature distribution throughout the cell stack. Figure 73 shows the temperature distribution within the stack at five axial cell locations such as corner-, side-, and central-positions. The temperatures were measured inside the cells with a movable type S thermocouple. The largest temperature spread is observed between the cells located at the colder and hotter sides of the cold-end insulation package. The spread within the active cell

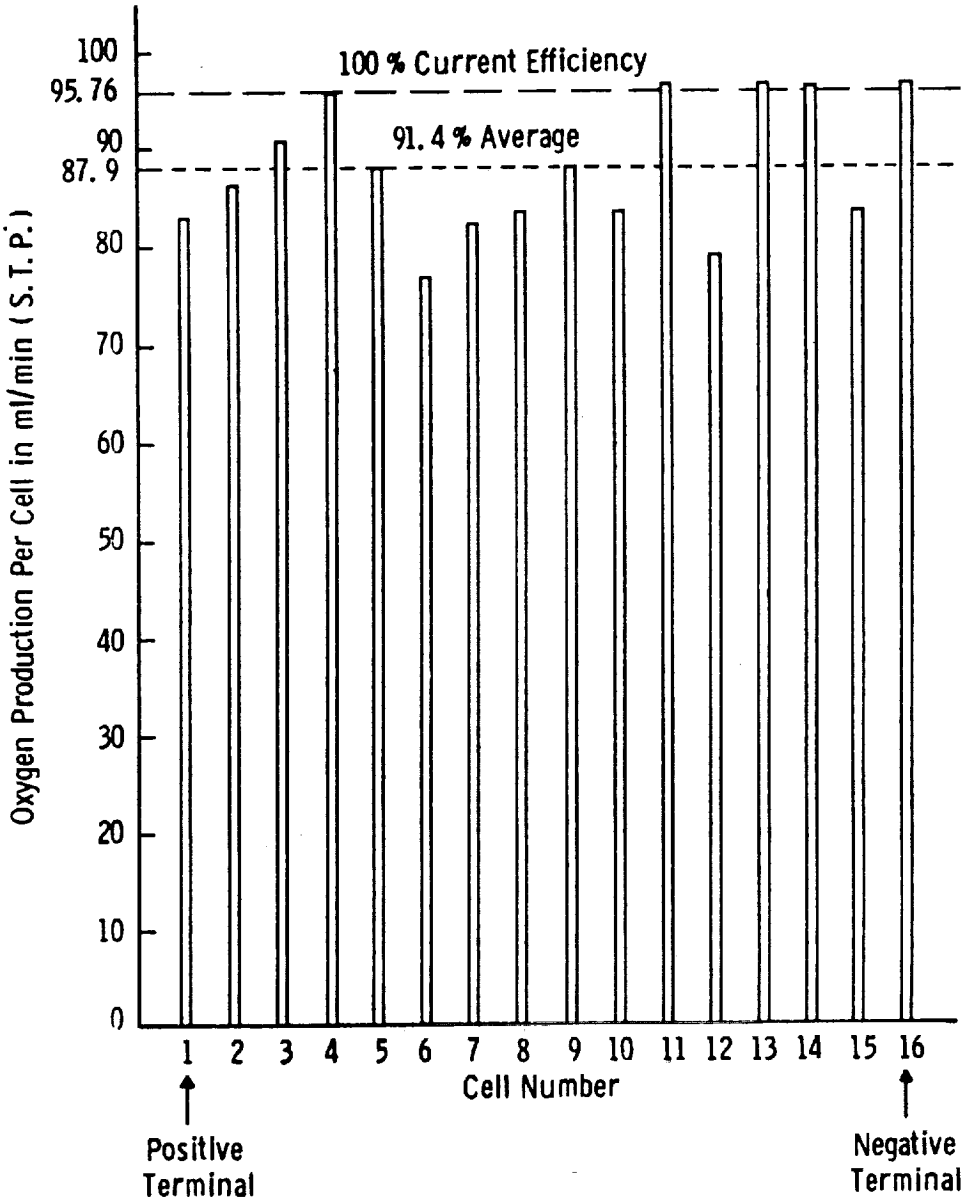

Figure 72. Oxygen Generation of Individual Stack Cells

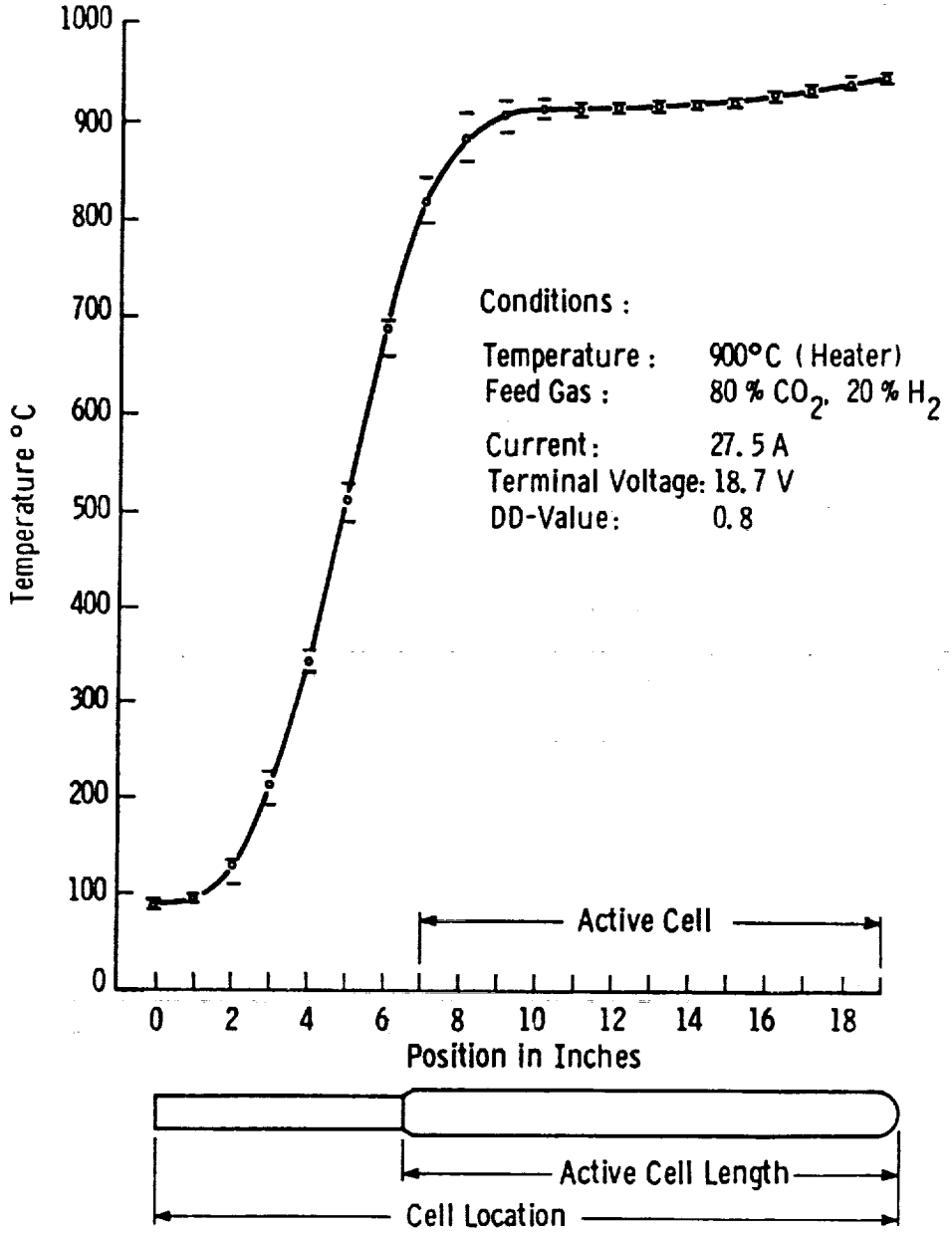

Figure 73. Temperature Distribution In Cell Stack At Three-Zone Heater Setpoints of 900°C

region is minimal. The temperature profile throughout the electrolyzer, measured during operation, is considered to be excellent and well within expected limits.

The electrical performance of the electrolyzer was measured by establishing voltage/current characteristics at constant cathode feed gas conversion rates. Constant conversion rates are measured by the DD-value (see section 3.4.2). The performance expectations for the three-person electrolyzer are based on the performance of qualification cells which were taken from the batches of production cells that provided the electrolyzer cells. The endurance performance of qualification cells is shown in Figure 74 for a cell current density of 250 mA/cm^2. This figure also compares the performance of qualification cell with that of the single cell performance established in Phase I of this program and was selected as candidate cell for the breadboard (see section 3.4.3).

Figure 75 through 79 represent the performance characteristics of the electrolyzer stack under a variety of cathode feed gas compositions, DD-values, and at two temperatures. The matrix of test conditions reflects those that were established during Phase I for testing the breadboard candidate cell. Using Figure 74, breadboard cells show a higher performance level than the qualification cells (1.16V average vs. 1.22V average). The reasons for the improved electrical performance are, a higher average temperature in the stack (925°C) as compared to the temperature in individual qualification cell tests (900°C), as well as more ideal electrical contacting.

Figure 77 represents V-I characteristics that are to be expected when operating the electrolyzer in a closed loop system which would include a carbon deposition reactor. Since the CO concentration in the cathode feed is high, a bucking voltage raises the required electrolysis voltage above that shown in Figure 76. The continuous operation of the breadboard under simulated closed loop feed gas conditions would require the storage of considerable quantities of bottled CO, therefore, these test conditions were applied only for the time period necessary of establishing the V-I characteristics. Furthermore, breadboard cell performance comparison can

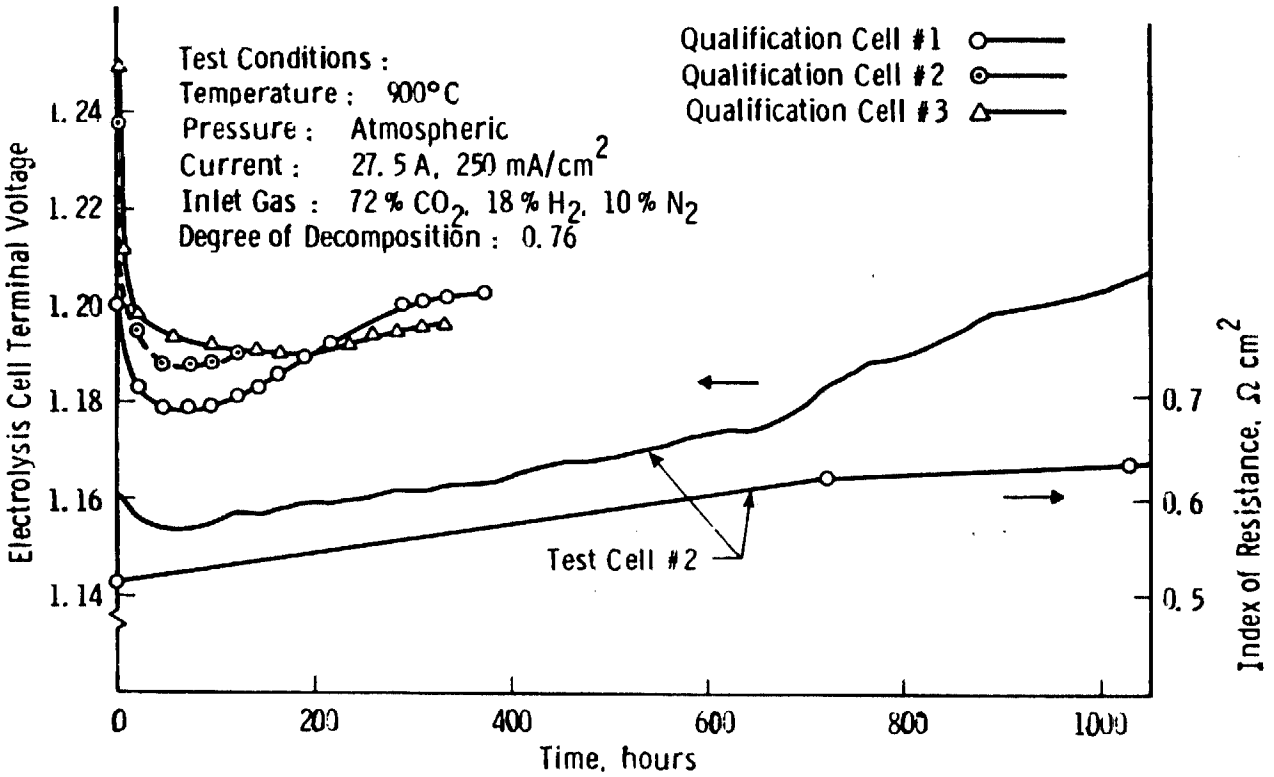

Figure 74. Performance of Stack Qualification Cells and of Prototype Breadboard Cell (Test Cell No. 2)

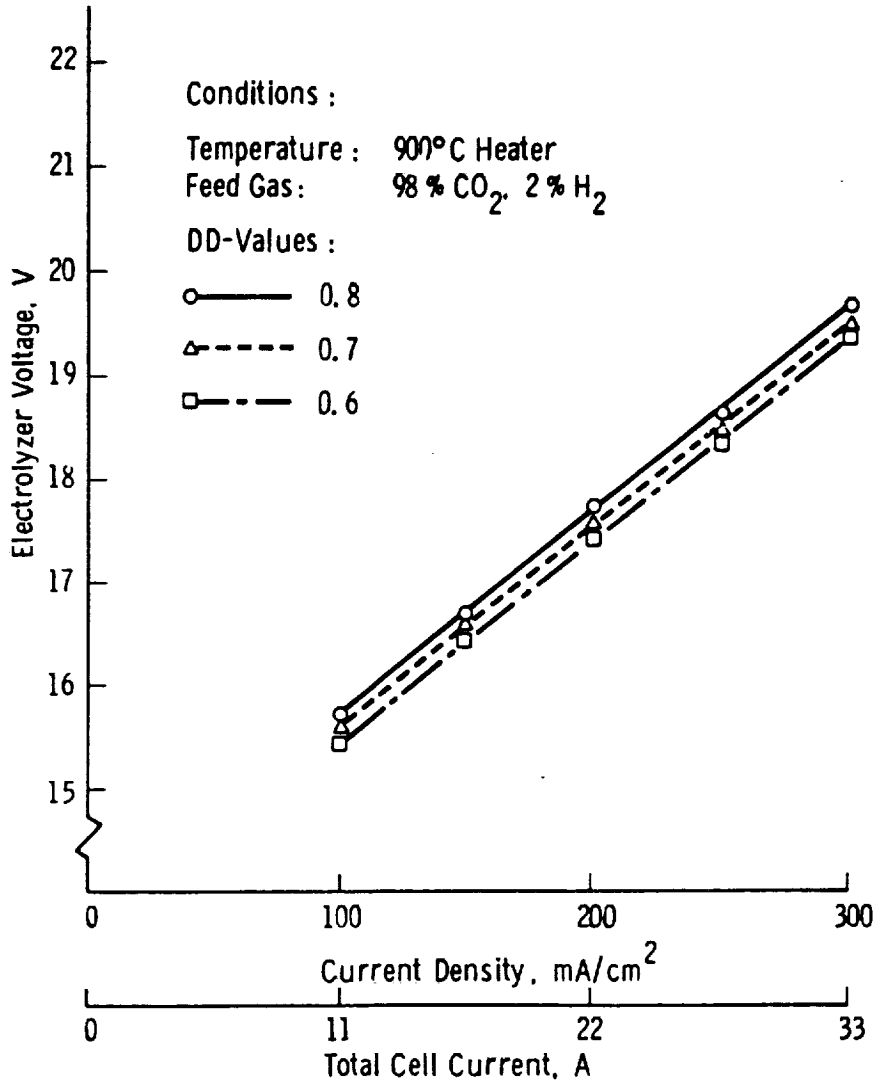

Figure 75. Performance Characteristics of 16-Cell CO_2-H_2O Electrolyzer

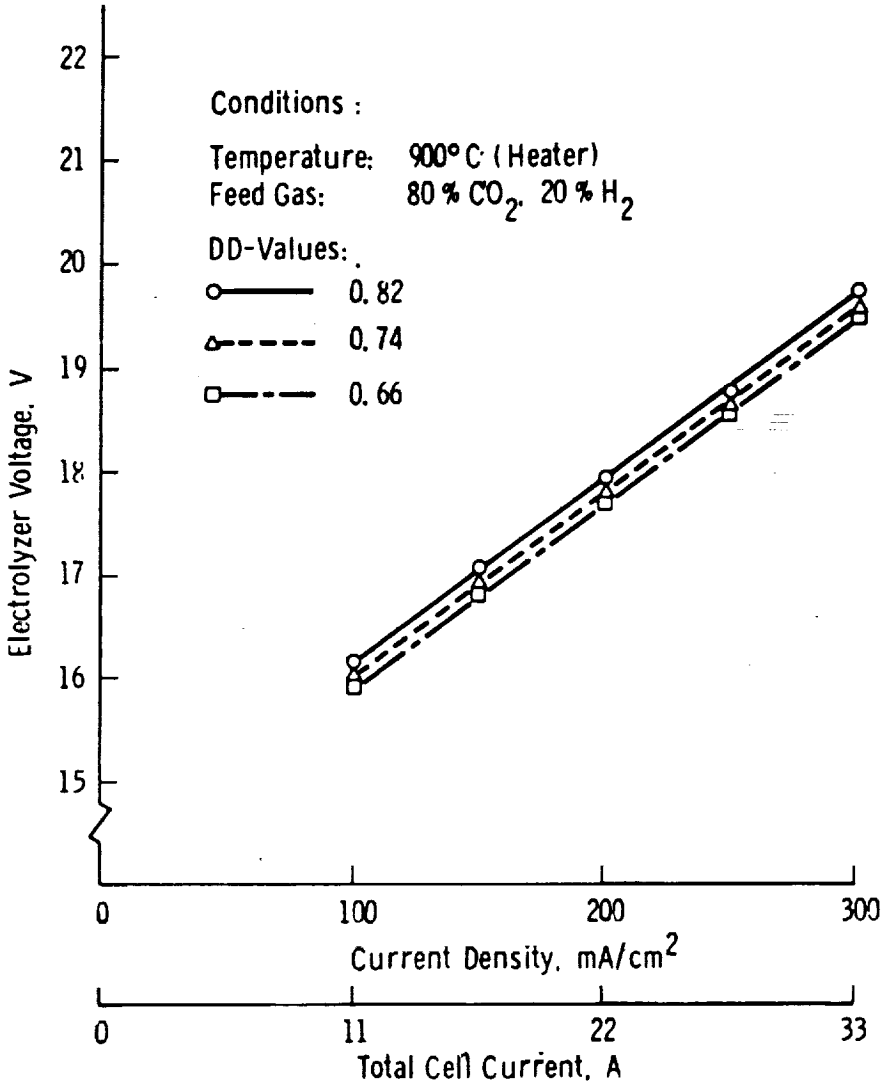

Figure 76. Performance Characteristics of 16-Cell CO_2/H_2O Electrolyzer

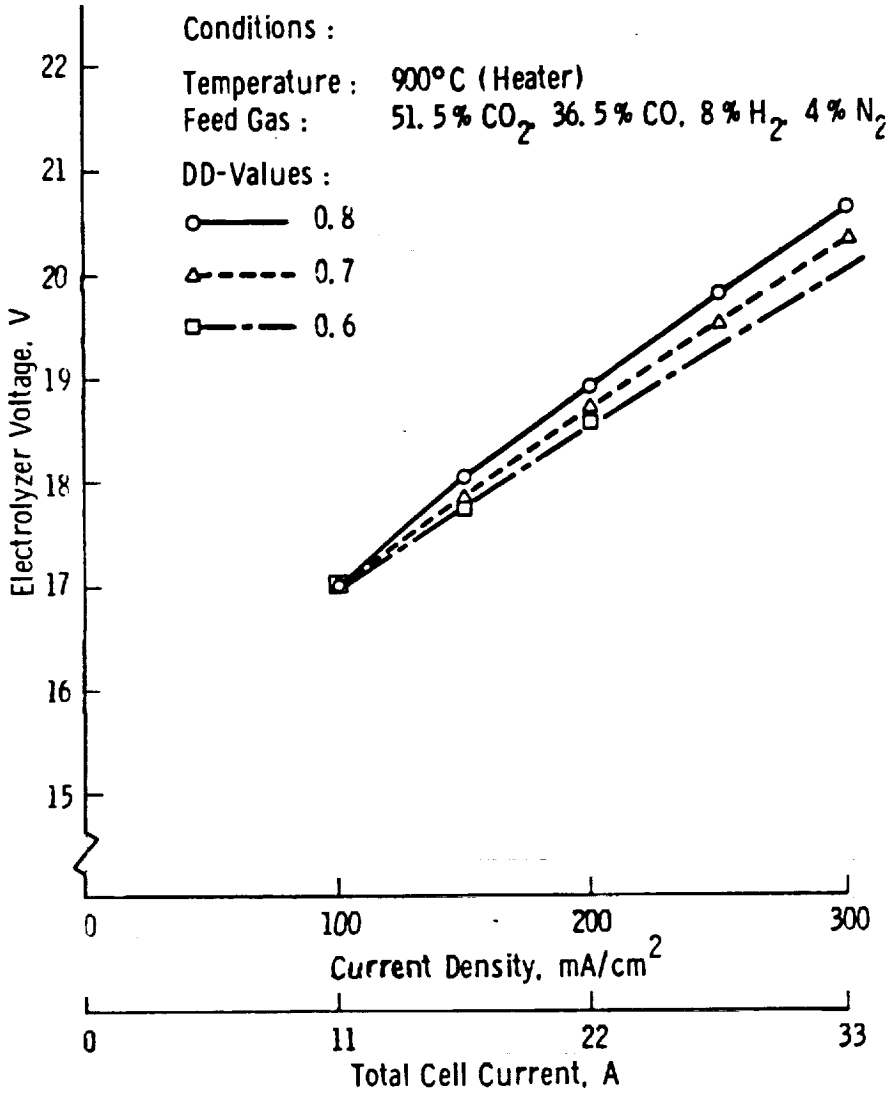

Figure 77. Performance Characteristics of 16-Cell CO_2/H_2O Electrolyzer

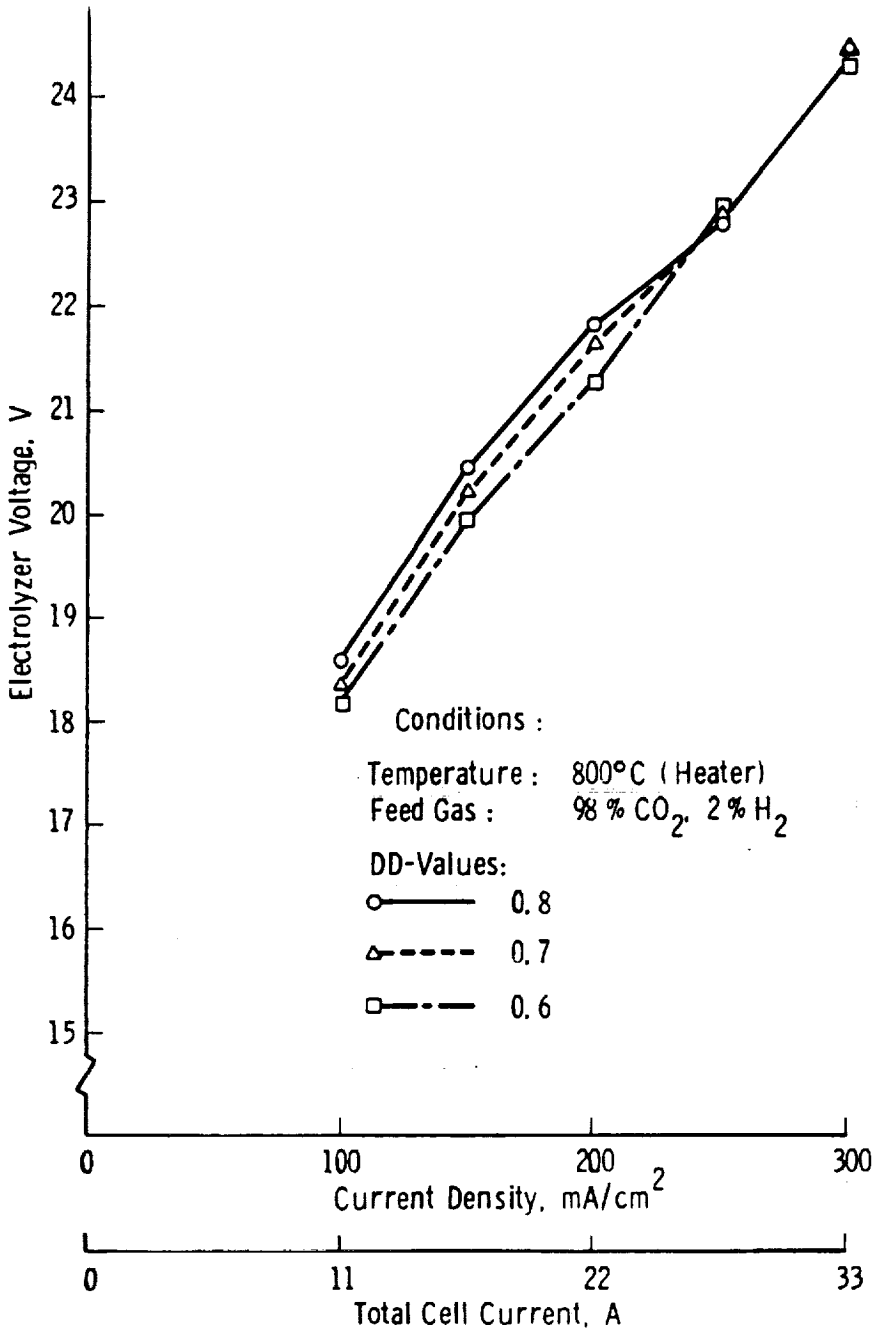

Figure 78. Performance Characteristics of 16-Cell CO_2/H_2O Electrolyzer

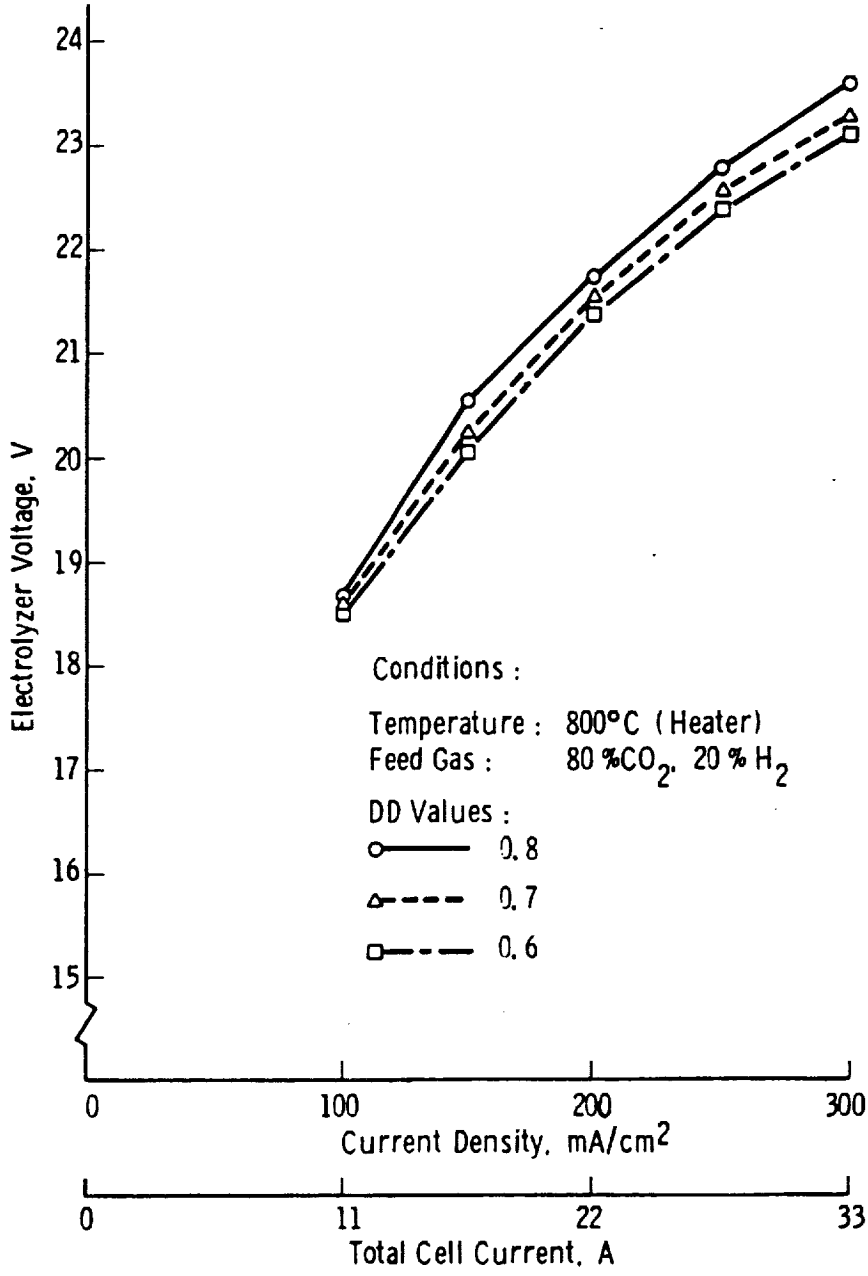

Figure 79. Performance Characteristics of 16-Cell CO_2/H_2O Electrolyzer

be made with test cell No. 2 shown in Figure 74 which was chosen as the prototypical breadboard cell.

Due to the fact that stack cells had developed leaks at an early stage of testing, any change of the stack temperature profile was avoided in order to minimize stresses in the cell structure, which potentially could have resulted in increased leakage. Performance tests at 800°C, therefore, were done during the last two days of breadboard operation. The stack characteristics at 800°C are shown in Figures 78 and 79. As expected, the required stack voltage is increased due to the fact that the required thermodynamic voltage for electrolysis is higher at lower temperatures. The higher electrolysis voltage is due to the lower oxygen activity in the cathode gas as indicated by equations 16 and 17, since k-values for lower temperatures are lower. The ln-term in equation 15, therefore, becomes the dominant one, which determines the increased voltage level.

When comparing the stack performance at 800°C with that of the prototypical breadboard electrolysis cell of Phase I (see Figure 17) an improved average performance of stack cells at the design current density of 250 mA/cm^2 is observed which, again, is due to a modestly increased average stack temperature.

It was demonstrated therefore, that the D.C. electrical performance of the breadboard stack at 800°C and 900°C can be predicted accurately from individual cell performance test. Also, it is significant that the stack performance, despite damage to cells by leaks, was surprisingly stable during the entire test period.

In establishing the stack characteristics, the flow of individual reactants was determined for each current density, gas mixture, and DD-value. Table 2 gives an example of cathode gas component flows, that were used in the test matrix.

A summary of significant breadboard overall performance data of the test period is shown in Table 3.

Table 2

Example Of Cathode Gas Flows For Breadboard Performance Tests

	Feed Gas Composition In Percent	Cathode Gas Component Flow In Liter Per Minute At mA/cm^2														
		DD = 0.6					DD = 0.7					DD = 0.8				
		100	150	200	250	300	100	150	200	250	300	100	150	200	250	300
System Recirculation Gas	51.5 CO_2	4.82	7.23	9.64	Flow Too High	Flow Too High	2.78	4.17	5.56	6.95	8.34	1.95	2.93	3.91	4.89	5.86
	36.5 CO	3.41	5.12	6.82			1.97	2.93	3.94	4.93	5.91	1.38	2.08	2.77	3.46	4.15
	8.0 H_2	0.75	1.13	1.50			0.43	0.65	0.86	1.08	1.29	0.30	0.46	0.61	0.76	0.91
	4.0 N_2	0.37	0.56	0.74			0.22	0.33	0.44	0.55	0.66	0.15	0.23	0.30	0.38	0.46
Breadboard Design Gas	80 CO_2	2.45	3.68	4.90	6.13	7.35	1.96	2.94	3.92	4.90	5.88	1.63	2.45	3.26	4.08	4.89
	20 H_2	0.61	0.92	1.22	1.53	1.83	0.49	0.74	0.98	1.23	1.47	0.41	0.62	0.82	1.03	1.23
Carbon Dioxide	99 CO_2	2.05	3.07	4.09	5.11	6.22	1.75	2.63	3.50	4.38	5.34	1.53	2.30	3.06	3.83	4.60
	1 H_2	0.02	0.03	0.04	0.05	0.06	0.02	0.03	0.04	0.04	0.05	0.02	0.02	0.03	0.04	0.05

Table 3. Three-Person Breadboard Performance

	Expected:	Actual:
Oxygen Production:	4.8 lb/day (minimum)	5.86 - 6.08 lb/day (at 250 mA/cm^2)
Average D.C. Power:	528 watt (at 250 mA/cm^2)	522 watt (15 250 mA/cm^2)
Current Efficiency:	85% (minimum)	100% (~5 hours after start-up) 85.3% average over 26 days
Total Oxygen Production		25.2 lb/10 days 94.9 lb/16 days
Total Carbon Dioxide Consumption		seven 60 lb. ea. cylinders of CO_2
During Test Period		~420 lb.
Degree of Decomposition DD = 0.80 nominal		326 lb CO_2 as O_2-equivalent or 78.5% conversion of CO_2 to O_2
Oxygen Purity		
Start of test:	100%	96.4% - balance CO_2
End of test:		92.9% - " "
A.C. heater requirement	400 watt	750 watt

4.4.3 Auxiliary Breadboard Performance

The functions of breadboard subsystems was described in section 4.3. All sub-systems performanced as expected. Due to the fact, however, that the hydrogen removal system was deactivated during most of the test this sub-system was not subjected to long-term testing, yet the vacuum pump was operated continuously with the inlet port of the pump closed. This was done to establish the reliability of the pump.

4.4.4 Data Handling Sub-System Performance

All vital breadboard performance data are scanned and recorded within seconds. A print-out is provided at selected time intervals in tabular form. In addition, the Factory Link software package allows the display of data in a variety of screens of which the Figures 80-83 are an example. These screens are selected and printed only when desired. Figure 80 represents the display of the raw data which are reduced to actual data by the software by taking into consideration calibration constants. The channels 9 and 10 are cathode gas inlet- and outlet-potentials, as measured by the oxygen sensors.

Due to cell leakage, some cell potentials indicated either excessively high or low voltages, these cases were observed always between adjacent cells. The faulty data are explained by the oxidation of the nickel potential wire contacts which are common to the two adjacent cells and the contacts are in the locations where cell leaks (and Pd tube leaks) had developed (contact to nickel felt at cathode gas inlet). This situation explains the values of channel inputs 12/13, 17/18, and 22/23.

Figure 81 is an example of a process overview. Figure 82 displays the voltage distribution in the cell stack and essential data which are calculated from the measured values of gas flow rates, current, and voltages. Figure 83 is an example of data trends. It shows the maximum, minimum, and average cell voltage over the last 24 hour time period (read from right to left). A sixty minutes plot on the same screen allows the viewing of the last hours performance on a less compressed time scale.

The Factory Link software package could provide considerably more control and display functions. It is greatly under-used as compared to its capabilities. However, the DHS system is a very cost effective and may be of considerable future value should a combination of the breadboard with a carbon deposition reactor be desired.

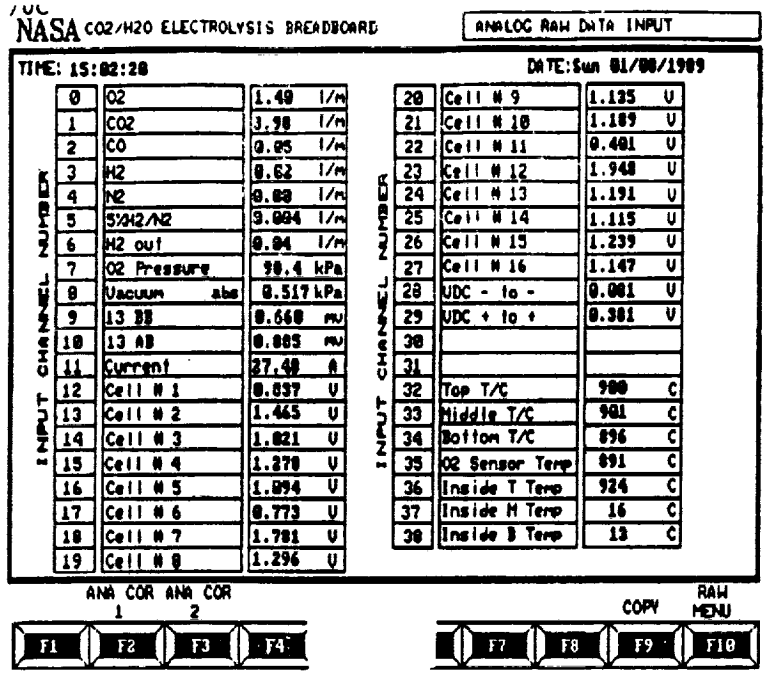

Figure 80. CRT Printout of Measured Data of CO_2/H_2O Electrolysis Breadboard

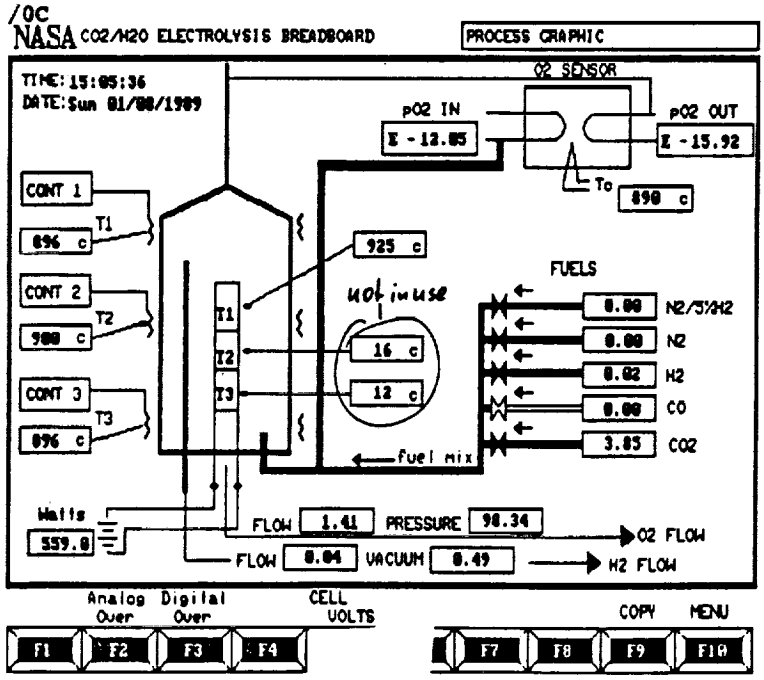

Figure 81. Printout of Process Graphics and System Overview of CO_2/H_2O Electrolysis Breadboard

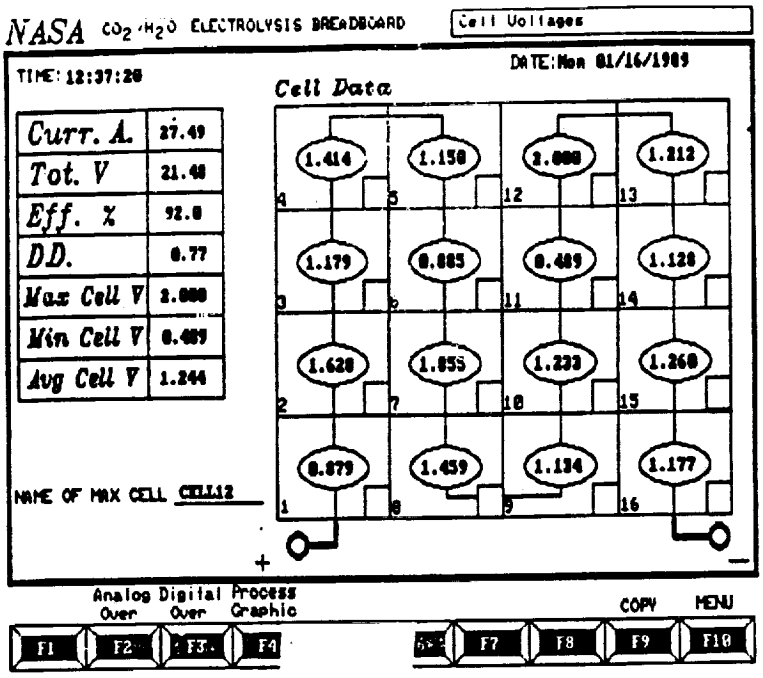

Figure 82. CRT Printout of Individual Cell Voltages and Process Parameters of CO_2/H_2O Electrolysis Breadboard

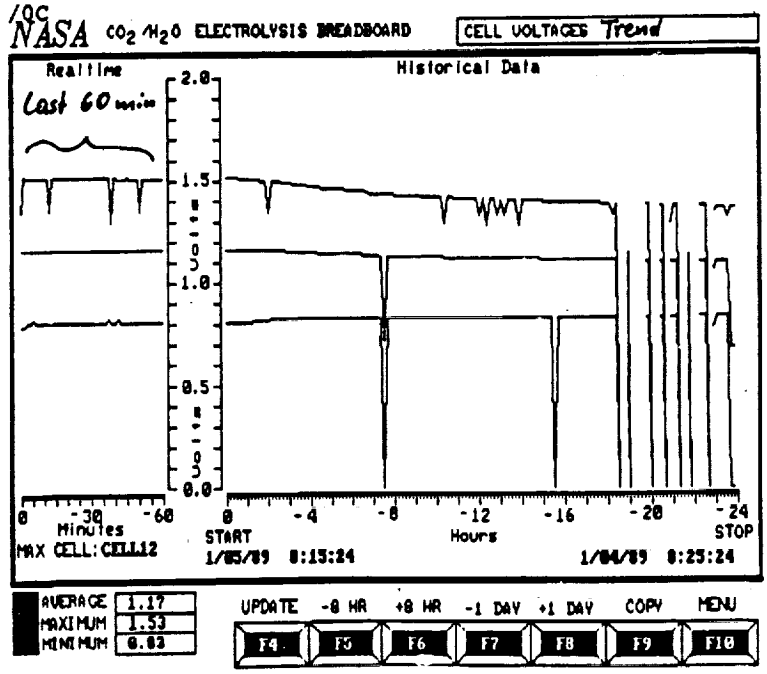

Figure 83. CRT Printout of Voltage Vs. Time Trend During CO_2/H_2 Electrolysis Breadboard Operation

4.5 Physical Characteristics of Breadboard

The following paragraphs describe some essential physical and operational data that are helpful to design and optimize future electrolysis units.

4.5.1 Electrolysis Unit Dimensions and Weight

The electrolysis unit was not designed as a prototypical unit, however, the core of the unit, i.e., the Inconel 600 stack canister and content, including cold end seals and metal cell adapters are considered near prototypical as far as volume and weight for state-of-the-art cells is concerned. Of course, further improvement in cell performance will reduce the volumetric as well as gravimetric figures of merit (watt/liter, watt/kg) of power consumption. Table 4 shows the weight and dimensions of the electrolysis unit components.

4.5.2 Thermal Characteristics and A.C. Power Consumption

The thermal insulation of the electrolysis unit has an average thickness of 5.5 inches which surrounds the stack canister. A power loss of 400 watt had been anticipated, based on the thermal conductivity values for Duraboard 3000 (Carborundum Co.). However a change in product density had been made by the manufacturer in the meantime without changing product designation. The actually applied stack insulation, therefore, lost more heat than what had been calculated previously. This fact became known only after the breadboard testing had commenced and after the electrolysis housing wall temperatures had been measured and found to be abnormally high.

The aluminum housing wall temperatures were measured with an iron/constantane thermocouple (5 mil wires) which was taped with a very thin adhesive tape to various wall locations (15 positions on vertical walls, 9 positions on bottom plate, 9 positions on top plate). The vertical walls

Table 4. Electrolysis Unit Physical Characteristics

Cell dimension	495mm (19.5")	15.5mm (0.610") 12.7mm (0.500")	O.D. active O.D. inactive
Total unit dimensions	610mm (24")	by 381mm (15")	by 394mm (15.5")
Inconel canister dimensions	118mm (4.65")	by 98mm (3.86")	by 495mm (19.5")
Electrolyzer total unit, wt.	24,400g	(53.8 lb)	
Insulation, wt.	16,700g	(36.8 lb)	
Aluminum shell, wt.	7,070g	(15.6 lb)	
Inconel canister, wt.	2,430g	(5.36 lb)	
Canister heaters, wt.	1,760g	(3.88 lb)	
Cell stack, wt.	7,700g	(17.0 lb)	
Total electrolyzer core, wt.	11,890g	(26.2 lb)	
16 bare cells in stack, wt.	3,200g	(7.05 lb)	

had an identical average temperature of 76°C. The bottom and top average plate temperatures were 79°C and 66°C respectively. Since the unit was free-standing, one can approximate a heat loss of 700 watts for the 1.23 m^2 of outer surface and a room temperature of 22°C. Of course, this is a very rough assumption, which could be inaccurate by plus/minus twenty percent. The emissivity of the smooth aluminum walls was considered as being insignificant.

The canister heater power consumption was measured for 900°C in equilibrium with the surrounding air and at the design point of operation. The canister heater resistance, current, and applied voltage were measured for each zone. They are:

top heater	12.0 Ω,	3.7 A,	43.6 V,	161 watt
center heater	6.6 Ω,	5.72 A,	36.7 V,	210 watt
bottom heater	10.0 Ω,	5.98 A,	56.3 V,	337 watt

These measurements indicate that the heat loss toward the cold end is the largest, which can be explained to a large degree by the heat conduction of the Inconel 600 canister wall. Assuming that the heat loss by conduction through the exit gas pipe at the top of the canister is minimal, one can estimate that nearly 160 watt of electric power are required to cover losses by heat-conduction via canister wall and cell extensions at the cold end of the stack. This type of heat loss can be reduced mainly by the design of a thinner canister wall. Since the Inconel 600 sheet wall is 0.037 inch thick one can reduce it in future electrolyzers to 0.015 inch in the lower temperature region where the danger of metal oxidation is minimal (500°C to room temperature). The thermal conduction via the cell tubes is much less than that of the canister due to the ceramic nature of the cells.

The energy of preheating the cathode feed gas (4 l CO_2/min), to 900°C requires a heat equivalent of 120 watt this energy is lost entirely with the hot exit gases. In a total system, therefore, this heat loss must be minimized by heat exchange between incoming cathode feed gas and exiting product gas.

The major energy loss, however, is due to the poor insulation characteristics of the electrolysis unit. For prototype electrolyzers one must employ low loss insulation such as evacuated ceramic foam insulation.

APPENDIX 1

Improved Cermet Cathode

This work was performed during a one month extension of the program during Phase I in order to evaluate an improved nickel/zirconia cermet cathode.

The method of cermet cathode attachment is described in section 3.1.4. The strength of the zirconia skeleton in such an electrode determines the degree of mechanical stability and bond strength to the electrolyte. A thicker zirconia skeleton can be achieved by increasing the porosity in the applied metal powder layer, which is fixed to the electrolyte by the EVD process. The selected approach of increasing the porosity of the cermet cathode was through the use of nickel oxide instead of nickel powder. The chemical reduction of the oxide to metal creates the additional porosity. This type of electrode was tested for test cell No. 4, which is described in section 3.4.6.

The electrode preparation involved the following procedures:

a. Milling of black nickel oxide (NiO) in n-butyl acetate to 5μm average particle size (zirconia grinding media in polyethylene container).

b. Adding 10ml of 9 wt% nickel resinate solution (in benzene) to 100ml of the decanted oxide slurry (decanted after five minutes of settling of oxide particles).

c. Spraying of oxide slurry onto the cell electrolyte to achieve a surface loading of approximately 40 mg/cm^2. The cell is rotated axially during this process. A Pasche air-brush-type spray gun is recommended. Cell areas which are not to be coated with cathode material are tape-masked.

d. Reduction of the nickel oxide by hydrogen is performed in the EVD reactor immediately before the vapor deposition of zirconia which forms the skeleton. The reduction is accomplished with a flow of hydrogen at a pressure of 100mm Hg for approximately 30 minutes. The end of reduction is indicated on the external glass connection to the EVD reactor, which, when cooled by dry-ice, shows condensation of water vapor.

The absence of condensation indicates completeness of nickel oxide reduction.

e. The EVD attachment of the porous nickel layer which follows is performed under standard vapor deposition conditions of cathode attachment.

The endurance test for test cell No. 4 (Figure 32) indicates that the cell performance deterioration slows down significantly to a lower rate after 1300 hours of continuous cell operation. This behavior is being attributed to a better mechanical attachment.

APPENDIX 2

Preliminary Failure Analysis of Palladium Tubes

This work was performed during an extension of the program in order to shed light onto the reasons for palladium tube failure which either preceded or coincided with the development of leaks in the electrolysis cells.

Visual Cell Bundle Inspection

The electrolyzer unit was removed from the breadboard housing and the cell bundle was extracted. This procedure demonstrated the capability of a smooth exchange of cell bundles when required for repair purposes.

The bundle showed evidence of damage to some peripheral cells but only at the feed gas inlet side. This explains why the cell performance was reasonably stable and good, since most other active cell areas were in excellent condition. The affected cell areas was next to the site where palladium tubes had failed. The palladium tube failure is unique and is observed only in the feed gas inlet side, 1/2" to 1" into the active cell region. The typical tube flaw is shown in Figure 84, which shows a large hole where a palladium grain was pulled into the tube cavity by the applied vacuum. Peripheral palladium tubes show several of these holes each. There is microscopic evidence, than an intergranular melt was present at the time of failure.

At this point, it was concluded that the palladium tube failure led to the development of cell leaks, possibly by establishing a nonuniform temperature profile in a sensitive stack area. The disturbed profile would be due to the fact that unknown quantities of cathode gas was drawn from hotter and cooler zones to the holes, until the vacuum pump was shut down because of a pressure rise in the hydrogen manifold above 15mm Hg.

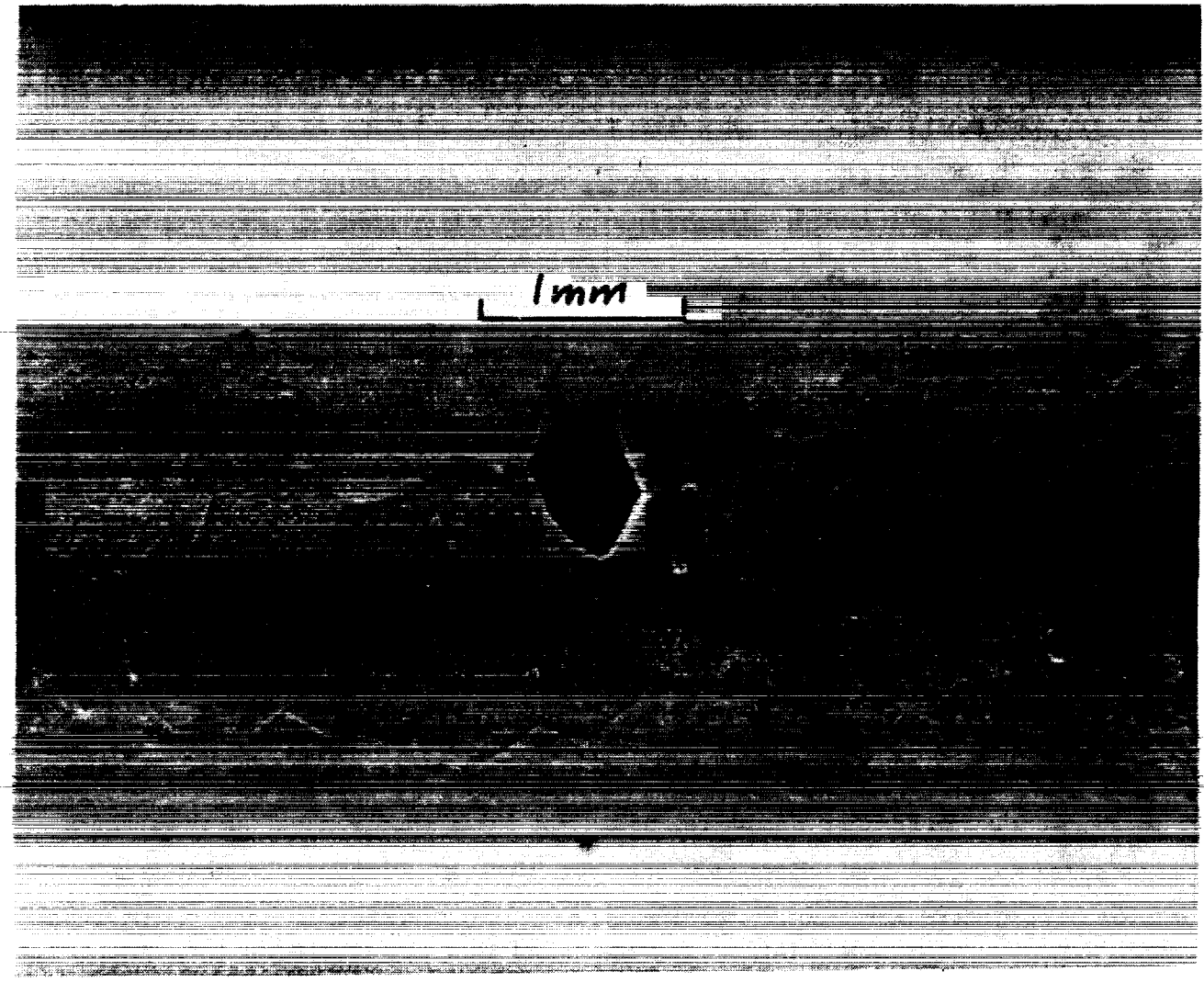

Figure 84. Hole Formation in Palladium Tube Through Intergranular Melt Formation

Failure Tests for Palladium Tubes

A major question arose as to the sequence of events that led to Pd tube failure and development of leaks in cell tubes during a relatively short time interval. The question is: Did leaks develop first in cell tubes which then led to oxygen attack on neighboring Pd tubes, or did the Pd tube leaks develop first, resulting in a severely distorted temperature profile on cells and thus create cell leaks due to thermal stresses.

The following experiments were performed. A new Pd tube was inserted into an alumina tube and a small bore alumina tube was placed beside it with its open end placed in the center of the heated Pd tube section. The assembly was heated to 900°C and the Pd tube was evacuated. A cathode gas flow, consisting of a mixture of CO_2, H_2 and N_2 passed over the samples. The gas composition and flow rate was representative of conditions during the occurrence of Pd tube leaks in the cell bundle.

In the first test, as shown in Figure 85a, a small oxygen flow was introduced into the cathode gas stream through the small bore alumina tube and was maintained for hours. No leak development was observed even over a 24 hour test period. The Pd tube surface appearance was excellent after this test.

A second test was performed to evaluate the possibility of cathode gas contamination due to a ceramic cement component, containing phosphate bonding constituents. This cement (Ceramabond 600) was tested before use in the cell bundle with respect to stability in contact with nickel felt, and alumina. No deleterious reactions were observed. In this test, as shown schematically in Figure 85b, dried and fired cement samples were positioned near the Pd tube in the test duct, but were not touching the Pd tubes. Using the same "cathode gas flow" conditions, (no oxygen flow), the Pd tube developed severe leaks of the same type that were observed on tubes from the breadboard cell bundle. Leak development was observed within 40 minutes.

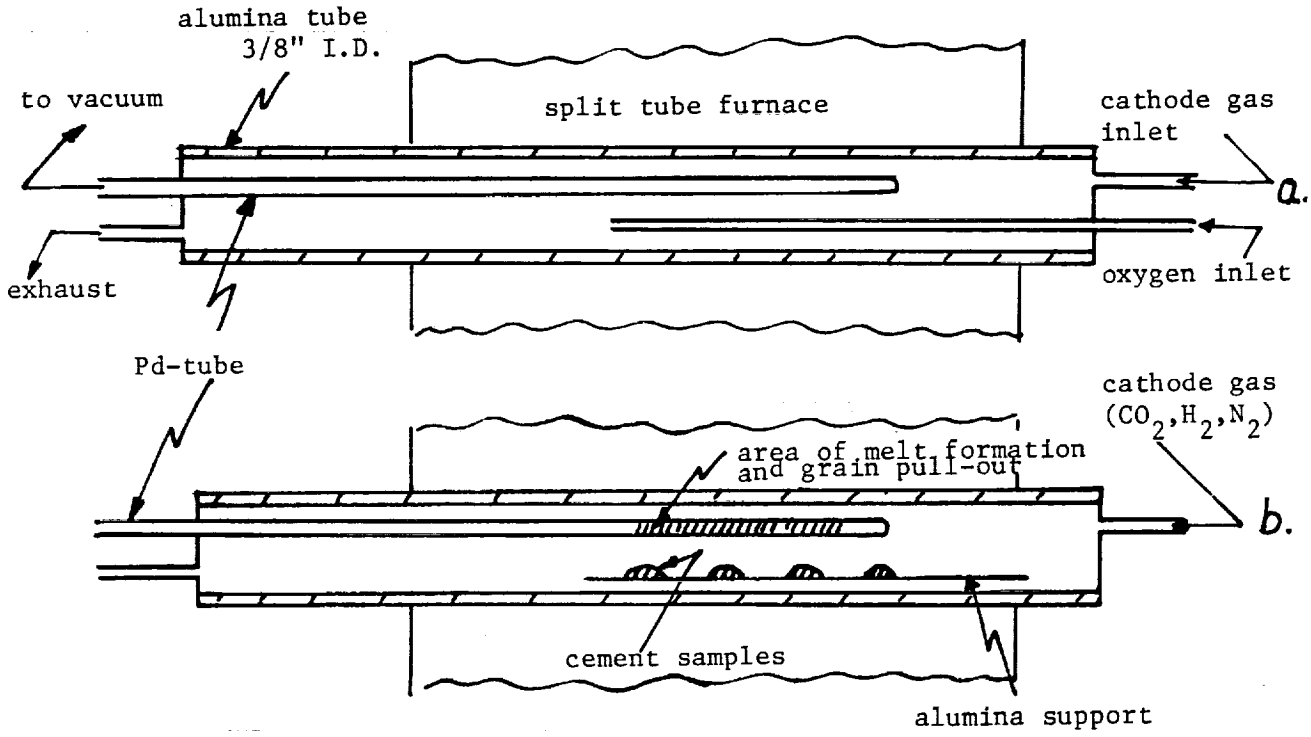

Figure 85. Test Arrangement for Determination of Pd-Tube Failure Mechanism

The surface of the cooled Pd tube showed enhanced attack by a melt. It is concluded that the formation of a eutectic melt of palladium phosphide caused the hole formation in the Pd test sample as well as in the Pd tubes of the cell bundle. A low melting point of 788°C is reported in the literature for a 20 atom percent phosphorous-palladium alloy[4]. It is also concluded from these tests that the Pd tube leak development occurred first and caused flow conditions which led to cell tube failure. This information is of great value for the construction of future electrolysis cell test stacks.

LITERATURE REFERENCES

1. Elikan, L.; Morris, J. P.; Wu, C. K.: "Development of a Solid Electrolyte Carbon Dioxide and Water Reduction System for Oxygen Recovery". NASA-Contract No. NAS1 8896, Report No. NASA CR-2014.

2. Isenberg, A. O.: "Growth of Refractory Oxide Layers by Electrochemical Vapor Deposition (EVD) at Elevated Temperatures". ECS-Symposium, Electrode Materials and Processes for Energy Conversion and Storage, Proceedings, Vol. 77-6.

3. Gmelin; Handbook of Inorganic Chemistry, 8th Edition, Palladium, System No. 65, 1942 Berlin, Verlag Chemie, pp. 116-131.

4. Hansen, M.; "Constitution of Binary Alloys", McGraw-Hill Book Co., 1958, p. 1084.